

**Natural Fractures and Lineaments of the  
East-Central Greater Green River Basin**

**GRI Contract Number 5091-221-2146**

Institute for Energy Research  
University of Wyoming  
Laramie, Wyoming 82071-4068

**TOPICAL REPORT**  
**August 1995**

for

Gas Research Institute  
GRI Project Manager  
John Hansen

## GRI Disclaimer

**LEGAL NOTICE** This report was prepared by Cheryl Jaworowski for Dr. Ronald C. Surdam, Principal Investigator, Institute for Energy Research, the University of Wyoming as an account of work sponsored by the Gas Research Institute (GRI). Neither GRI, members of GRI, nor any person acting on behalf of either:

- a. Makes any warranty or representation, express or implied, with respect to the accuracy, completeness, or usefulness of the information contained in this report, or that the use of any apparatus, method, or process disclosed in this report may not infringe privately owned rights; or
- b. Assumes any liability with respect to the use of, or for damage resulting from the use of any information, apparatus, method, or process disclosed in this report.

REPORT DOCUMENTATION PAGE			Form Approved OMB No. 0704-0188	
Public reporting burden for this collection of information is estimated to average 1 hour per response, including the time for reviewing instructions, searching existing data sources, gathering and maintaining the data needed, and completing and reviewing the collection of information. Send comments regarding this burden estimate or any other aspect of this collection of information, including suggestions for reducing this burden, to Washington Headquarters Services, Directorate for Information Operations and Reports, 1215 Jefferson Davis Highway, Suite 1204, Arlington, VA 22202-4302, and to the Office of Management and Budget, Paperwork Reduction Project (0704-0188), Washington, DC 20503.				
1. AGENCY USE ONLY (Leave Blank)	2. REPORT DATE August 1995	3. REPORT TYPE AND DATES COVERED Topical Report: May 1992-August 1995		
4. TITLE AND SUBTITLE Natural Fractures and Lineaments of the East-Central Greater Green River Basin			5. FUNDING NUMBERS 5091-221-2146	
6. AUTHOR(S) Jaworowski, C., G.E. Christiansen, M.A. Grout, H.P. Heasler, W.P. Iverson, R.S. Martinsen, M.A. Olson, R. Simon, R.C. Surdam (P.I), and E.R. Verbeek				
7. PERFORMING ORGANIZATION NAME(S) AND ADDRESS(ES) Institute for Energy Research University of Wyoming P.O. Box 4068 Laramie, WY 82071-4068			8. PERFORMING ORGANIZATION REPORT NUMBER	
9. SPONSORING/MONITORING AGENCY NAME(S) AND ADDRESS(ES) Gas Research Institute 8600 Bryn Mawr Avenue Chicago, Illinois 60631			10. SPONSORING/MONITORING AGENCY REPORT NUMBER GRI-95/0306	
11. SUPPLEMENTARY NOTES				
12a. DISTRIBUTION/AVAILABILITY STATEMENT Unclassified			12b. DISTRIBUTION CODE	
13. ABSTRACT (Maximum 200 words)  This topical report addresses the relationship of natural fractures and lineaments to hydrocarbon production of the east-central Greater Green River Basin. The tight gas sands of the Cretaceous Mesaverde Formation are the primary focus of this work. IER and USGS researchers have (1) demonstrated that east-northeast and northeast-trending regional fractures and lineaments are important to hydrocarbon production; (2) recognized the east-northeast regional joint set near two horizontal wells (Champlin 254 Amoco B 2-H and Champlin 320 C-1A-H) in the Washakie and Great Divide basins, respectively; (3) related Cretaceous Almond Formation thickness and facies to northeast-trending faults; (4) developed a program to automatically derive lineaments from small linear features; (5) associated oil and gas production data with east-northeast and northeast-trending lineaments and linear features; and (6) digitally compared lineaments with potentiometric maps of the Mesaverde and Frontier formations. The construction of a digital geologic database (geology, satellite images, linear features, lineaments, digital elevation data, township-range, oil and gas fields, gravity, magnetics, production and potentiometric maps) has been an integral part of this effort.				
14. SUBJECT TERMS			15. NUMBER OF PAGES	
			16. PRICE CODE	
17. SECURITY CLASSIFICATION OF THIS REPORT Unclassified	18. SECURITY CLASSIFICATION OF THIS PAGE Unclassified	19. SECURITY CLASSIFICATION OF ABSTRACT Unclassified	20. LIMITATION OF ABSTRACT	

# Research Summary

- Title** Natural Fractures and Lineaments of the East-Central Greater Green River Basin
- Authors** C. Jaworowski, G. Christiansen, M. Grout, H. Heasler, W. Iverson, R. Martinsen, M. Olson, R. Simon, R. Surdam, and E. Verbeek
- Contractor** Institute for Energy Research  
University of Wyoming
- Contract** GRI Contract No. 5091-221-2146
- Contract Period** May 1993 - September 1995 (extended to March 1996)
- Principal Investigator** R. Surdam
- Report Period** August 1995  
Topical Report
- Objective** The overall objective of the project is to develop an innovative exploration and production strategy to optimize the efficient exploitation of gas resources, particularly those in “tight” gas sands in the upper Cretaceous (100-65 million years) Mesaverde Group of the Greater Green River Basin (GGRB), Wyoming. This topical report explores the relationship of basement-lineaments (probable faults in 2.7 to 2.0 billion year-old rocks) to regional fractures, sedimentation, fluid flow, and hydrocarbon production. Our work is an integrated part of the larger project *Natural Gas Resource Characterization Study of the Mesaverde Group in the Greater Green River Basin, Wyoming: A Strategic Plan for the Exploitation of Tight Gas Sands*.
- Technical Perspective** Several variables affect hydrocarbon accumulation: type of rock, temperature and depth of burial of rock, degree and timing of cementation, development of fractures, the timing of fluid flow through rocks, and the folding and faulting of rocks. Fractures are thought to be an important factor in the production of hydrocarbons from “tight” gas sands. Lineaments influence hydrocarbon production by affecting the thickness of sediments, the type of sediments, the flow of fluids in permeable rocks as well as the folding and faulting of rocks. By understanding these relationships, it will be possible to reduce exploration risks.
- Results** The concept of movement along east-northeast and northeast trending lineaments—probable deep-seated faults—is useful for understanding the production of significant hydrocarbon production in the east-central Greater Green River Basin (Washakie and Great Divide basins). These lineaments bound or terminate areas of significant hydrocarbon production throughout the basin. Surface fractures near two horizontal wells (Champlin 254 Amoco

B 2-H and Champlin 320 C1A-H) show an east-northeast or northeast trend similar to lineaments, linear features, and natural fractures in Cretaceous sediments at 10,000 ft-depth in the Washakie and Great Divide basins. Producing trends in the vicinity of these horizontal wells are terminated by an east-northeast lineament or northeast linear feature. A detailed subsurface correlation of the Cretaceous sediments in the Washakie and Great Divide basins showed that northeast-trending lineaments affect sedimentary thickness and type of sediment. We tested our delineation of lineaments by developing a program that automatically defines lineaments from small, local linear features. Finally, we used our digital geologic database of the Greater Green River Basin to demonstrate an innovative approach for establishing the subsurface significance of surface lineaments; we digitally combined lineaments, faults, gravity, and potentiometric maps to show that areas of high fluid flow ("sweet spots") are associated with lineaments and faults.

**Technical Approach**

Our study uses both standard methods (field work on fractures, analysis of cores, well logs, stereoscopic aerial photographs) and computer-assisted analysis of satellite images and digital geologic data to investigate regional fractures and lineaments. The initial phase of our work involved the acquisition of public domain digital geologic data and generation of digital geologic data for the east-central Greater Green River Basin. The integration of various types of digital geologic data (e.g., linear features, lineaments, gravity, magnetics, potentiometric maps, topography, oil and gas fields, township-range) allowed a graphical display of relationships between linear features, lineaments, faults, gravity, potentiometric maps, and oil and gas fields. Field work on fractures and the development of accurate stratigraphy and sedimentology was concurrent with the establishment of a digital geologic database.

**Project Implications**

Techniques have been developed to predict subsurface fractures using image interpretation and joint data. A better understanding of regional fractures, lineaments, fluid flow, and Mesaverde stratigraphy in the Washakie and Great Divide basins will allow GRI clients to make more informed exploration and production risk assessments for the tight gas sands of the Mesaverde Group. All interested parties can focus their attention and resources on selected target areas or "sweet spots."

GRI Project Manager  
John Hansen

# Table Of Contents

<b>Chapter 1</b> .....	<b>1</b>
Introduction	
<i>Cheryl Jaworowski and Ronald Surdam</i>	
<b>Chapter 2</b> .....	<b>5</b>
The Significance of Northeast-Trending Lineaments, Regional Fractures, and Digital Geologic Data to Oil and Gas Production within the East-Central Greater Green River Basin, Wyoming	
<i>Cheryl Jaworowski, Robert Simon, and Ronald Surdam</i>	
<b>Chapter 3</b> .....	<b>23</b>
Stratigraphy and Lithofacies of the Almond Formation, Washakie and Great Divide Basins	
<i>Randi Martinsen, Glen Christiansen, and Mark Olson</i>	
<b>Chapter 4</b> .....	<b>37</b>
Joint Sets in the Wamsutter Area: Relation to Fracture History of the Rawlins and Rock Springs Uplifts, Washakie Basin, Southern Wyoming	
<i>Earl Verbeek, Marilyn Grout, and Cheryl Jaworowski</i>	
<b>Chapter 5</b> .....	<b>47</b>
Oil and Gas Production Data	
<i>William Iverson</i>	
<b>Chapter 6</b> .....	<b>57</b>
Automated Recognition of Lineaments from Linear Features	
<i>Robert Simon and Cheryl Jaworowski</i>	
<b>Chapter 7</b> .....	<b>65</b>
Comparison of Lineaments and Potentiometric Surfaces	
<i>Henry Heasler and Cheryl Jaworowski</i>	
<b>References</b> .....	<b>71</b>
<b>Appendix A</b> .....	<b>77</b>

# List Of Tables

Table		page
2-1	Studies of photolinear elements in the GGRB .....	8
2-2	Studies of joints in the GGRB .....	9
2-3	Panchromatic SPOT satellite images .....	10
4-1	Station number and set designation for joints .....	40
4-2	Possible correlations between median strikes of joints .....	42
4-3	Orientations and relative ages of joint sets F2, F4, and F5 .....	44

# List Of Figures

Figure		page
2-1	Digital elevation model for Wyoming .....	6
2-2	Plot showing major structural features .....	7
2-3	Wamsutter-Latham NHAP color-infrared aerial photograph .....	11
2-4A	Non-length-weighted rose diagram, from photo, Wamsutter .....	12
2-4B	Length-weighted rose diagram, from photo, Wamsutter .....	12
2-4C	Rose diagram of Wamsutter-Latham joints .....	13
2-4D	Rose diagram of natural fractures in horizontal core, Wamsutter .....	13
2-5	Linear features from SPOT images, Wamsutter .....	13
2-6A	Non-length-weighted rose diagram, from SPOT images, Wamsutter .....	14
2-6B	Length-weighted rose diagram, from SPOT images, Wamsutter .....	14
2-7	Linear features from SPOT images, Red Desert .....	15
2-8A	Non-length-weighted rose diagram, from SPOT images, Red Desert .....	15
2-8B	Length-weighted rose diagram, from SPOT images, Red Desert .....	15
2-8C	Rose diagram of Red Desert joints .....	16
2-8D	Rose diagram of linear features, from photos, Red Desert .....	16
2-8E	Rose diagram of natural fractures in horizontal core, Red Desert .....	16
2-9	Plot identifying oil and gas fields in Figures 2-10 to 2-12 .....	17
2-10	Plot of Bouguer gravity, GGRB .....	19
2-11	Plot of magnetic intensity, GGRB .....	19
2-12	SPOT mosaic of east-central GGRB, showing oil and gas fields .....	20
3-1	Oil and gas map of GGRB area .....	24
3-2	Structure contour map of GGRB .....	25
3-3	Diagrammatic cross section showing restored Upper Cretaceous rocks .....	26
3-4	Well-log cross section constructed across T17N .....	27
3-5	Isopachous map of interval underlying "hot shale" .....	27
3-6	Diagrammatic cross section showing relationship of Almond members .....	28
3-7	Isopachous map of total net coal, Almond Formation .....	30
3-8	Base map of Dripping Rock-Mulligan fields .....	35
4-1	Map of joint stations, Wamsutter area .....	39
5-1	Cumulative gas production vs. cumulative oil production .....	48
5-2	Defined worth of 181 fields in the study area vs. year of discovery .....	49
5-3	Contour map of the net present worth (NPW) of individual wells .....	51
5-4	Well logs, Champlin 254 Amoco B 2-H well, Wamsutter area .....	52
5-5	Well logs, PTS #14-4 well, a prolific Echo Springs producer .....	52
5-6	Great Divide and Lost Creek gas fields, Champlin 320 C-1A-H well .....	53
5-7	Well logs, vertical parent of Champlin 320 C-1A-H well .....	54
6-1	Parameterization of a line .....	58
6-2	Shape in the image space of a point when $Dq$ is large .....	59
6-3	Shape in the image space of a point when $Dr$ is large .....	59
6-4	Input for test .....	60
6-5A-C	Output for test, various parameters .....	60
6-6	Map of lineaments and linear features using various parameters .....	61

6-7	Map of lineaments and linear features using various parameters .....	62
6-8	Map of lineaments and linear features using various parameters .....	62
6-9	Map of lineaments and linear features using various parameters .....	63
7-1	Contoured potentiometric surface, Mesaverde Formation .....	66
7-2	Faults associated with SPOT lineaments .....	67
7-3	Contoured potentiometric surface with fault lines, Mesaverde Formation .....	67
7-4	Contoured potentiometric surface, Frontier Formation .....	68
7-5	Potentiometric surface with oil and gas fields and SPOT lineaments .....	69
7-6	Potentiometric surface with oil and gas fields and gravity gradients .....	69
7-7	Potentiometric surface with oil and gas fields and gravity gradients .....	70

## List Of Plates

Plate 1. East-west well-log cross section A-A' of the upper Ericson through lower Lewis interval is hung on the base of the "hot shale." Line of section shown in Figure 4-2. Well-log cross section B-B' across Barrel Springs Field, shows stratigraphic relationships within the Almond and the location of inferred syndepositional faults. The interval designated "middle Almond shale marker" is correlatable across the central and eastern Washakie and Great Divide basins. Datum is a marker in the lower Lewis. Line of section shown in Figure 4-2. Gamma-ray - resistivity-log cross section C-C' of the Almond Formation in the Dripping Rock-Mulligan Draw fields area. Line of section is shown in Figure 4-10. Cross section trends northwest-southeast and is hung on a bentonite datum in the Lewis Shale. The location and relative motion of inferred faults are shown. Gamma-ray - resistivity-log cross section D-D' of the Almond Formation in the Dripping Rock field. Cross section is of two adjacent wells, and is hung on a bentonite datum in the Lewis Shale. Also shown are location and relative motion of inferred fault. Line of section is shown in Figure 4-10.

Plate 2. Well-log cross section grid of Almond Units 1 and 2 within the Coal Gulch field.

# Chapter 1

## Introduction

*Cheryl Jaworowski and Ronald Surdam*

Lineaments (probable basement faults) affect production of oil and gas by influencing sedimentary thickness, facies, fluid flow, and structure. Using the Washakie and Great Divide basins as examples, the effect of lineaments upon these geologic parameters is discussed in succeeding chapters. Each chapter addresses a different aspect of regional fractures and lineaments: east-northeast-trending regional fractures, lineaments, and significant production of hydrocarbons; the impact of northeast-trending lineaments on Cretaceous Almond Formation sedimentary thickness and facies; regional fractures and their relationship to joint history; application of oil and gas production data to east-northeast-trending lineaments; an automated method of defining lineaments from linear features; and comparison of lineaments with potentiometric maps. A brief synopsis of each chapter follows.

Chapter 2, entitled "*The Significance of East-Northeast-Trending Lineaments, Regional Fractures, and Digital Geologic Data to Oil And Gas Production Within the East-Central Greater Green River Basin,*" introduces the concept of east-northeast and northeast-trending, basement-related lineaments and regional fractures in the Washakie and Great Divide basins. East-northeast-trending basement faults may have been reactivated and east-northeast-striking joints may have formed during a period of middle Tertiary extension. Site-specific studies of joints and linear features near two horizontal wells (Champlin 254 Amoco B 2-H and Champlin 320 C-1A-H) indicate that east-northeast trending regional fractures are present at the surface. The same set of east-northeast-

trending regional fractures was encountered in the subsurface by these horizontal wells. Dominant east-northeast-striking regional fractures near these wells are parallel or subparallel to mapped faults.

Martinsen et al. discuss the correlation of facies within the Cretaceous Almond Formation in Chapter 3, "*Stratigraphy and Lithofacies of the Almond Formation, Washakie and Great Divide Basins.*" The authors recognize three genetic units of the Almond Formation: Unit 1, a barrier-bar and coal-bearing facies associated with back-barrier environments (youngest), Unit 2, a dominantly marine facies of coarsening-upward shale and sandstone sequences, and Unit 3, a fluviially-dominated, coal-bearing unit (oldest). They attribute changes in reservoir thickness and facies of Almond sediments to movement along basement faults in the Washakie and Great Divide basins. The sands in Unit 2 are depositionally similar to the productive upper Almond sands, and may be viable exploration targets.

In Chapter 4, entitled "*Joints Sets in the Wamsutter Area: Relation to Fracture History of the Rawlins and Rock Springs Uplifts, Washakie Basin, Southern Wyoming,*" Verbeek, Grout, and Jaworowski discuss the relationship of a dominant east-northeast joint set near the Champlin 254 Amoco B 2-H well to a previously documented joint history of the Rawlins and Rock Springs uplifts. Their work suggests that the dominant east-northeast joint set near Champlin 254 Amoco B 2H probably is no older than Miocene. In their study of gilsonite dikes in the eastern Uinta Basin, Verbeek and Grout (1993) recognized that

Age  
Available  
data

normal faults and a joint set can be different products of the same period of regional extension. This work clearly demonstrates the correlation between the geometric properties of the surface network of regional fractures and the subsurface fracture in Upper Cretaceous reservoir rocks, particularly in the Washakie Basin.

In Chapter 5, "Oil and Gas Production Data," Iverson uses well production figures from Petroleum Information to classify oil and gas fields within the eastcentral Greater Green River Basin into four categories: largest, significant, small, and smallest fields. The largest fields, which have >500 Bscfe (\$500 million) cumulative production and significant fields, which have 50-500 Bscfe (\$50-500 million) cumulative production, are associated with lineaments. Iverson's contour plots of production values for two areas near Champlin 254 Amoco B 2-H east of Wamsutter and Champlin 320 C-1A-H in the Red Desert show termination of production by an east-northeast or northeast-trending lineament. Iverson recognizes fractures as a significant, but not necessarily primary, factor affecting the production of hydrocarbons.

In an attempt to test lineaments interpreted from satellite images, R. Simon has developed a computer program that constructs lineaments from small linear features. In Chapter 6, "Automated Recognition of Lineaments from Linear Features," Simon and Jaworowski use the program rather than a human interpreter to identify large regional fractures or lineaments. First, linear features are identified by a human interpreter on satellite images. Using a Hough transform, the program identifies lineaments by drawing a line along a dense concentration of linear features. Then, by adjusting length, width, number, and angle, the program derives different lineaments from linear features. Continued testing of a computer program to directly identify lineaments from an image

will eventually result in a map of lineaments that can be reproduced by different users of the computer program.

Comparison of lineaments with mapped faults and potentiometric maps indicates that lineaments are associated with discontinuities in the fluid-flow regime. In Chapter 7, "Comparison of Lineaments and Potentiometric Surfaces," Heasler and Jaworowski demonstrate that high values of hydraulic head in the Frontier and Mesaverde formations correlate best with previously mapped faults. Several mapped faults correlate with lineaments derived from satellite images. On the potentiometric map of the Frontier Formation, a north-east-trending zone of moderate hydraulic head is associated with the Brady Field.

The following topics discussed in the present study are currently applicable to hydrocarbon exploration in other Laramide basins in the Rocky Mountains: (1) recurrent movement along Precambrian zones of weakness and the associated influence on the overlying sedimentary section, (2) an exploration approach that utilizes stereo images (satellite images or aerial photographs) to define structural linear features, and (3) an integrated geologic approach to problem solving using digital geologic data.

Future work on lineaments (probable basement faults) must address certain key questions, including:

- what is the timing and movement on the most conspicuous basement faults?
- what type(s) of movement has occurred along these faults?
- how do these basement faults relate to regional tectonics?
- does recurrent movement along these lineaments produce wrench duplexes?

The Cretaceous Almond sediments are probably not the only formation affected by episodic movement of basement faults; study of other formations is needed to

demonstrate movement during other geologic intervals. Our use of public domain, low resolution geophysical data shows only the most conspicuous basement faults. High resolution aeromagnetic maps can help to more accurately define the subsurface location of these faults. Continued field work on natural fractures and faults near other wells will further test the correlation between surface natural fractures and subsurface fractures. Continued study of regional fractures, faults, lineaments, and other formations will expand upon ideas generated by this initial assessment of important regional fractures and basement faults.

## Chapter 2

# The Significance of East-Northeast-Trending Lineaments, Regional Fractures, and Digital Geologic Data to Oil and Gas Production within the East-Central Greater Green River Basin, Wyoming

*Cheryl Jaworowski, Robert Simon, and Ronald Surdam*

### ABSTRACT

Basinwide and site-specific studies of regional fractures have shown that basement-related lineaments are associated with oil and gas production within the east-central Greater Green River Basin (GGRB). Specifically, northeast- and east-northeast-trending surface and gravity lineaments are associated with those oil and gas fields that individually have more than 5 Bscfe (\$5 million) cumulative production. In the Rocky Mountain region, recurrent movement along basement-related lineaments has been correlated with changes in sediment thickness, facies, and production from structural traps.

In our basinwide study, digital databases (linear features, oil and gas fields, geology, Bouguer gravity, magnetic data, digital elevation data, and production data) were used to illustrate the relationship between lineaments and oil and gas production. Surface lineaments from analysis of 10-meter SPOT panchromatic images were correlated to magnetic and gravity gradients. Graphical display of lineaments with oil and gas fields indicates that lineaments bound or traverse producing fields.

In our site-specific studies of regional fractures, we predicted the orientation of subsurface fractures by image interpretation and joint measurements. In the Red Desert (Champlin 320 C-1A-H) and near Wamsutter (Champlin 254 Amoco B 2-H),

linear features and joints correlated with the orientation of fractures measured in cores from two horizontal wells. At both sites, a dominant east-northeast-trending regional fracture was measured at outcrop and in horizontal core.

### GEOLOGIC SETTING

The Greater Green River Basin (GGRB) of southwestern Wyoming (Figure 2-1) contains several major geologic structures: the Rock Springs Uplift, the Great Divide Basin, the Wamsutter Arch, the Washakie Basin, and the Green River Basin (Figure 2-2). The Wamsutter Arch separates the Great Divide Basin from the Washakie Basin. The Wind River Thrust, Thrust Belt, Uinta Mountains, Sierra Madre, and Rawlins Uplift define the northwestern, western, southwestern, southeastern, and northeastern margins of the GGRB, respectively (Figure 2-2). The regional fractures and lineaments in the east-central part of the GGRB are the focus of this paper.

### INTRODUCTION

Photogeologic analyses of streams and studies of joints indicate that fracture patterns change from dominant east-northeast and northwest trends in the northern portion of the study area to northwest and east-west trends near the

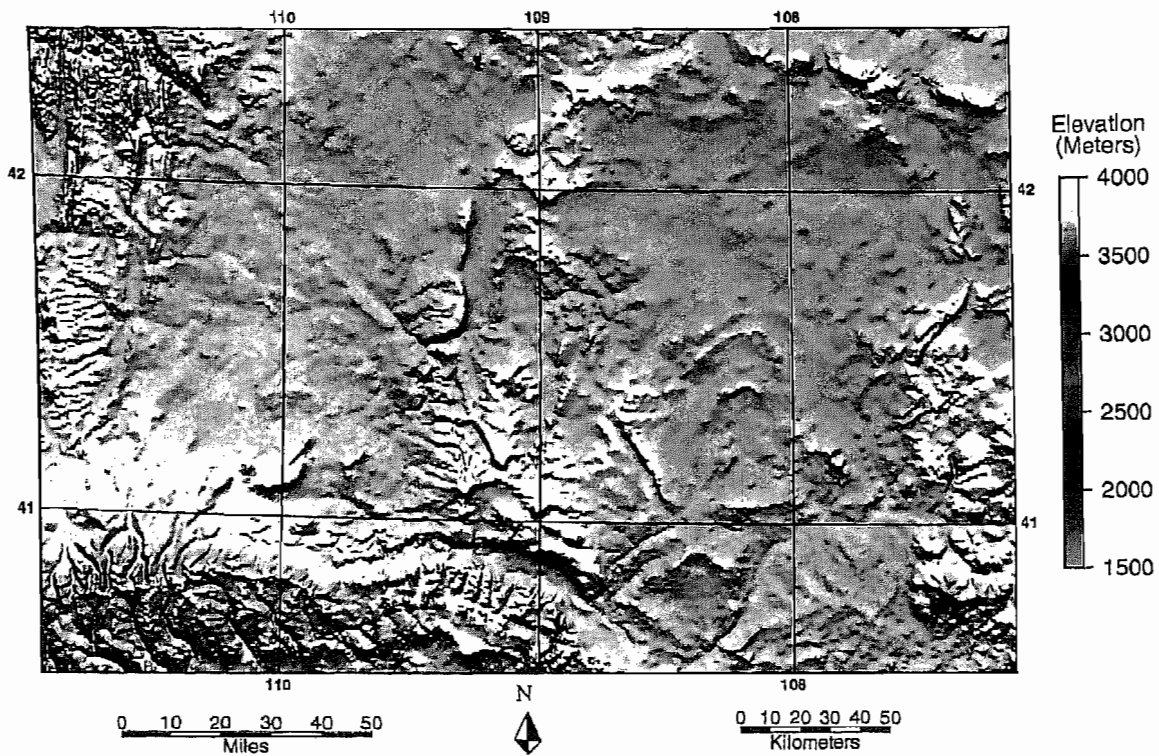


**Figure 2-1.** Digital elevation model for the GGRB (Lambert conic conformal projection, 1-km grid, 0° solar azimuth). The area between 107.5 and 111 west longitude and 39.5 to 42.5 latitude encompasses the majority of the GGRB of southwestern Wyoming. Elevation ranges from 1500 m (ochre) to 4000 m (grey).

Wyoming-Colorado border. The north-to-south change in dominant fracture pattern coincides with north-to-south changes in the orientation of major faults. The goals of these basinwide and site-specific studies of regional fractures and lineaments in the east-central GGRB are: (1) to document the spatial variation of regional fracture patterns using 10-meter SPOT satellite images, (2) to compare linear features to joint orientations and subsurface fractures, (3) to correlate surface lineaments with similar subsurface features, and (4) to determine if an association exists between basement-related lineaments and production of oil and gas.

A structural photo-interpretation of topography, satellite images, and aerial photographs provides a reasonable assessment of regional fractures for most of the GGRB. Such an interpretation shows

stream patterns that reflect structural influence on drainage, such as opposing linear tributaries, right-angle bends in streams, radial drainage, and streams parallel to the strike of beds or fractures (Doeringsfeld and Ivey, 1992; Penney, 1992). Stream courses reflect not only structure, but also adjustment to progressive late Cenozoic basin excavation. Barbed drainage patterns, indicative of stream piracy, are seen. Stream piracy and other changes in stream courses may reflect a Quaternary drainage reversal (Hansen, 1969, 1984, 1985).

Use of drainage as an indicator of structure is less helpful in areas covered by significant eolian sediments. The "Wyoming wind corridor" cuts across the Green River and Great Divide basins (Kolm, 1982). In the Red Desert of central Wyoming, scour streaks and linear depressions

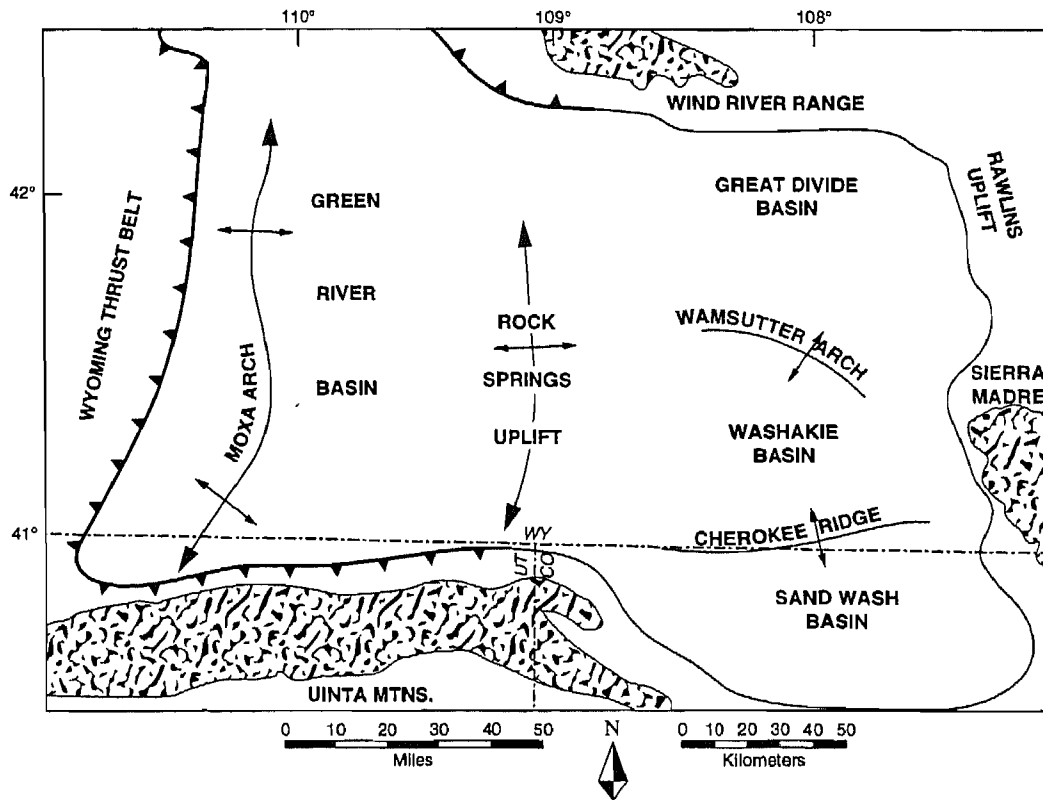


**Figure 2-2.** Plot of major structural features of the GGRB; the Wyoming thrust belt forms the western basin border; the Sierra Madre and Rawlins Uplift form the eastern border; and the Uinta and Wind River mountains form the southern and northern borders, respectively. Figures 2-7 to 2-9 show the same area.

result from persistent unidirectional winds (Marrs and Gaylord, 1982). Eolian features with a N75°E trend are responsible for the strongly striped ground seen on satellite images and color-infrared aerial photographs (Blackstone, 1973). Eolian processes can obscure as well as follow structural trends. Thus, linear features (topographic alignments, tonal changes, and vegetation lines) mapped in areas with eolian and other Quaternary sediments may contain a significant percentage of nonstructural linear features.

## PREVIOUS STUDIES

Researchers, observing photo-linear features on satellite images and aerial photographs, have related these features to Laramide tectonics and late Miocene

faulting south of the Washakie Basin (Thomas, 1971; Earle, 1975; Paylor, 1983). Studies of linear features and lineaments in the GGRB (Table 2-1) have identified N60-80°E and N25-60°W regional trends (Thomas, 1971; Blackstone, 1972, 1973; Earle, 1975). Using photogeologic maps of southwest Wyoming, Thomas (1971) identified major northeast-trending (Wamsutter, Bitter Creek, and Rock Springs) and northwest-trending lineaments (Alkali Creek and Cherokee Ridge). Using an early August ERTS-1 image (ID # 1013-17300-5; ERTS-1 is also known as Landsat-1), Blackstone (1972, 1973) confirmed the N65E (Red Desert lineament) and the N40°W (Farson lineament) structural trends. The northwest-trending Farson lineament, which is subparallel to a zone of normal faults (McGrew and Berman, 1955), aligns with

**Table 2-1.** Studies of photolinear elements in the GGRB, Wyoming.

Researcher	Location	Major Trends	Lineament	Comments
Thomas (1971)	GGRB	NE NW	Bitter Creek Wamsutter Alkali Creek La Barge	Photogeologic study
Blackstone (1973)	GGRB	N65°E N40°W	Red Desert Farson	ERTS-1 image
Earle (1975)	Rock Springs	ENE		Landsat-1 winter mosaic
Paylor (1983)	Table Rock	N10-20°E, N40-50°E, N60-70°E, N80-80°E, N70-90°W, N40-50°W, N-N20°W		
Peiterson (1992)	Washakie Basin	N-N10°E, N40-50°E, N60-80°E, N30-40°W		Landsat MSS image (80-m resolution)

the Pleistocene volcanic vents of the Leucite Hills (Bradley, 1961; Blackstone, 1972). A reconnaissance study of major lineaments and linear features on a winter Landsat-1 photomosaic encompassing Wyoming (Earle, 1975) mentions similar trends: (1) a dominant east-northeast trend and a subordinate west-northwest trend for the Rock Springs Uplift, and (2) north-northeast, northeast, and northwest trends in the Great Divide, Washakie, and Yampa basins (the Yampa Basin is south of Wyoming).

Researchers studying joints in the Cretaceous Mesaverde Group around the Rock Springs Uplift (García-González, 1992; Grout and Verbeek, 1992; Laubach et al., 1992; Leite, 1992) (Table 2-2) consistently identify two regional trends, N60-80°E and N30-40°W. Grout and Verbeek (1992) document a dominant N30-40°W trend as the oldest trend on the Rock Springs Uplift (Table 2-2). The N60-80°E strike is the third-oldest joint set. Two northwest trends (N20-45°W and N55-85°W) are the youngest joint sets on the Rock Springs Uplift (Grout and Verbeek, 1992). Grout and Verbeek (1992) argue that a second northwest-trending joint set (N20-45°W) developed

approximately on strike with the oldest northwest joint set on the Rock Springs Uplift. The younger N20-45°W joint set may be associated with Blackstone's Farson lineament and Pleistocene activity in the Leucite Hills. Grout and Verbeek (1992) state that the joint history suggests a counterclockwise rotation of the stress field in post-Cretaceous time. In apparent contrast to this assessment of joint history, Laubach et al. (1992) state that east- and east-northeast-trending joint sets on coals predate a nonsystematic set of northwest-striking joints, and suggest that regional fracture patterns in Cretaceous and Tertiary coal beds are related to the trace of the Cordilleran thrust belt.

## METHODS

For our basinwide study of regional fractures, panchromatic SPOT (Satellite Pour l'Observation de la Terre) satellite images (10-meter spatial resolution) were acquired for the Rock Springs Uplift, Washakie Basin, Wamsutter Arch, and Great Divide Basin (Table 2-3). Because low solar elevation enhances subtle geomorphic features, a snow-free mosaic of October

**Table 2-2.** Studies of joints in the Greater Green River Basin.

Researcher	Location	Strike	Unit
Grout and Verbeek	Rawlins Uplift	N10-30°E, N05-30°W, N45-65°W, N75-80°W, N50-75°E, N25-45°W, N55-65°W	Mesaverde (1992) Group
	Rock Springs Uplift	N30-40°W, N55-65°W, N20-45°E, N60-80°E, N20-45°W, N55-85°W	Mesaverde Group
Laubach et al. (1992)	Rock Springs Uplift	N60-80°E	Cretaceous coals
García-González (1992)	Rock Springs Uplift	N15-45°W, N80°E	Almond/Lance
Leite (1992)	Rock Springs Uplift	N-N10°W, N20-30°W, N50-70°W, N80-90°W, N20-30°E, N60-70°E	Almond
		N20-30°W, N30-40°W, N40-60°E	Basal Blair Ss

images was attempted for the east-central Greater Green River Basin. Linear features from the Rock Springs Uplift to the Rawlins Uplift were mapped using SPOT panchromatic images and a commercially available image processing program, ER Mapper. The 10-meter spatial resolution allowed identification of linear features as fractures, cliffs, streams, and previously mapped faults. Interpretation of linear features with SPOT satellite images enabled efficient digital mapping over broad areas with minimal distortion. Using ER Mapper's annotation program, nearly 17,300 linear features were mapped digitally over a 6430-mi<sup>2</sup> (16,655-km<sup>2</sup>) area of the east-central GGRB.

Digital mapping of linear features using SPOT images allowed for integration with other digital data (e.g., geology, oil and gas fields, Bouguer gravity, magnetic data, potentiometric maps, township-range grids). Lineaments were delineated by noting aligned linear fea-

tures or areas with a high density of linear features. An automated method of determining lineaments from our digital database of linear features is under investigation (Chapter 6, this volume).

A lineament, or fracture of regional extent (Hoppin, 1974), should be apparent in the subsurface. Bouguer gravity and magnetic anomaly data were used to test the subsurface significance of SPOT surface lineaments. The 3804 points of Bouguer gravity data from Bankey and Kulik (1989) were gridded by the use of an inversesquare interpolation (Robert Simon's program GRIDIT). After importation into ER Mapper, the gravity was warped to an appropriate projection, annotated, and overlaid with oil and gas fields. Digital magnetic data for the United States were downloaded from the National Geophysical Data Center CD-ROM of geophysical data grids onto our workstation and imported into ER Mapper.

**Table 2-3.** Panchromatic SPOT satellite images used in the present study.

Area	Scene I.D. (k-j-date-hms)*	Solar Azimuth	Solar Elevation	Comments
Northern Rock Springs Uplift	555-266-102489-181611	167°	36°	good quality image
Southern Rock Springs Uplift	555-267-102489-181619	167°	36°	good quality image
Great Divide & NW Washakie Basins	556-266-102489-181609	167°	36°	good quality image
SW Washakie Basin	556-267-102489-181617	167°	36°	good quality image
Great Divide & Washakie Basins	557-266-102088-181150	166°	37°	good quality image
Washakie Basin	557-267-102088-181159	166°	37°	good quality image
Great Divide & NE Washakie Basin	558-266-103188-180020	165°	33°	light snow
SE Washakie Basin	558-267-100292-181416	164°	44°	light snow

\*Each grid point on the SPOT Grid Reference System is identified by a pair of letters (k, j): k = column number and j = row number.

2D  
 For our site-specific studies of regional fractures in the Red Desert and near Wamsutter, linear features were mapped using National High Altitude color-infrared (CIR) transparencies (scale 1:58,000) and panchromatic SPOT images. Unless CIR aerial photographs are digitized, imported, and rectified to an appropriate projection, linear features must be analyzed manually. The length and orientation of CIR linear features were measured manually and entered into an ASCII file for plotting rose diagrams. For linear features derived from panchromatic SPOT images, rose diagrams were generated using several programs. Robert Simon's C-language program, LINES, determined the length, direction, number, and percent of linear features in a selected area. The ASCII output of the LINES program was edited and imported into a Postscript-language program for plotting publication-quality rose diagrams.

As part of the site-specific studies, joint sets were measured in the vicinity of the Champlin 254 Amoco B 2-H (Wamsutter) and Champlin 320 C-1A-H (Red Desert) horizontal wells. Joint sets were compared with the linear features seen on color-infrared aerial photographs and panchromatic SPOT images, as well as with fractures encountered by the two horizontal wells.

**CORRELATION OF LINEAR FEATURES WITH JOINTS AND SUBSURFACE FRACTURES**  
**Wamsutter Horizontal Well (Champlin 254 Amoco B 2-H)**

Using a stereoscope and color-infrared aerial photographs, linear features with structural significance were identified over a 306-km<sup>2</sup> (118-mi<sup>2</sup>) area east of Wamsutter (Figure 2-3). This area pro-

vides a test for correlation between surface and subsurface fractures. A plot of the number and orientation of linear features (Figure 2-4A) near Wamsutter shows a major east-northeast trend (N40-60°E) and a subordinate west-northwest trend (N50-60°W). A plot of percent total length of linear features (Figure 2-4B) shows similar east-northeast (N50-60°E) and west-northwest (N50-70°W) trends. Length-weighting of linear features changes the pattern of the rose (compare Figures 2-4A and 2-4B) by weighting longer northeast-trending linear features more than shorter north

and northwest-trending linear features. Length-weighting of linear features is computed as

$$\% \text{ total length} = \frac{\text{total length of linear features in a } 10^\circ \text{ increment}}{\text{total length of all linear features}} \times 100.$$

Subsurface fractures from the horizontal core of the Champlin 254 Amoco B 2-H well show an orientation similar to that of linear features identified by structural photo-interpretation of color-infrared aerial

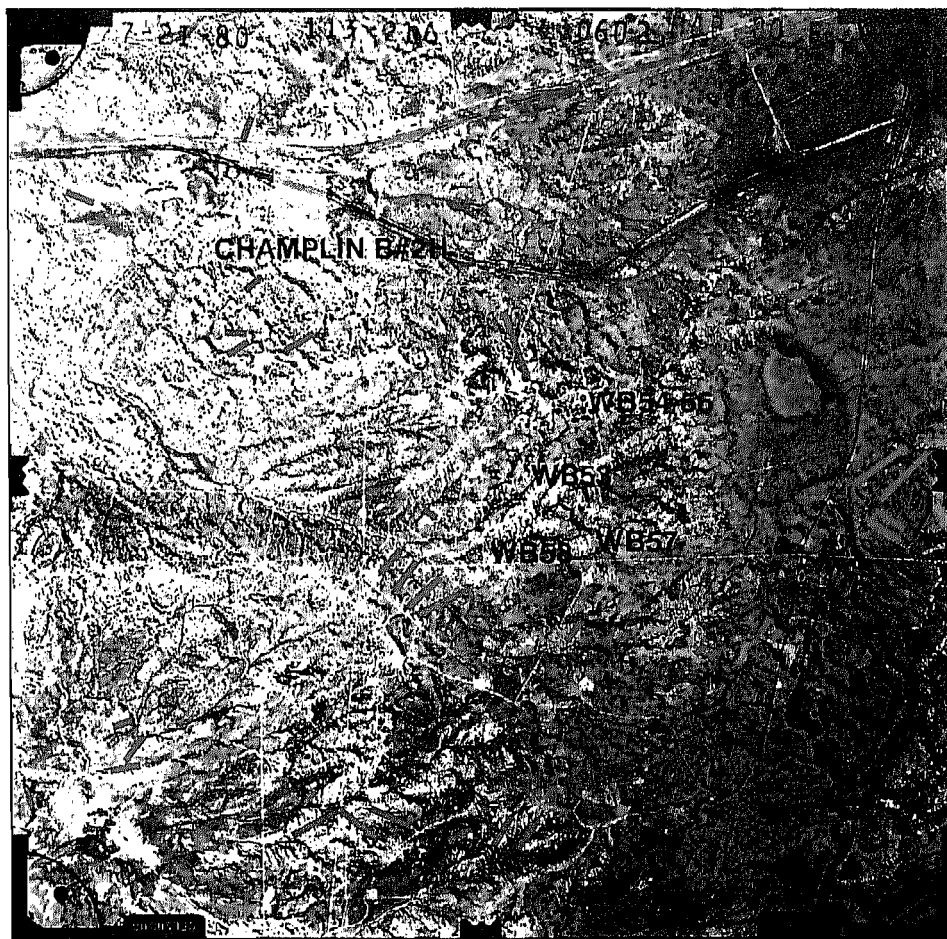


**Figure 2-3.** Wamsutter-Latham NHAP color-infrared aerial photograph. The Amoco Champlin 254B-2H horizontal well (yellow box) is located south of the interstate and railroad. Linear features (dark pink) and joint localities (WB53-58) also are shown. Four color-infrared aerial photographs are required to cover the area shown in Figure 2-5.

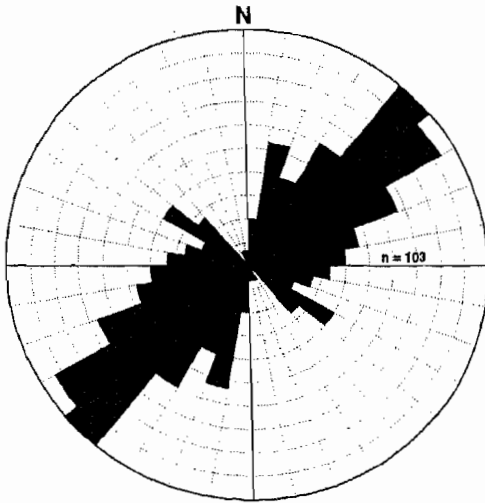


**Figure 2-4A.** Non-length-weighted rose diagram (10-degree increments) of linear features mapped using colorinfrared stereo aerial photographs of the Wamsutter-Latham area. The rose diagram shows a major trend of N40-60°E and minor trends of N10-20°E and N50-60°W.

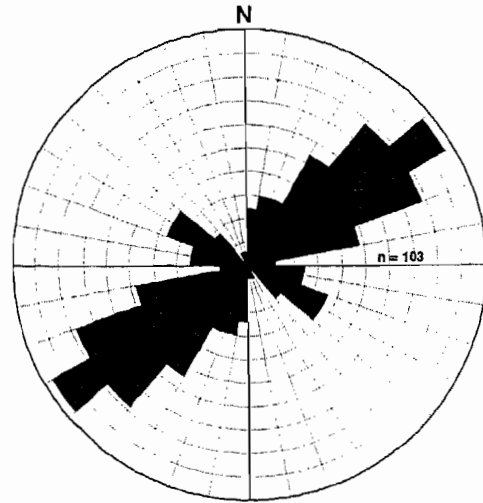


**Figure 2-4B.** Length-weighted rose diagram (10-degree increments) of linear features mapped using color-infrared stereo aerial photographs of the Wamsutter-Latham area. The rose diagram shows a N50-60°E major trend and a N50-70°W minor trend. Note that the rose changes when length-weighting of linear features is applied (compare Figures 2-4A and 2-4B).

photographs and joint data (Figure 2-4C). The rose diagrams of joint orientations from five localities (Figure 2-4C), non-lengthweighted linear features (Figure 2-4A), and subsurface fractures (Figure 2-4D) reveal a dominant east-northeast trend. However, a 20° counterclockwise shift is apparent between the N40-60°E major trend of linear features (Figure 2-4A) and N60-70°E trend of natural fractures in an Almond sandstone at approximately 10,000 ft depth (Figure 2-4D). East of Wamsutter, joints in outcrops of Tertiary bedrock within a 4mi<sup>2</sup> area show one major joint set, N61-84°E (see Chapter 4, this volume). Joints measured at N52°E were controlled by a lens of sandstone in a mixed-lithology outcrop of Tertiary sedimentary rocks.

Almost 1000 linear features were identified on panchromatic SPOT images over the same 306-km<sup>2</sup> (118-mi<sup>2</sup>) area east of Wamsutter (Figure 2-5). A rose diagram of non-length-weighted linear features (Fig-

ure 2-6A) shows three major directions: N10-20°W, N10-30°E, and N40-50°W. A length-weighted rose diagram of the same 1000 linear features (Figure 2-6B) shows similar major trends: N10-20°W, N20-40°E, and N40-50°W. The differences between the trends identified on the panchromatic SPOT images (Figure 2-6B) and on the color-infrared aerial photographs (Figure 2-4B) may be due to the following factors: (1) a far greater number of linear features identified on the SPOT image, (2) more nonstructural linear features identified on the SPOT image, (3) stereoscopic versus monoscopic viewing of the area, and (4) solar azimuth of the satellite image.

### **Red Desert Horizontal Well (Champlin 320 C-1A-H)**

A second comparison of surface and subsurface fractures in the Red Desert (Figure 2-7) indicated good correlation

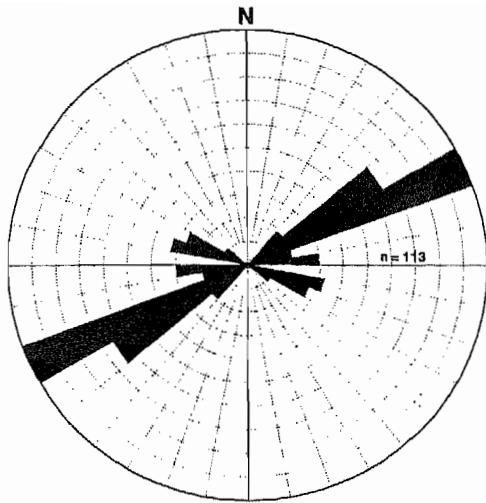


**Figure 2-4C.** Wamsutter-Latham joints (10-degree increments). The joint orientations from five localities (Figure 2-3) are plotted for comparison with non-length weighted linear features (Figure 2-4A) and subsurface fractures (Figure 2-4D).

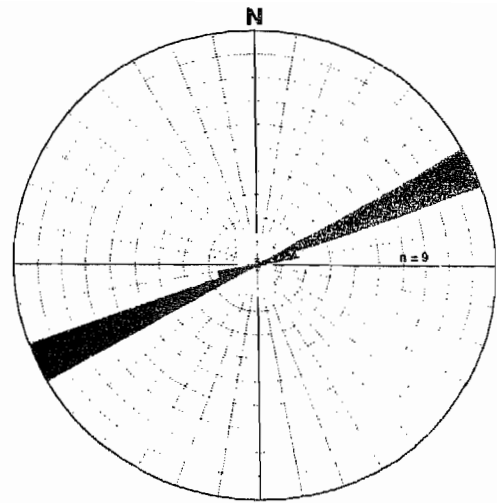


**Figure 2-4D.** Rose diagram of natural fractures in horizontal cores of the Champlin 254 Amoco B 2-H well. Modified from Hill (1995).

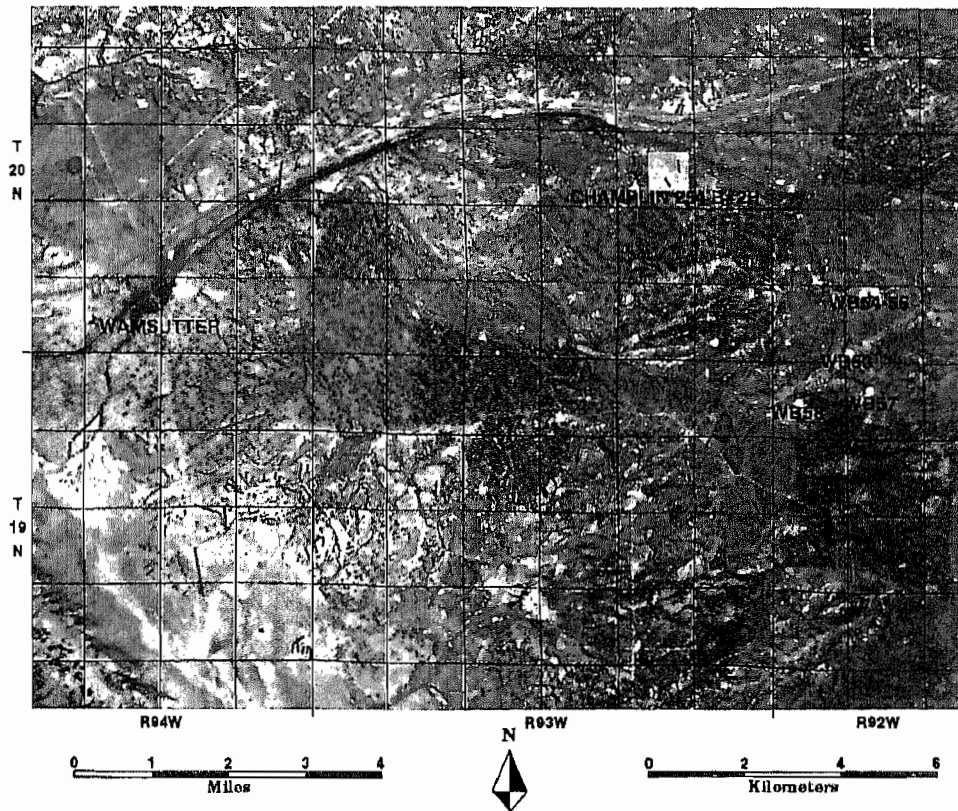


**Figure 2-5.** Linear features (dark pink) were mapped from panchromatic SPOT images of the Wamsutter-Latham area. A portion of this area showing Amoco Champlin 254B-2H (yellow box) and joint localities (WB53-58) is shown on the color infrared aerial photograph of the Wamsutter-Latham area (Figure 2-3). The township-range grid (navy blue) was generated from U.S. Geological Survey digital line graph files of the Public Land Survey System.

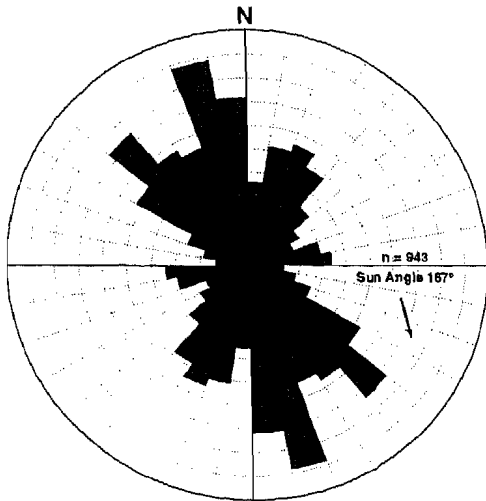


**Figure 2-6A.** Non-length-weighted rose diagram of linear features from panchromatic SPOT image of the Wamsutter-Latham area (10-degree increments). North-northwest, north-northeast, and north-northwest trends are dominant. North-northwest and north-northeast trends appear enhanced by the solar azimuth of the SPOT image.

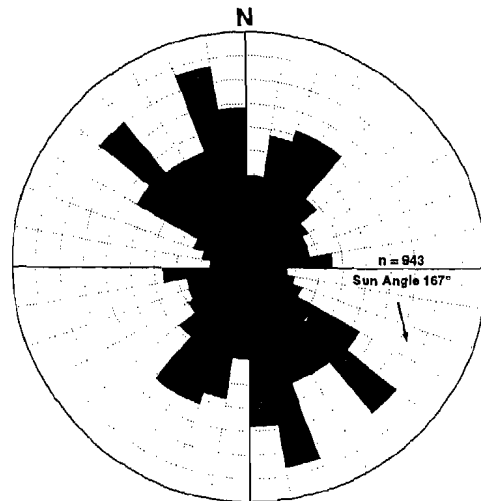


**Figure 2-6B.** Length-weighted rose diagram of linear features from a panchromatic SPOT image of the Wamsutter-Latham area (10-degree increments), showing three major trends: N10-20W, N40-50W, and N20-40E. Note that longer, northeast-trending linear features (N20-40E) become more dominant than shorter, north-northwest (N10-20W) linear features when length-weighting is applied to the data (compare Figures 2-6A,B).

between a dominant joint set, the structural photo-interpretation of linear features, and subsurface fractures. Rose diagrams of non-length-weighted linear features mapped from panchromatic SPOT images of the Red Desert (Figure 2-8A) show a dominant trend of N10-20°W and subordinate trends of N30-50°E, N70-80°E, and N50-60°W. In contrast, rose diagrams of length-weighted linear features (Figure 2-8B) show a dominant trend of N40-50°E and subordinate trends of N70-80°E, N10-20°W, and N50-60°W. During a reconnaissance study of jointed Tertiary rocks, one dominant joint set striking N73-90°E and a subordinate set striking N3-27°W were measured. A second, younger set of joints subparallel to the N73-90°E set was also noted. It is interesting that the best correspondence between SPOT linear features and joint sets is shown on the length-weighted rose diagram of SPOT linear features (Figure 2-8B). A plot of the orientation of joints measured in a 4-mi<sup>2</sup> of the horizontal well shows a major strike of

N80-90°E and a subordinate strike of N10-20°W (Figure 2-8C). Hill (1995) reported a nearly east-west strike of natural fractures (N87°E) from his study of the Champlin 320 C-1A-H horizontal core (Figure 2-8E). The non-length-weighted rose diagram of joints (Figure 2-8C) and the non-length-weighted rose diagram of natural fractures in the core (Figure 2-8E) show good correlation.

Structural photo-interpretation of NHAP color-infrared aerial photographs in the immediate vicinity of the Champlin 320 C-1A-H well showed a major east-northeast-trending linear feature (Figure 2-8D). Love and Christiansen (1985) map this same linear feature as a fault between Quaternary terraces. An assessment of faults within the Red Desert (Wyoming State Geological Survey, 1987) shows suspected active faults, inactive faults, and photo-lineaments with east-west, east-northeast, west-northwest, and northwest trends. Minor faults with strikes of N65°E

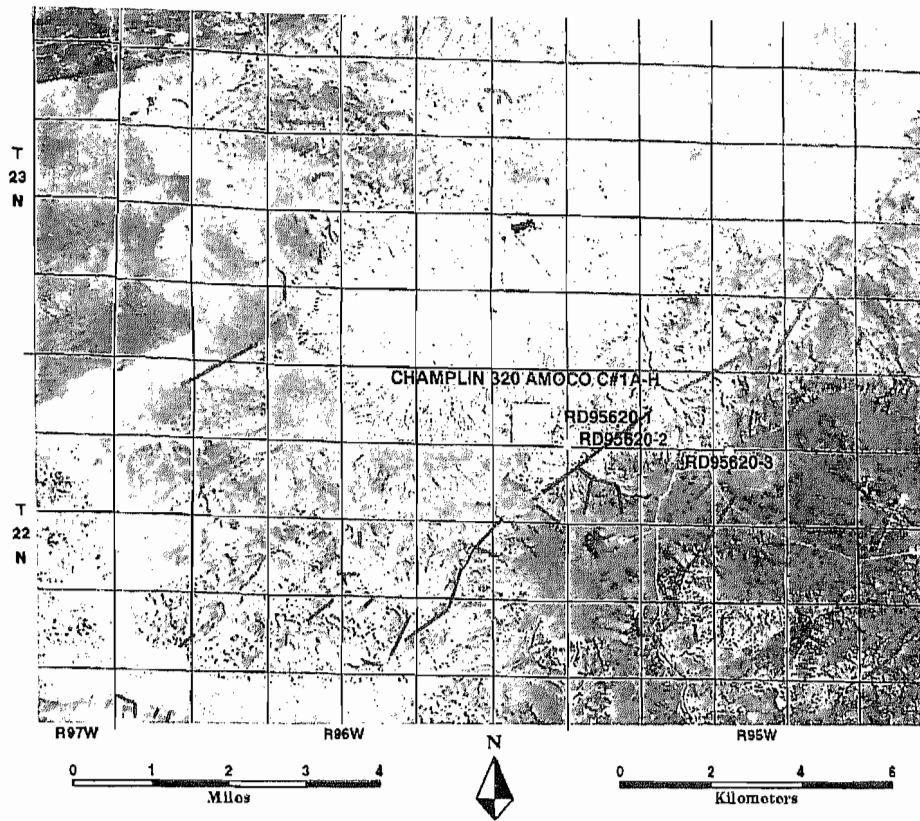


**Figure 2-7.** Linear features (dark pink) were mapped from panchromatic SPOT image of the Red Desert. Joint sets were measured at three stations (RD95620-1, RD95620-2, and RD95620-3) within a few miles of the Amoco Champlin 320C-1AH horizontal well (yellow box). The township-range grid (navy blue) was generated from U.S. Geological Survey digital line graph files of the Public Land Survey System.

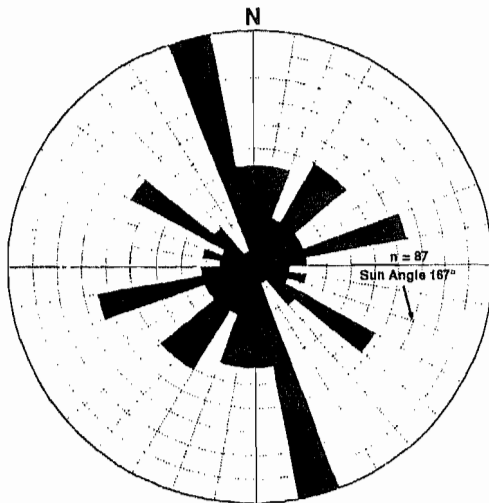


**Figure 2-8A.** Non-length-weighted rose diagram (10-degree increments) of linear features mapped near the Champlin 320 C-1A-H well from SPOT panchromatic images. N20-30W is the major trend when all linear features are weighted equally.

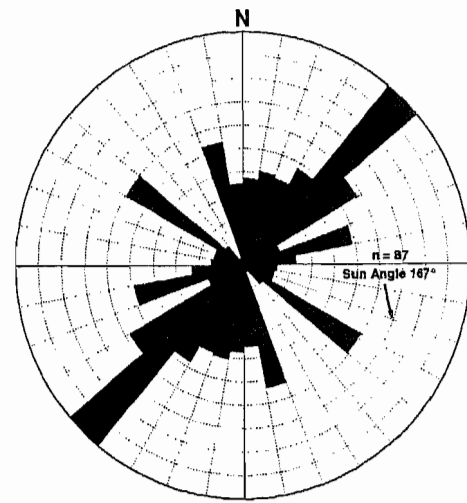


**Figure 2-8B.** Length-weighted rose diagram (10-degree increments) of linear features mapped near the Champlin 320 C-1A-H well from panchromatic SPOT images. Note the marked change in the rose when length-weighting is applied to linear features (see Figures 2-8A,B). N50-70E is the major trend when the longer east-northeast linear features are weighted more than shorter linear features.

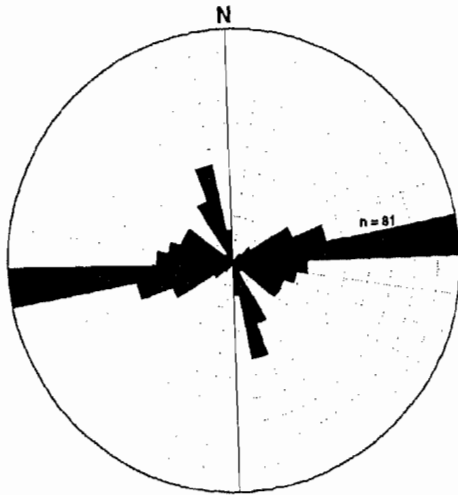


**Figure 2-8C.** Rose diagram of joints near the Champlin 320 C-1A-H well in the Red Desert (10-degree increments). The joint orientations from three localities (Figure 2-3) are plotted for comparison with non-length weighted linear features (Figure 2-8A), length-weighted linear features (Figure 2-8B), and subsurface fractures (Figure 2-8E).

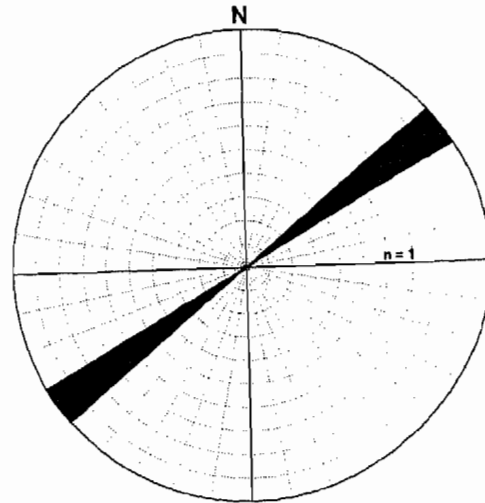


**Figure 2-8D.** Rose diagram (10-degree increments) of linear features identified by stereoscopic analysis of color infrared aerial photographs. This is the only linear feature with structural significance in the immediate vicinity of the Champlin 320 C-1A-H well. This linear feature is mapped by Love and Christiansen (1985) as a fault between Quaternary terraces.

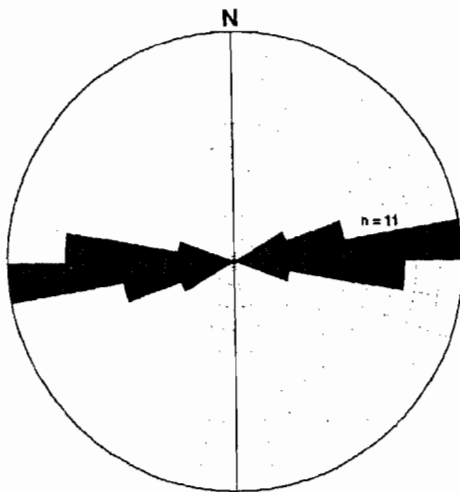


**Figure 2-8E.** Rose diagram (10-degree increments) of natural fractures measured in the horizontal core of the Champlin 320 C-1A-H well. The orientation of fractures in this core closely resembles that of the dominant joint set (Figure 2-8C) in the vicinity of the well. A dominant northeast (Figure 2-8B) to east-northeast trend (Figure 2-8D) is predicted by analysis of linear features on satellite images and color-infrared aerial photographs.

have been reported in the Great Divide Basin (Pipiringos, 1961; Masursky, 1962). However, subsurface studies of drill records from petroleum exploration have not revealed major northeast faults (Blackstone, 1973). The preliminary finding that dominant east-northeast joints are found at the surface and in the subsurface near the Red Desert (Champlin 320 C-1A-H) and Wamsutter (Champlin 254 Amoco B 2-H) horizontal wells suggests that this joint set is an important regional joint set (see Chapter 4, this volume). Being parallel or subparallel to previously mapped faults, its relationship to faulting, time of fault movement, type of movement, and regional stresses are important questions. It is possible that joints and faults may be different products of the same period of extension. In the eastern Uinta Basin of Utah, Verbeek and Grout (1993) document that a basinwide period of extension produced by both joints and faults.

## BASEMENT LINEAMENTS

Determining if any relationship exists between hydrocarbon production and regionally prominent lineaments (e.g., basement faults) is of primary importance. The concept that reactivated basement faults influence sedimentation, structure, and hydrocarbon production has been discussed by many researchers in the Rocky Mountain and Plains states (Thomas, 1971; Weimer, 1980; Marrs and Raines, 1984; Martinsen and Marrs, 1985; Shurr et al., 1991; Stone, 1995; Martinsen et al., 1995). Studies in the Powder River Basin of northeastern Wyoming have demonstrated the effect of major northeast-trending and smaller northwest-trending lineaments on sedimentation and petroleum production (Marrs and Raines, 1984; Martinsen and Marrs,

1985). In the eastern Powder River Basin, petroleum production has been correlated with northeast-trending linear features (Slack, 1981).

In the Greater Green River Basin, Thomas (1971) associated northeast-trending basement lineaments (Wamsutter and Bitter Creek lineaments) with the variable thickness of the Cretaceous Almond Formation, control of sedimentary facies, the development of intrabasinal folds, and a structural influence on oil and gas accumulation in the Table Rock and Patrick Draw fields (Figure 2-9). Martinsen et al. (Chapter 3, this volume) attribute patterns in Cretaceous Almond lithofacies and thickness to syndepositional movement along northeast-trending faults throughout the Washakie and Great Divide basins.

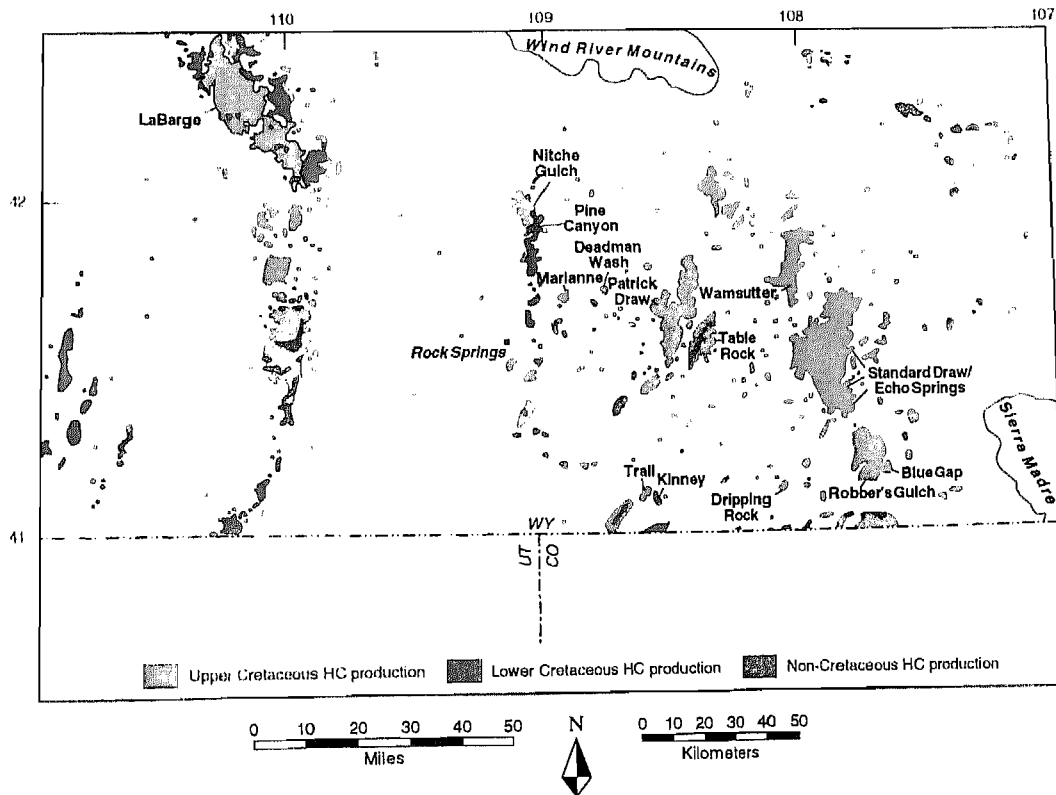


Figure 2-9. Map of oil and gas fields shown in Figures 2-10 to 2-12.

In the Laramie Basin of southeastern Wyoming, Stone (1995) discusses the complex structure and kinematics of the Quealy wrench duplex. Stone's discussion of Permian and Laramide movement along the Precambrian Cheyenne Belt is most relevant to the Precambrian shear zones in the southeastern Washakie Basin.

During our basinwide analysis of regional fractures, the surface lineaments on the SPOT mosaic of the east-central Greater Green River Basin were tested for expression in the subsurface. Surface lineaments were compared with gravity gradients (Figure 2-10), magnetic gradients (Figure 2-11), and oil and gas fields (Figure 2-12). Many surface lineaments, gravity gradients, and magnetic gradients bound or traverse oil and gas fields (see Figures 2-10 to 2-12). A few east-northeast- and northeast-trending surface lineaments, gravity gradients, and magnetic gradients are associated with production of hydrocarbons in the basin from fields classified, as discussed below, as "largest" and "significant" (Figure 2-12).

## BASEMENT LINEAMENTS AND PRODUCTION

Iverson (Chapter 5, this volume) used oil and gas production data to classify oil and gas fields within the Greater Green River Basin into four categories. Cumulative production of >500 Bscfe (>\$500 million) constitutes a *largest* field; 50 to 500 Bscfe (\$50 to 500 million), a *significant* field; 5 to 50 Bscfe (\$5 to 50 million), a *small* field; and <5 Bscfe (<\$5 million), a *smallest* field. The present chapter addresses those fields in the east-central GGRB located between 41 and 42° north latitude and 107 to 109° west longitude.

Figure 2-12 shows the spatial relationship between the regional lineaments and the hydrocarbon accumulations. There is an obvious relationship between the distribution of hydrocarbon accumulations in fields with greater than 5 Bscfe (\$5 million) cumulative production and the most

prominent regional lineaments. For example, most of the accumulations in these fields are either cut or terminated by the lineaments (Figure 2-12). Conversely, few of the smallest fields (< 5 Bscfe) are associated with mapped regional lineaments (Figure 2-12).

A good illustration of this relationship is the hydrocarbon accumulation at the Standard Draw - Echo Springs field (Figure 2-12). One lineament forms the northernmost limit of production in this field, whereas a second parallel subsurface lineament cuts through a saddle in the isopach map of the Almond bar sandstone. This saddle coincides with some of the most productive wells in the field. The coincidence of thinning of the bar sand and the position of the geophysical lineament suggests that basement faults were reactivated during deposition of the bar sand.

An east-northeast-trending surface lineament and geophysical gradients (both gravity and magnetics) also coincide with the southern terminus of this field. The fact that some hydrocarbon accumulations are bounded by the lineaments further supports the hypothesis that a significant cause-and-effect relationship exists between the regional lineaments and the more significant hydrocarbon accumulations in the Washakie Basin (Chapter 5, this volume).

### Largest Fields: >500 Bscfe (>\$500 million)

Largest fields, such as Table Rock and Brady, are described as structural and stratigraphic traps (Wyoming Geological Association, 1979). Other large fields, such as Patrick Draw and Arch, are primarily stratigraphic traps. However, hydrocarbon production within the North Patrick Draw field is abruptly terminated by a northeast trend (Wyoming Geological Association, 1979). Reactivation of basement faults

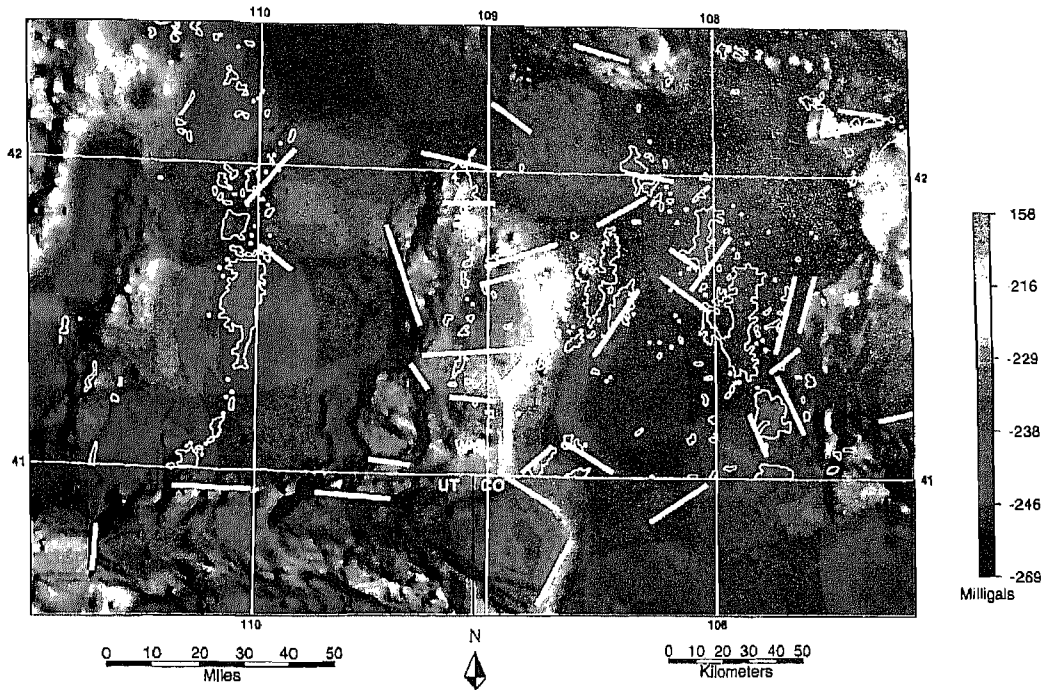


**Figure 2-10.** Plot of Bouguer gravity (milligals for the GGRB; modified from Bankey and Kulik, 1989). Orange, red, and yellow colors show gravity highs such as the Rock Springs Uplift (center), the Uinta Mountains (bottom left), the Sierra Madre (bottom right), and the southeastern Wind River range (top center). Green, blue, and blue-violet colors show gravity lows such as the Washakie Basin (bottom right, north of Wyoming-Colorado border), northern Green River Basin (top center), and the Great Divide Basin (top right). Many steep gravity gradients (thick white lines) bound oil and gas fields.

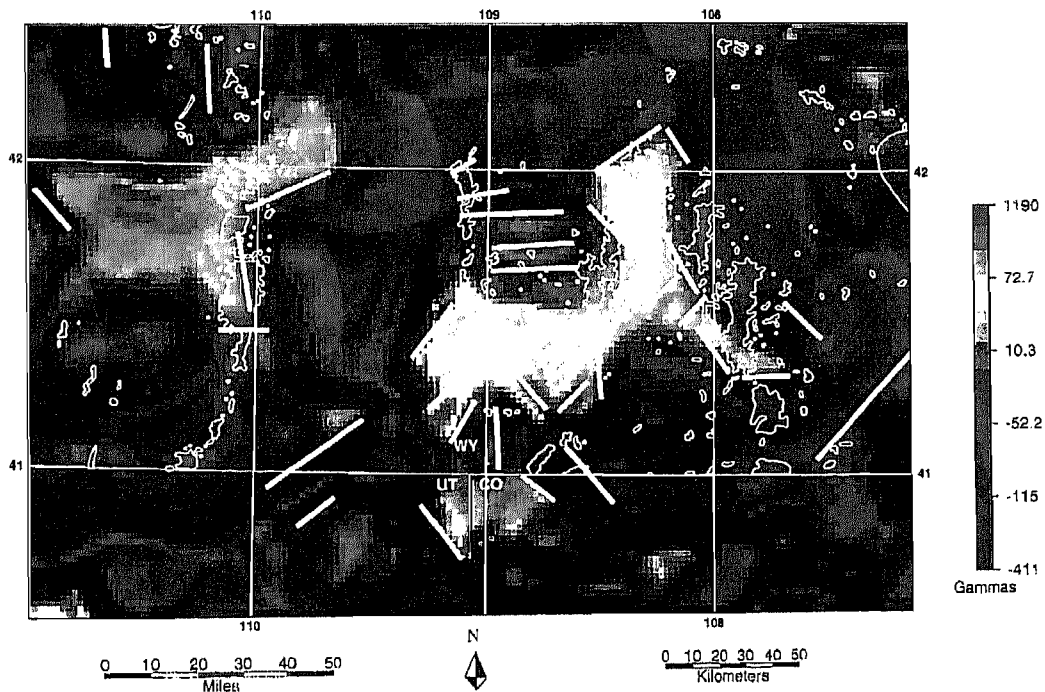


**Figure 2-11.** Plot of magnetic intensity for the GGRB. The area depicted is the same as in Figures 2-2 and 2-9 to 2-11. Magnetic data (2-kilometer grid) from the National Geophysical Data Center was imported into a commercial image processing program. The magnetic data for Wyoming were projected from an Albers projection into a Lambert conic conformal projection. The magnetic data were smoothed with a  $3 \times 3$  (pixels) average filter, and the histogram was equalized. Warm colors (red, orange, yellow) represent higher values of magnetic intensity (gammas).

may have affected the limits of sedimentary facies or the thickness of the Patrick Draw - Arch units, whereas reactivation of basement faults at the Table Rock and Brady fields caused intrabasinal folding and, possibly, faulting of strata. Recently completed three-dimensional seismic surveys support this concept of movement along northeast basement faults for the Table Rock and Brady fields (Russell and Stone, 1995).

The Table Rock oil and gas field (a structural and stratigraphic trap) is associated with east-northeast and northeast surface, gravity, and magnetic lineaments (Figures 2-10 to 2-12). Dickinson (1992) mentions a basement-related fault that extends at least to Cretaceous-age rocks

and controls the structure on the west side of the Table Rock Field. Dickinson's (1992) structure contour map of the Frontier Formation and isopach values of greater than 8% porosity show a prominent northeast trend, similar to the northeast-trending gravity and magnetic gradients (Figures 2-10 and 2-11).

The Brady field (a structural trap), which produces from several formations, also appears to be affected by reactivation of faults along northeast-trending basement lineaments. The Brady field produces from numerous hydrocarbon-bearing intervals, Paleozoic to Late Cretaceous. In the Paleozoic rocks, a northeast-trending basement lineaments. The Brady field produces from

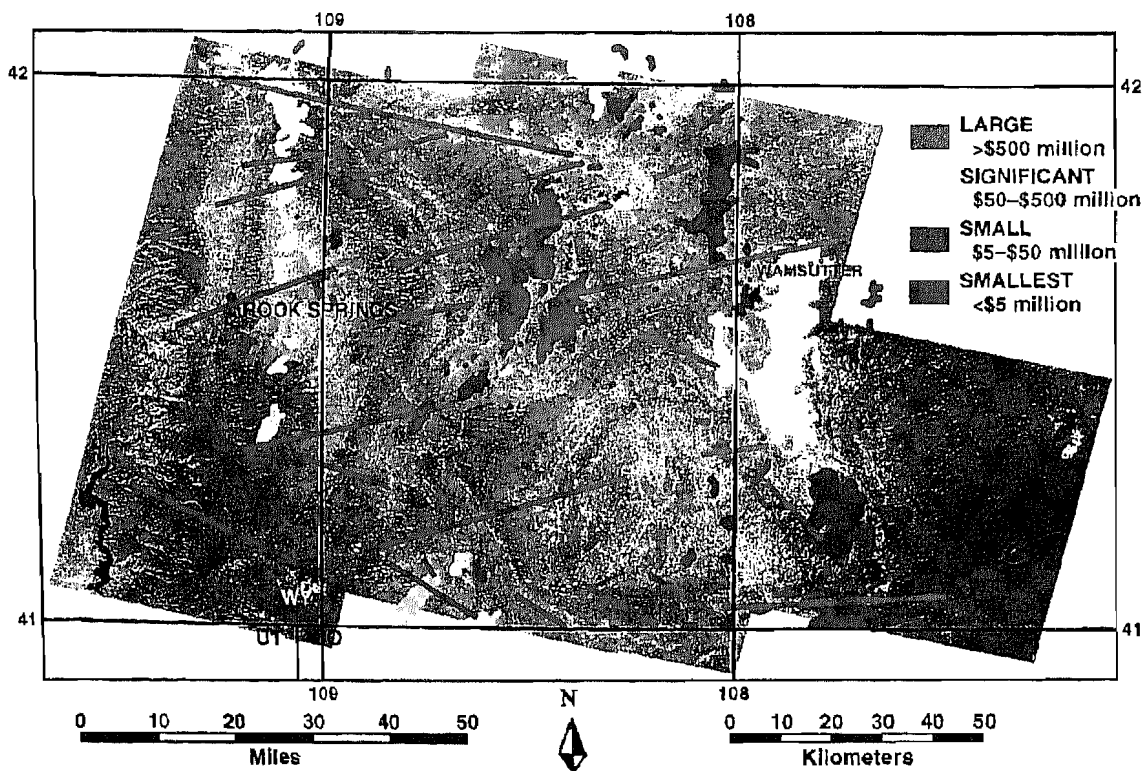


**Figure 2-12.** SPOT mosaic of the east-central GGRB showing oil and gas fields (red, yellow, green, and blue) and surface lineaments (solid pink). The dotted pink line, suparallel to solid pink line near Wamsutter, is associated with a gravity gradient and a saddle in the isopach map of the Almond bar sandstone. Oil and gas fields are color-coded according to oil and gas production: red for *largest* producers; yellow for *significant* producers, green for *small* producers; and blue for *smallest* producers, which are not economically viable. Compare this figure with Figures 2-10 and 2-11 to see the relationship of the surface lineaments to gravity and magnetic gradients. On this two-dimensional plot, lineaments cut across or bound oil and gas fields. The *largest* and *significant* fields are associated with east-northeast- and northeast-trending surface, gravity, and magnetic lineaments.

numerous hydrocarbon-bearing intervals, Paleozoic to Late Cretaceous. In the Paleozoic rocks, a northeast-trending fault is a significant element in the hydrocarbon trap, but as this fault is traced upsection into the Cretaceous rocks, it evolves into a drape fold. The crest of the drape fold is also an important element in forming a trap for hydrocarbon accumulation. In each case, the trace of the fault and the crest of the fold are parallel to and part of the regional lineament system in the Washakie Basin.

### **Significant Fields: 50-500 Bscfe (\$50-500 million)**

Stratigraphic and structural plays in significant oil and gas fields such as Baxter Basin, Echo Springs, Standard Draw, Nitchie Gulch, Playa, and Desert Springs probably are related to the reactivation of northeast- and east-northeast-trending basement faults. As already discussed, reactivation of basement faults affects the limits of porous sands in primarily stratigraphic plays within the Echo Springs - Standard Draw and Desert Springs fields. Movement along basement faults may also cause intrabasinal folding and faulting associated with other significant producers of oil and gas (Baxter Basin, Nitchie Gulch, and Playa).

The northern boundary of the Echo Springs field is terminated by east-northeast- and northeast-trending surface lineaments, gravity gradients, and magnetic gradients (Figures 2-9 to 2-12). Iverson (Chapter 5, this volume) further documents the association of the northern boundary of gas-condensate production at Echo Springs field with an east-northeast trending lineament. On its southern boundary, the Standard Draw field is bounded by an east-northeast-trending gravity gradient, magnetic gradient, and surface lineament. On its western edge, the Standard Draw field is bounded by a

northwest-trending magnetic gradient, gravity gradient, and surface lineament. Within the Desert Springs field, changes in the limits of porous Lewis E' Sand and Almond B<sub>1</sub> Sand suggest reactivation of northeast- or east-northeast-trending basement faults. The Nitchie Gulch oil and gas fields on the northernmost Rock Springs Uplift are cut by nearly east-west-, east-northeast-, and northeast-trending surface, gravity, and magnetic lineaments (Figures 2-9 to 2-12). In the Nitchie Gulch field, stratigraphic plays within the Frontier and Dakota formations are traversed by northeast-trending faults (Wyoming Geological Association, 1992). At the Nitchie Gulch field, an impermeable, clay-filled boundary within the Frontier Formation shows an east-northeast trend (Wyoming Geological Association, 1979). Reactivation of northeast-trending basement faults with associated intrabasinal folding and faulting may explain production of gas from multiple horizons within the Baxter Basin fields (North, Middle, and South). Many northeast-trending faults cut across the producing anticlinal structures at Middle Baxter Basin and South Baxter Basin (Wyoming Geological Association, 1979). The Cretaceous Lewis play in the Playa field also may be associated with intrabasinal folding near a northeast- or east-northeast-trending basement fault.

### **Small Fields: 5-50 Bscfe (\$5-50 million)**

The reactivation of northeast-trending basement faults and associated facies change, variation in thickness of sediments, folding, and faulting affect several small fields. In the Red Desert of south-central Wyoming, Iverson (Chapter 5, this volume) has found that the Great Divide gas field apparently is truncated by a northeast-trending linear feature. At Ten Mile Draw, a northeast-trending normal fault is associated with a limit of the gas-producing Lewis sand. At the Joyce Creek field, the northeast trend of the faulted anticlinal nose and the anticline may

be associated with the reactivation of north-east-trending basement faults. The smallest fields (<5 Bscfe) in the Washakie Basin do not show correlation between regional lineaments and the position of hydrocarbon accumulations (Figure 2-12).

## SUMMARY

East-northeast-trending and north-east-trending basement-related lineaments affect the production of hydrocarbons in the east-central Greater Green River Basin by influencing sedimentary thickness, facies, porosity, and structure. Surface lineaments determined from satellite images correspond to previously mapped faults as well as to geophysical gradients, demonstrating that many surface lineaments are structurally significant. Many lineaments and geophysical gradients bound or traverse oil and gas fields. Within largest and significant oil and gas fields, producing trends are terminated by east-northeast- and north-west-trending lineaments. Digital databases aided the graphical display of hydrocarbon production with lineaments and geophysical gradients.

Dominant east-northeast regional fractures have been measured at the surface and in the subsurface in the vicinity of two horizontal wells (Champlin 254 Amoco B 2-H and Champlin 320 C-1A-H). These fractures are parallel or subparallel to previously mapped east-northeast faults, suggesting that these fractures were formed and faults were reactivated during a similar period of extension.

Future work in the Greater Green River Basin should address the timing of movement on basement faults. Demonstration of east-northeast or northeast trends in isopach maps of Paleozoic and Mesozoic rocks will show that recurrent movement along basement faults have affected sediments other than the Cretaceous Almond Formation. Continued field

work on joints will further test the hypothesis that dominant east-northeast joints formed during a period of middle Tertiary extension. Continued application of our techniques to other areas will extend our analyses to the entire Greater Green River Basin.

## ACKNOWLEDGMENTS

The authors appreciate the support of the Gas Research Institute (Contract No. 5091-221-2146) and the NSF-EPSCoR-ADP Fossil Energy program (Contract No. EHR-910-8774). Public domain digital data from the Wyoming Geological Survey (oil and gas fields) and the U.S. Geological Survey (Bouguer gravity and magnetics) confirmed the geologic significance of surface lineaments. We are grateful to Allory Deiss for his assistance with diagrams. Also, we wish to thank the editors and reviewers of this manuscript for their suggestions.

## Chapter 3

# Stratigraphy And Lithofacies Of The Almond Formation, Washakie And Great Divide Basins

*Randi Martinsen, Glen Christiansen, and Mark Olson*

### ABSTRACT

The Almond Formation in the Washakie and Great Divide basins varies from 250 to more than 500 ft in thickness. Both the upper contact of the Almond Formation with the Lewis Shale and the lower contact with the Ericson Sandstone rise stratigraphically to the west. Variations in formation thickness and in lithofacies are interpreted as being due, at least in part, to syndepositional movements along basement block faults.

Commonly, the Almond is informally divided into the upper and main Almond. The upper Almond consists dominantly of shoreface sandstone tongues that interfinger with the Lewis, and the main Almond consists of interbedded marine to nonmarine sandstones, siltstones, shales, and coals. In the eastern parts of the basins, the Almond can be subdivided into three genetic units: (1) an upper unit, Unit 1, including a highly productive barrier-bar facies and a coal-bearing facies deposited dominantly in back-barrier environments; a middle unit, Unit 2, consisting of several dominantly marine, coarsening upward shale-to-sandstone sequences that contain little to no coal; and a lower, fluvially dominated, coal-bearing unit, Unit 3. The upper unit is transgressive in origin and is generally correlative with the lower Almond of the Rock Springs Uplift. The middle unit is bounded above and below by unconformities, pinches out to the west, and appears to correlate with a marine shale in the lowermost Almond on the Rawlins Uplift. The lowermost unit may correlate to the east with the Pine Ridge Sandstone, but

what happens to it to the west is unclear. The presence of numerous coals in the main Almond, as well as reservoir-type sandstones, some of which are depositionally similar to upper Almond sands, suggests that the main Almond may have significant gas potential.

### INTRODUCTION

The Almond Formation in the area of the Rock Springs Uplift and western Wamsutter Arch has been widely studied (Jacka, 1965; Weimer, 1965, 1966; Weimer et al., 1985; McCubbin and Brady, 1969; Meyers, 1977; Flores, 1978; Van Horn, 1979; Roehler, 1988, 1990; Szpakiewicz et al., 1991; Jackson and Rawn-Schatzinger 1993). Little work has been done on the Almond as it occurs farther east, even though significant gas production has been established there in recent years (Figures 3-1 and 3-2). The purpose of this chapter is to compare and contrast the Almond Formation of the Rock Springs Uplift with the Almond Formation in the area of the Washakie and Great Divide basins and eastern Wamsutter Arch (Figure 3-2).

### REGIONAL STRATIGRAPHY

The Almond is well exposed along the flanks of the Rock Springs Uplift, and extends eastward in the subsurface of the Great Divide and Washakie basins. It also crops out along the eastern margins of these basins, and to the east along the

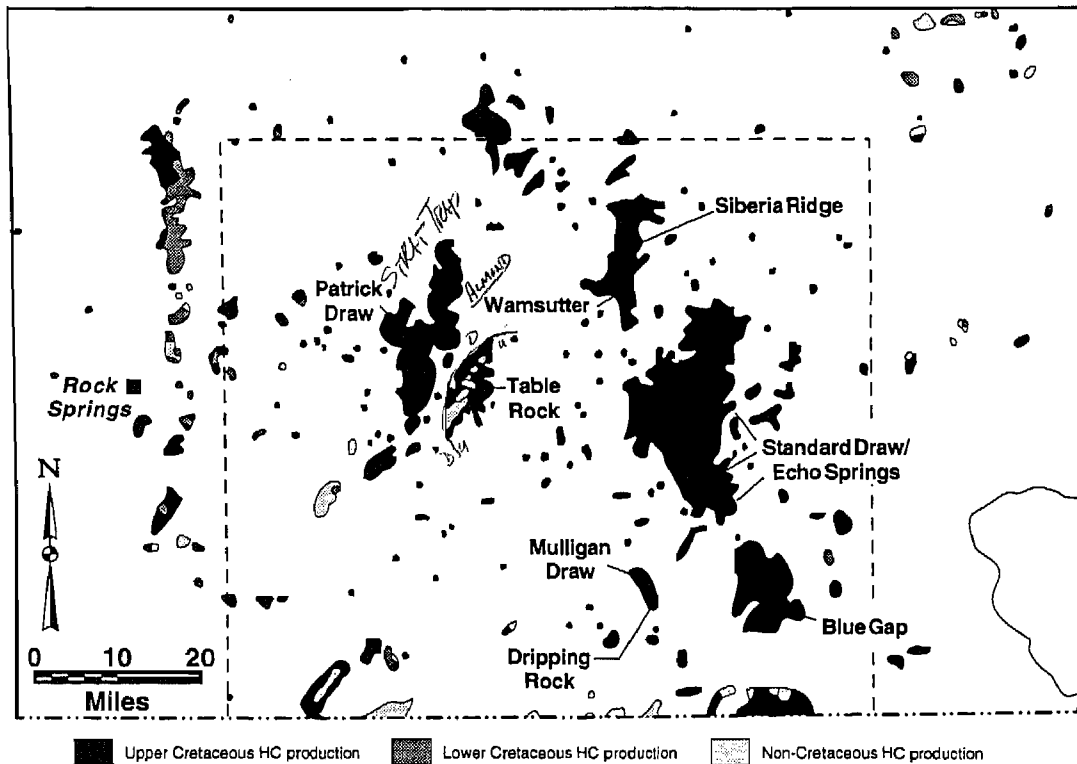


**Figure 3-1.** Oil and gas map of the eastern Greater Green River Basin area. Fields with significant Almond production are named. Outlined area is area of Figure 3-5.

western margins of the Hanna, Carbon, and Laramie basins. The Almond is believed to be absent east of the Laramie Basin (Gill et al., 1970), where it has changed facies and is designated Lewis Shale. The Almond Formation cannot be distinguished from overlying and underlying strata very far west of the Rock Springs Uplift (Figure 3-3).

The Almond is the youngest formation in the Mesaverde Group of south-central Wyoming; it is overlain by, and interfingers with, the marine Lewis Shale. Where it can be distinguished, the Almond-Lewis contact generally is sharp, is easily recognizable in outcrop and on well logs, and consistently represents a transgressive surface of erosion (TSE). Although numerous small transgressive-regressive cycles characterize the Almond, overall indications of marine conditions increase upsection, which suggests that the Almond is dominantly transgressive in origin (Meyers, 1977; Flores, 1978; Van Horn, 1979; Roehler, 1990).

The top of the Almond rises intermittently from east to west (Van Wagonner et al. 1990; see Figure 3-4), and can be characterized as a series of back-stepping parasequence sets. Figure 3-5, an isopachous map of an interval in the lower Lewis Shale displays the rise in plain view. The top of the mapped interval is the base of a regionally recognizable zone within the lower Lewis, herein denoted the "hot shale." The "hot shale" is characterized by very high gamma-ray response that is typically associated with a high resistivity response, and by downlap of units above it; it probably represents a condensed zone formed during a period of rapid transgression. The base of the mapped interval is the top of the Almond. The steep rise in the stratigraphic elevation of the top of the Almond corresponds to a zone of abrupt thinning near the middle of the map ( $\approx$  R96W).

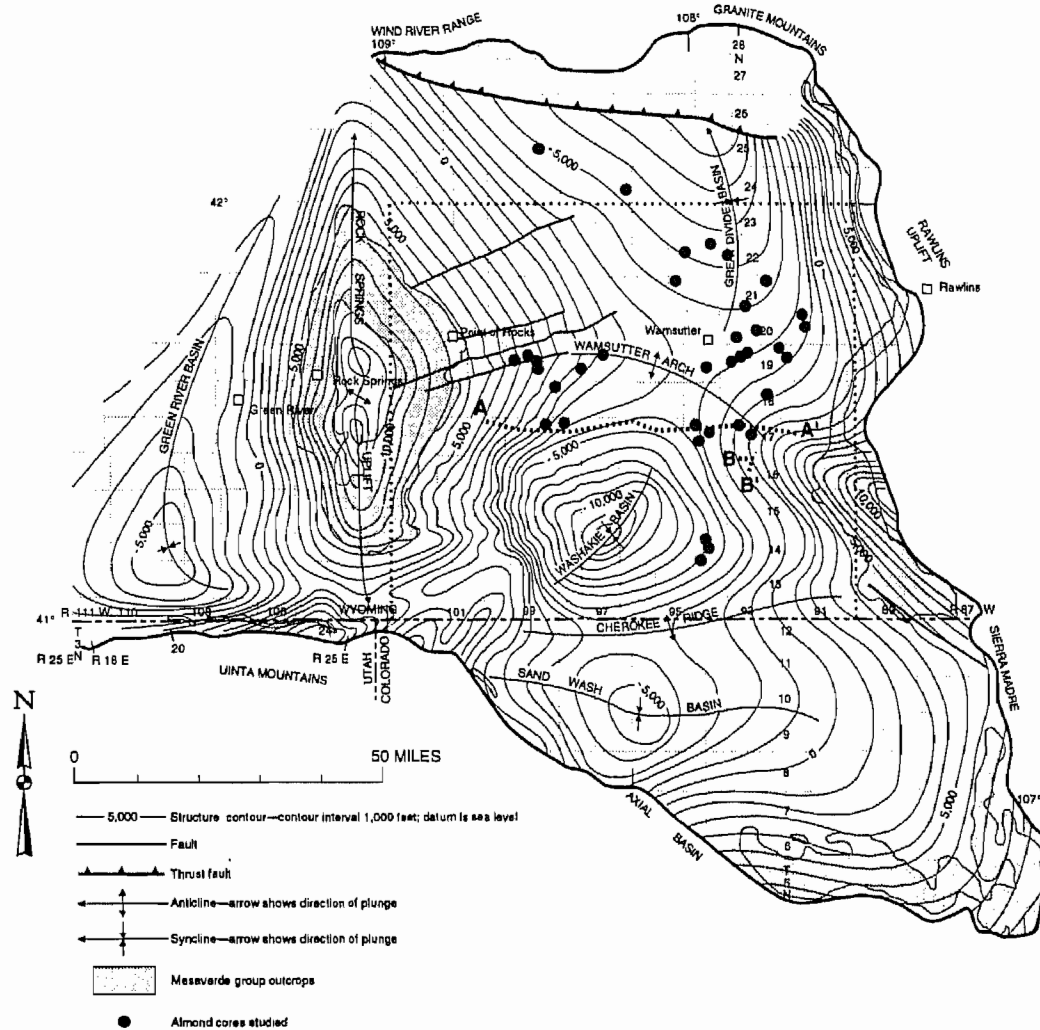


**Figure 3-2.** Structure contour map of the GRB. Mesaverde Group outcrops are superimposed on structure contours at the top of the Ericson and Pine Ridge Sandstones. Contours are approximately located, and are projected in places where the datum is eroded. Solid circles are the locations of cores examined; outlined area is area of Figure 3-5. Also shown are the locations of cross sections A-A' (Plate 1) and B-B' (Plate 1). Compiled from Roehler (1990, his Figures 1 and 2).

The Almond is underlain by the Ericson Formation in the area of the Rock Springs Uplift and by the Pine Ridge Sandstone in the area of the Rawlins Uplift (Figure 3-3). Generally, the Almond-Ericson contact is easily and consistently picked both in outcrop and in well logs in the western Washakie Basin. Farther to the east, however, as indicated from Petroleum Information historical data files, the top of the Ericson has been picked at many different stratigraphic intervals. In the present study, the Al-

mond-Ericson contact is picked where the section changes upward from a section of thick, amalgamated sand to a section of interbedded shale, coal, and sandstone (cross sections A-A' and B-B', Plate 1). Typically, the contact is sharp. Because sands in the lower Almond are commonly laterally discontinuous, are associated with coals, and have fining-upward profiles on logs, they are usually easily distinguished from upper Ericson sands, which have very blocky log profiles. Locally, thick amalgamated sands do

occur in the lower Almond, however, and give the appearance of interfingering between the two formations, making the Almond-Ericson contact difficult to pick accurately in these areas.

The Almond-Ericson contact rises from east to west; the rise is similar to the rise of the Lewis-Almond contact, and is often abrupt. The most abrupt rise in the top of the Ericson (>100 ft) is observed in the vicinity of R96W, which is just east of where the most abrupt rise in the top of the Almond occurs (near well 4, Figure 3-4). Abrupt changes in the elevation of the

Almond-Ericson contact between closely spaced wells (~1 mi spacing) are observed from north to south. It is unknown whether these changes are solely the result of facies change, or the contact was elevated and eroded along fault blocks progressively uplifted toward the Rock Springs Uplift.

On the Rock Springs Uplift, however, Van Horn (1979) interpreted the contact to be conformable due to interfingering between lower Almond- and Ericson-type lithologies. Paleocurrent directions in the lowermost Almond and Ericson on the uplift also both indicate south to southeast flow

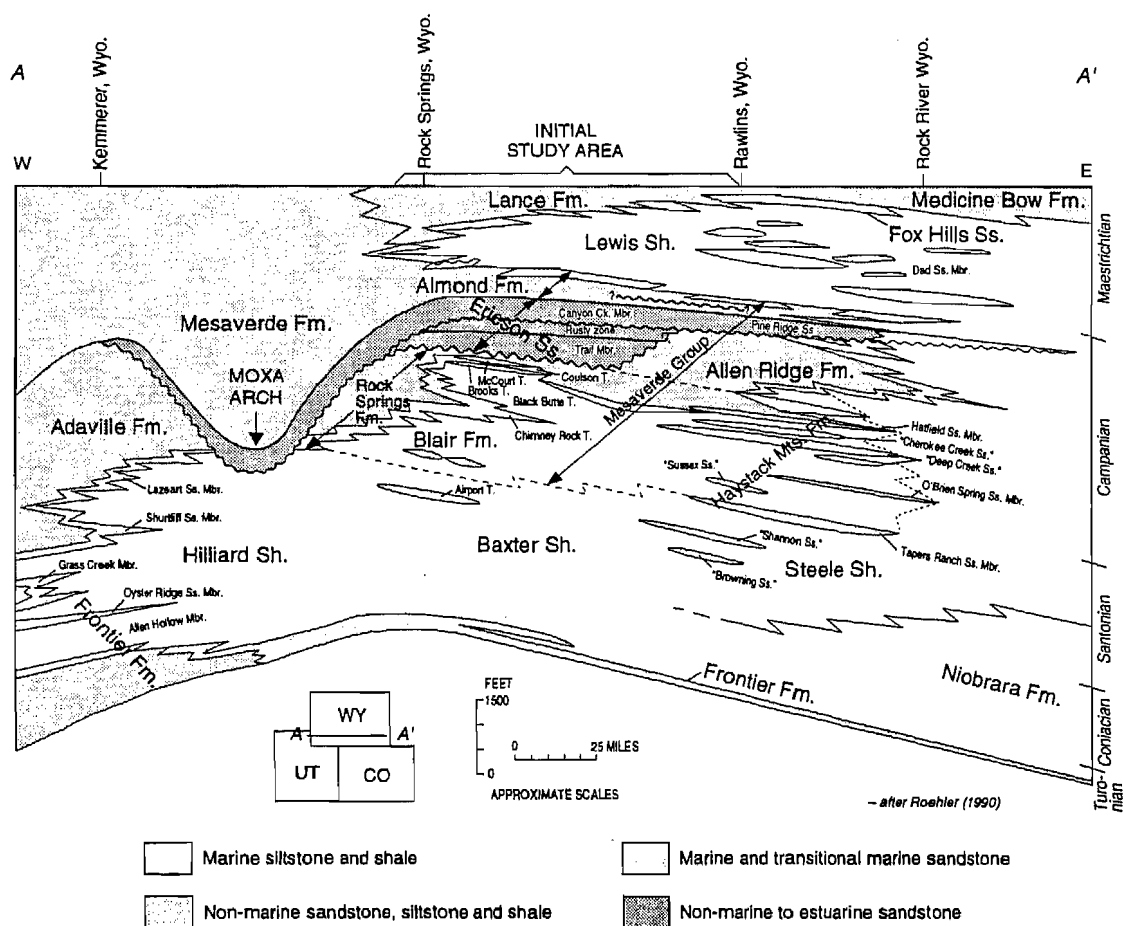


**Figure 3-3.** Diagrammatic cross section showing restored Upper Cretaceous rocks across northern Utah and southern Wyoming. Rocks of continental origin are shaded; alluvial-plain and marine-shoreline, shelf, slope, and basin sandstone and siltstone units are shown by dot pattern; marine shale and limestone are unpatterned. The location of subaerially-formed unconformities is indicated by the squiggly line. Modified from Roehler (1990).

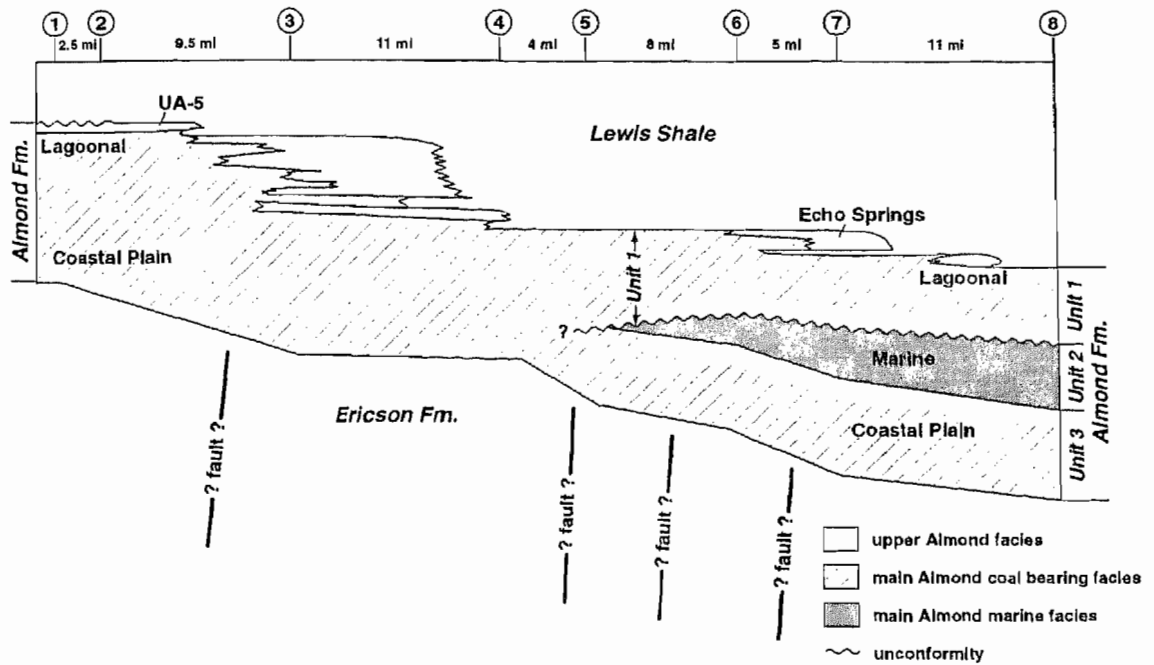


Figure 3-4. Schematic representation of well-log cross section constructed across T17N (Plate 1). Cross section is hung on the "hot shale" zone of the lower Lewis Shale. Circled numbers refer to locations of wells in Plate 1.

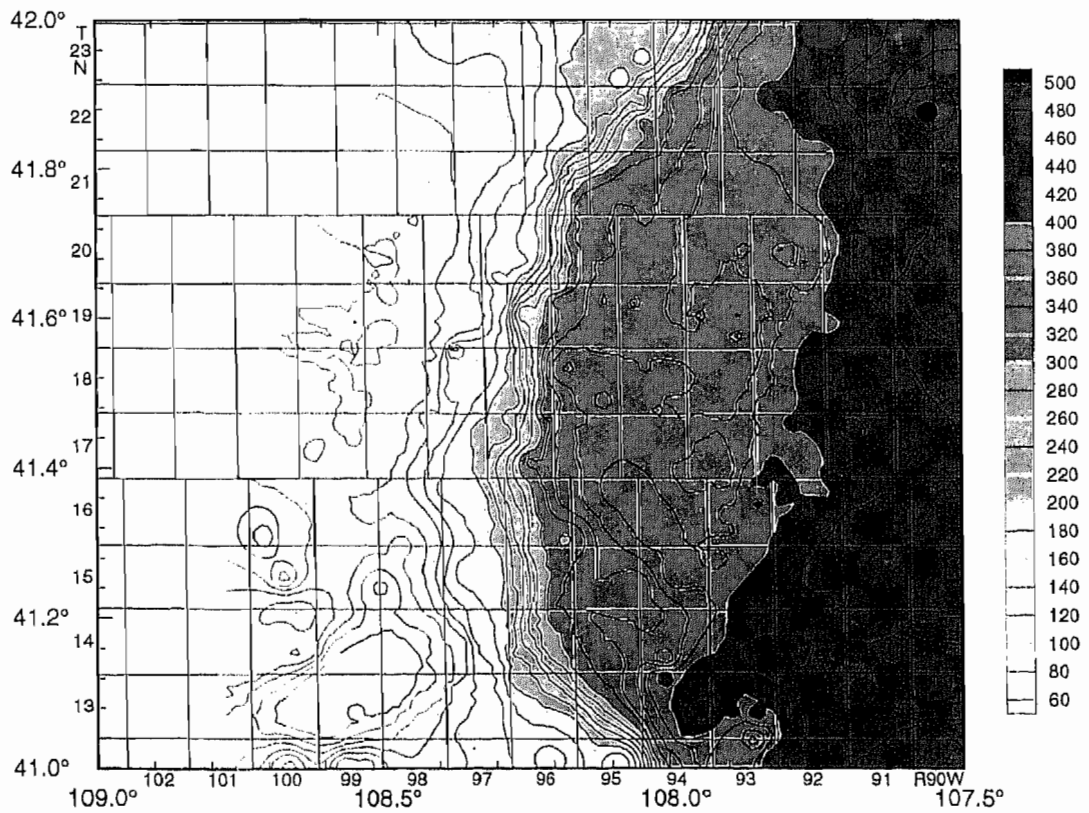


Figure 3-5. Isopachous map of the interval in the Lewis that is bounded by the base of the "hot shale" and below by the top of the Almond Formation. Map roughly covers T12-23N and R90-102W; outline of map area is shown in Figure 1.

(Meyers, 1977; Van Horn, 1979; Sherman, 1983), which supports the concept of a conformable contact. Recent studies indicate that the Ericson contains evidence of some marine influence, including *Ophiomorpha* and possible *Asterosoma* trace fossils as well as bidirectional cross-bed sets (Martinsen, 1994), whereas the basal Almond section, where it has been studied, is continental in origin and lacks evidence of marine influence (Meyers, 1977; Van Horn, 1979). The presence of marine indicators in the Ericson complicates the simple model of a facies change from upstream alluvial (Ericson) to coastal plain (lower Almond) sedimentation.

### STRATIGRAPHY AND DEPOSITIONAL ENVIRONMENTS OF THE ALMOND IN THE ROCK SPRINGS UPLIFT AREA

Many workers (Hale, 1950; Lewis, 1961; Jacka, 1965; Flores, 1978; Van Horn, 1979; Roehler, 1990) divide the

Almond Formation in the Rock Springs Uplift area into two mappable intervals: an upper interval consisting dominantly of sandstones of marine to brackish water origin (barrier-beach, tidal inlet, tidal delta, and upper, middle, and lower shoreface deposits), and a lower interval consisting of interbedded coals, shales, siltstones, and sandstones of continental and brackish water origin (fluvial channel, splay, overbank, swamp, fresh and salt water marsh, lagoon, tidal flat, and tidal channel deposits). Recognition of this division has informally established two Almond members, upper and lower, in this area. The contact between the two members is unconformable (Figure 3-6; Van Horn, 1979).

In this area, the lower Almond contains a basal interval of overall continental sedimentation (Meyers, 1977; Van Horn, 1979). That is, it consists mainly of fluvial-related deposits, including small, lenticular channel sandstones; thin, finer-grained levee, overbank, and floodplain

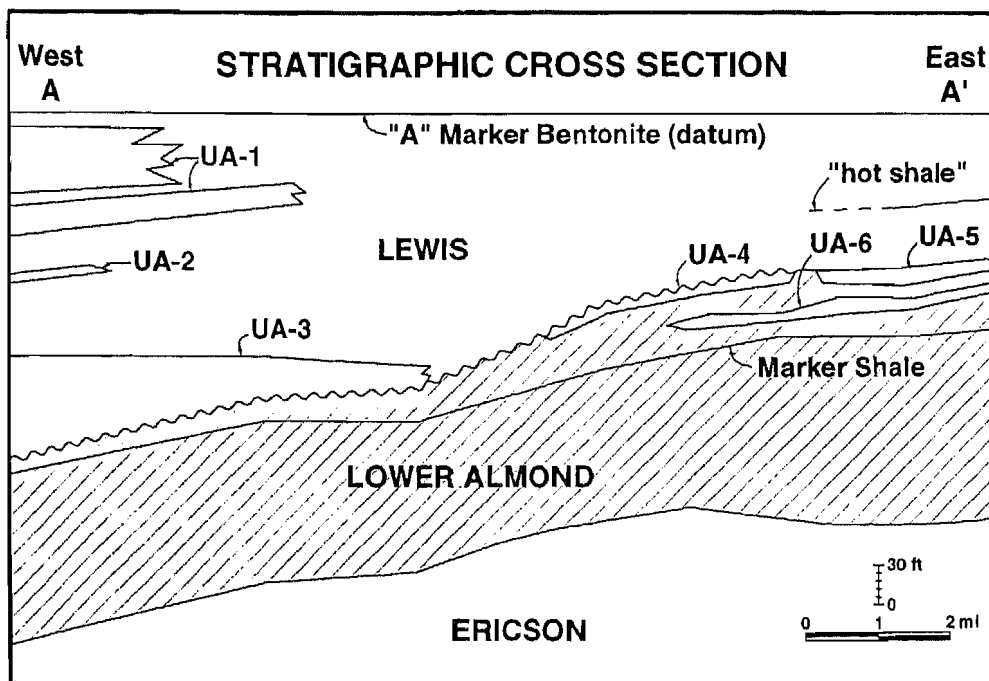


Figure 3-6. Diagrammatic west-east cross section showing the relationship between upper and lower Almond members over the Rock Springs Uplift and in the westernmost Washakie Basin. Modified from Van Horn (1979), whose subdivision of the upper Almond is designated UA-1 to UA-6.

sandstones, siltstones, and mudstones; and carbonaceous shales and coal beds deposited in flood-basin marshes and swamps. The shales contain abundant large, well-preserved cuticle fragments, few spores, and no dinoflagellates, and thus probably represent fresh-water deposits (Meyers, 1977). Burrows are sparse and of one type, *Planolites*.

The upper part of the lower Almond, in contrast, indicates alternating fresh- and brackish-water conditions (Meyers, 1977; Flores, 1978; Van Horn, 1979), and comprises cyclical sequences (parasequences) of freshwater coals and brackish water carbonaceous shales, mudstones, siltstones, and sandstones deposited in a variety of back-barrier tidal-flat / lagoonal environments. Burrows, mainly *Planolites*, and sporadic occurrences of marine palynomorphs increase upwards within the upper part of the lower Almond (Meyers, 1977), indicating that it is a transgressive deposit.

The upper Almond typically contains fewer and less extensive coal beds, shows a marked increase in both the abundance and diversity of trace fossils (including *Planolites*, *Ophiomorpha*, *Asterosoma*, *Teichichnus*, and *Zoophycos*) and dinoflagellates (Meyers, 1977), and was deposited within estuarine to open marine environments. The intertonguing of Lewis Shale with upper Almond sands further subdivides the upper Almond into three sandstone units, referred to by Van Horn (1979), oldest to youngest, as UA-3, UA-2, and UA-1. Although these units were deposited during an overall transgression, the UA-1 sand is seaward-stepping, unlike the underlying UA-2 sand (Figure 3-6), and distally downlaps onto the "hot shale." The upper Almond member pinches out into Lewis Shale just to the east of the Rock Springs Uplift, and thus is not present throughout most of the Washakie and Great Divide basins. Generally, the Almond Formation within the basins and the Wamsutter Arch

area is correlative to the lower Almond member of the Rock Springs Uplift.

## **STRATIGRAPHY AND DEPOSITIONAL ENVIRONMENTS OF THE ALMOND FORMATION IN THE WASHAKIE AND GREAT DIVIDE BASINS AND WAMSUTTER ARCH**

In the Washakie and Great Divide basins, the contact between the Almond and the Lewis is very sharp and is marked by a TSE. Often, the uppermost Almond comprises a marine sandstone facies that is commonly underlain and separated from the main Almond by a tongue of marine Lewis Shale. These marine sand tongues and the Lewis Shale tongues (where present) are denoted upper Almond, and the section below, main Almond. The Almond tongues are progressively younger from east to west (landward stepping), and thus cause the observed stratigraphic rise of the Almond-Lewis contact to the west. From east to west in a stratigraphic interval, facies typically change laterally from open marine (Lewis Shale) to shoreface and tidal inlet to back barrier, and the underlying marine shale tongues pinch out (between wells 3 and 4 and wells 6 and 7, cross section A-A', Plate 1). Westward of the underlying shale pinch-outs, upper Almond tongues merge with and become indistinguishable from the main Almond. Although upper Almond marine facies are similar to facies in the upper Almond member on the Rock Springs Uplift, they are chronostratigraphically older and a part of the lower Almond. Facies within the main Almond are similar to facies within the lower Almond member on the Rock Springs Uplift and are, at least in part, chronostratigraphically equivalent.

According to Roehler (1990), the Almond Formation is thickest in the Rock Springs Uplift area and progressively thins eastward, due to facies change into Lewis Shale. Within the Washakie Basin, the Almond varies from 250 to more than 500 ft thick,

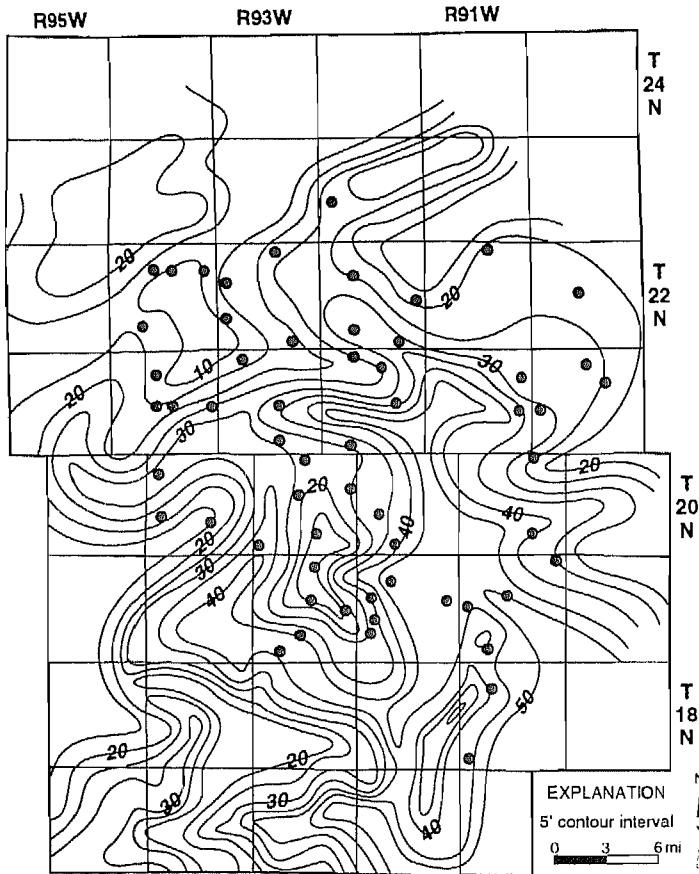


**Figure 3-7.** Isopachous map of total net coal in the Almond Formation, northern Washakie and southern Great Divide basins. Coals were identified by travel time greater than 115  $\mu$ s/ft, after the manner of Davis (1977). Patterned area indicates net coal thickness >40 ft.

but does not consistently thin to the east as Roehler (1990) suggests; both the upper and lower contacts rise from east to west (Figures 3-4 and 3-7; Plate 1). Local variations in thickness are probably related to syndepositional movements along basement block faults.

In the eastern Washakie and Great Divide basins, the Almond can be divided into three genetic units that encompass the whole formation: an upper unit (Unit 1) that includes the upper Almond marine sandstone tongues and a coal-bearing section; a middle unit (Unit 2) that contains significantly less coal than the units above and below it, and a lower unit (Unit 3) that contains numerous coals (cross sections A-A' and B-B', Plate 1). Because coals are easily identified using a combination of gamma-ray-resistivity and either neutron-density or sonic logs, these units can be readily correlated and mapped in

the eastern portions of the basins. Farther to the west, the middle, non-coal-bearing unit pinches out, and correlation becomes more difficult.

### Unit 1

Marine tongues of the uppermost Almond vary from zero to more than 150 ft thick, and are much thicker in the western part of the Washakie Basin than in the eastern part (Figure 3-4). Typically, they consist of one or more upward-coarsening sandstones that are continuous along strike (basically north-south) and are discontinuous in a dip direction. On gamma-ray logs, upper Almond sands display sharp upper contacts and gradational to sharp lower contacts, with profile shapes that are coarsening-upward to blocky. Landward (westward), sands thin gradually and become interbedded with shales, thus changing facies into "lower" or

“main” Almond-type lithologies. The upper Almond is indistinguishable from the main Almond west of the pinch-out of the underlying Lewis Shale tongues. Seaward (eastward), the sands thin and pinch out rapidly into Lewis Shale; for example, the upper Almond sand in the area of R96W is more than 100 ft thick, but pinches out to shale in less than three miles (between wells 2 and 3, cross section A-A', Plate 1).

As observed in cores, the upper Almond consists mainly of very-fine to fine grained sandstones, with minor interbedded shale and rare, thin coal beds. The sandstones are often subhorizontally laminated, cross bedded, or rippled. Burrows are rare to common, and include *Ophiomorpha*, *Teichichnus*, *Planolites*, and *Thalassinoides*. Cores indicate that at least some of the sharp-based units are tidal channels that cut into shoreface sandstones. The number of tidal channels observed in the area of Echo Springs Field is substantially less than observed in the Patrick Draw Field. Other sharp-based sands are interpreted to be shoreface sands. Tidal flat and washover fan sands have also been identified, but are far less common than shoreface sandstones. Transgressive disconformities separate the upper Almond from the overlying Lewis Shale and from the underlying main Almond.

The coal-bearing facies of Unit 1 is 160-250 ft thick, comprises interbedded sandstone, shale, and coal, and has an overall “spiky” log character due to the alternating lithologies. In general, the ratio of shale to sandstone within a stratigraphic interval increases to the west. Individual sandstones are generally 10-15 ft thick, but may be up to 25 ft thick. Coals are typically 1-4 ft thick, but may be up to 8 ft thick. The continuity of sandstones and coals is often on the order of several miles in all directions. Correlation of individual units can be accomplished wherever well control is good (e.g., within producing fields). An example is presented in Plate 2, which is a stacked grid of east-to-west trending cross-

sections for T17N, R 93W, Coal Gulch Field. The cross sections were constructed using detail-scale gamma-ray-resistivity logs, and porosity logs were also utilized to identify coals. Note how many individual sandstones and coals can be correlated across the township. Where well control is less dense, correlation of individual units is often not possible.

As observed in core, the sandstones are generally very-fine to fine grained, contain numerous coffee-grounds layers, and are rippled to flaser bedded. Both symmetric and asymmetric ripple forms occur, suggesting that both waves and currents were present. Tops of sandstones are commonly rooted. Shales are often carbonaceous and highly disturbed as a result of soft-sediment deformation or disturbance by plants and animals. Trace fossils are dominantly *Planolites*, with minor *Skolithos*, *Teichichnus*, and *Thalassinoides*. Erosional discontinuities are common, and units commonly coarsen upward, and less commonly fine upward.

Unit 1 was deposited in marginal marine back-barrier environments, including tidal flat, tidal channel (creek), washover fan, lagoon/bay, marsh, and swamp environments, and is depositionally similar to the upper portions of the lower Almond Formation of the Rock Springs Uplift. Overall, Unit 1 is transgressive in origin and correlates with part or all of the lower Almond section of the Rock Springs Uplift.

## Unit 2

Unit 2, the middle section of the main Almond, is a series of coarsening-upward shale-to-sandstone packages. The sandstones are up to 30 ft thick, with characteristic funnel-shaped gamma-ray log profiles. These sands are continuous over tens of miles in both the east-west and north-south directions, and thus can be correlated even across areas of sparse well control. Unit 2

is easily identified on well logs because it contains more continuous sands and significantly fewer coal beds than Units 1 and 3. Coal is commonly absent in the northern part of the study area; to the south, one continuous, thin coal seam occurs at the top of one of the sands.

Cores indicate that Unit 2 sandstones are very-fine grained, commonly contain organic debris, are dominantly low-angle to subhorizontally laminated or rippled, with occasional hummocky cross-stratified beds and cross beds, and display numerous subhorizontal truncations. The tops of the sandstones are sometimes rooted. The shales are silty, and much less carbonaceous than the shales in Units 1 and 3. Unit 2 shows greater abundance and diversity of trace fossils than Units 1 and 3, including *Ophiomorpha*, *Helminthopsis*, *Terebellina*, *Thalassinoides*, *Teichichnus*, and *Skolithos*. Deposition of Unit 2 was primarily in an open marine shoreface environment; some back-barrier tidal flat sandstones and lagoonal shales are present.

Both the upper and lower contacts of Unit 2 are erosional. The upper contact, often picked near the base of the lowermost coal in Unit 1, is a lowstand unconformity that progressively cuts downsection to the west. Up to 50 ft of local relief is observed along the unconformity (cross section B-B', Plates 1 and 2). An unpublished Union Pacific Resources report (1992) also identifies an unconformity in the same stratigraphic interval of Unit 2. The basal contact of Unit 2 is often picked near the top of the uppermost coal in Unit 3, and is a transgressive disconformity or possibly a transgressively modified lowstand unconformity.

Unit 2 is not present in the western Washakie Basin - Rock Springs area; it pinches out by a combination of erosional truncation below the unconformity, onlap onto Unit 3, and (possibly) facies change into coastal plain sediments (cross section A A, Plate 1). Tracing the unconformity west

of the pinchout is very difficult without the intervening middle unit to help distinguish Units 1 and 3.

Unit 2 can be traced as far east as well control exists, and reaches a maximum thickness of 140 ft. It correlates with the high-gamma-ray, low-resistivity portion of the basal Almond in the Rawlins Uplift, as presented by Roehler and Hansen (1989; = 12,850-12,960 ft, well #7, Amoco Champlin #272, Sec. 11-T21N-R90W). Gill et al. (1970, their Figure 2) indicate that this interval is a marine shale tongue of the Lewis.

### Unit 3

Unit 3 comprises 90 to 200 ft of interbedded coal, shale, siltstone, and sandstone; the sandstones are up to 45 ft thick. Thicker sands typically display fining-upward profiles on gamma-ray logs and are highly discontinuous. Coals are 4-6 ft thick, and commonly occur at the top of fining-upward sequences. Near the base of Unit 3 is a prominent coal zone that is more than 15 ft thick and continuous. In core, the sandstones are very-fine grained, often contain abundant shale clasts, and are dominantly ripple bedded. Shales are carbonaceous, and contain abundant plant remains. Burrows overall are sparse and of one type, *Planolites*.

Unit 3 was deposited in a coastal plain environment consisting of fluvial channels (thick, discontinuous sandstones), splays, marshes, and swamps, and represents the most continental deposition in the Almond.

Unit 3 thins to the west either by onlap onto the Ericson or by facies change to the Ericson, and by truncation below the lowstand unconformity that forms the base of Unit 1. Because it is difficult to trace the unconformity west of the pinch-out of Unit 2, it is not clear what happens to Unit 3 westward. The unconformity may continue to cut down, and to remove all of Unit 3. If

Unit 3 is not removed, then perhaps it is the chronostratigraphic equivalent of the lowermost Almond (continental facies) on the Rock Springs Uplift. Commonly, in the eastern Washakie and Great Divide basins, the top of Unit 3 is picked as the top of the Ericson, as reported in Petroleum Information's Historical Data Files. Note that Unit 3 corresponds to what Roehler and Hansen (1989, their wells 7 and 8, Map MF 2076) have identified as the Pine Ridge Sandstone.

### ALMOND PRODUCTION

Most of the gas production in the eastern Washakie and Great Divide basins and intervening Wamsutter Arch is from the dominantly marine sandstones of the upper Almond. Iverson and Surdam (1995) indicate that, at least within portions of the Echo Springs Field, production to date has exceeded the calculated gas-in-place within the upper Almond sand reservoirs. They state that additional gas production must be coming out of the main Almond, even where only the upper Almond sands are perforated. García-González and Surdam (1992) indicate that Almond coals in the Washakie Basin have generated both oil and gas and have expelled significant quantities of gas. Vitrinite reflectance data from the Standard Draw and Siberia Ridge fields indicate that the coals there are mature (Christiansen, 1995). The numerous, thick coals in the main Almond may be the source of the "excess" gas that has been produced from the upper Almond. Although the upper Almond is the primary exploration target, significant gas potential may also exist in the main Almond. The sands in the middle marine unit (Unit 2) are depositionally similar to the upper Almond sands, and may form viable reservoirs. They are generally very-fine grained in the few cores in which they were identified in this study; additional work will determine their grain size elsewhere.

### SEDIMENTATION AND TECTONICS

The influence of syndepositional movement along northeast-southwest-trending basement block faults during Almond deposition is well documented in the Rock Springs Uplift (Van Horn, 1979; Hendricks, 1983). According to Van Horn (1979), movement on the faults was dominantly vertical, and changes in relative sense of movement display up to 150 ft of displacement. Changes in lithofacies and interval thickness across these faults are common.

Evidence suggests that hydrocarbons migrated up along northeast-trending basement faults and fracture zones in the vicinity of Patrick Draw (Richers et al., 1982). Fluid movement along basement block faults may also help explain the strong northeast trend of mapped temperature anomalies throughout the basin noted by Law and Smith (1983). ✕

Evidence of syndepositional movement along basement block faults occurs throughout the Washakie and Great Divide basins. Northeast-trending offsets in the zone of abrupt thinning of the lower Lewis ← (Figure 3-5) are similar to northeast trending variations in lower Lewis thickness observed by Van Horn farther to the west (1979, his Figure 48). The overall very linear nature of this zone suggests possible tectonic influence. The strong north-south ← orientation of the zone in the basin center is interesting because nearly all the mapped faults and lineaments, both in the <sup>overprints</sup> basin and on the Rock Springs Uplift, are either northeast-southwest or northwest-southeast (Love and Christiansen, 1985; Thomas, 1973). Many gas fields in this area are oriented roughly north-south, including the greater Echo Springs - Standard Draw - Coal Gulch, Blue Gap, Desert Springs, and Siberia Ridge fields.

Abrupt changes in the stratigraphic elevation of the Almond-Ericson contact generally correspond to abrupt rises in the top of the Almond, and may be the result of

differential movement along basement block faults. Laterally abrupt changes in stratigraphic elevation of the top of the Ericson are observed on both east-west and north-south cross sections, and often coincide with laterally abrupt thickness or lithofacies changes observed within the Almond. The distribution of total net coal thickness in the main Almond interval shows trends of alternating thick and thin zones both to the northeast and the northwest (Figure 3-7).

Faults were probably active during the formation of the unconformity at the base of Unit 2 in the main Almond. Up to 50 ft of relief between adjacent wells (~1 mile spacing) is observed along the unconformity (cross section B-B', Plate 1; between Sections 9, 10, and 11, Plate 2). Additional section is preserved in intervals both directly above and below the unconformity in what are interpreted to be downdropped blocks. Commonly, abrupt variations in the elevation of the Almond-Ericson contact coincide with variations in relief observed along the unconformity.

Variations in the distribution of the upper Almond sand reservoir in the Dripping Rock / Mulligan Draw fields (Figure 3-1) also suggest syndepositional faulting. Figure 3-8, a structure map on top of the Almond over the area of these fields, indicates a gentle monoclinal dip to the southwest and no structural closure. Production, which is from upper Almond sandstones, is stratigraphically controlled, although fractures may also influence production.

A grid composed of cross sections of the Almond was constructed over the area. The locations of two of these cross sections (A-A' and B-B') are shown in Figure 8, and the cross sections are shown in Plate 1. The cross sections include the lower Lewis Shale as well as the upper Almond and a portion of the lower Almond; the datum is a bentonite marker in the Lewis Shale. The locations of inferred faults and their rela-

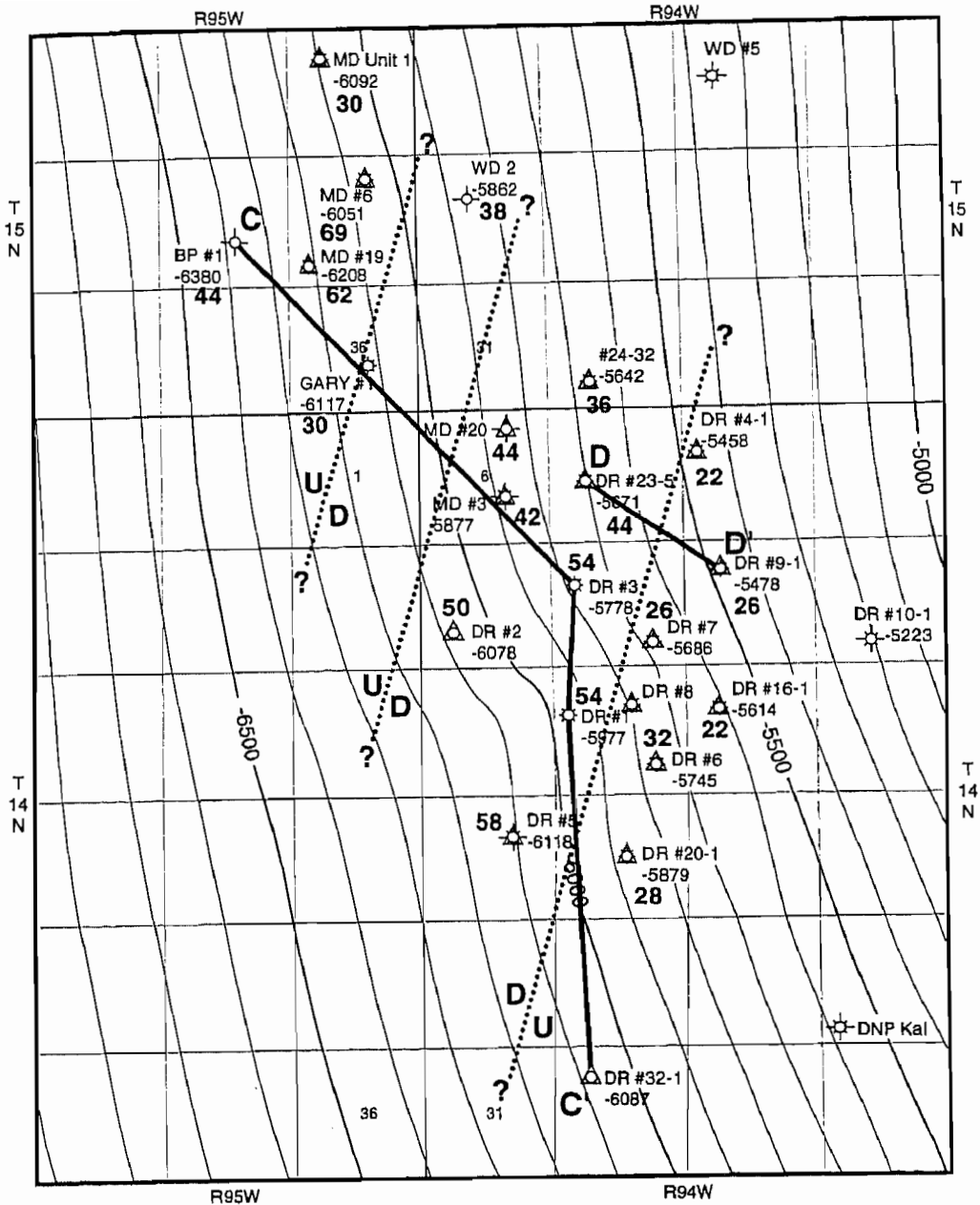
tive motions are indicated on the cross sections.

Correlations indicate that the upper Almond interval thickens by the addition of sandstone at the top of the Almond, and not by the thickening of any one sand. Note that the units both above and below the upper Almond are also thicker in the wells with the thickest upper Almond (Dripping Rock #3 and #1 wells, cross section C-C', Plate 1). If the additional sand at the top were depositionally positive (e.g., a thick bar sandstone), the shale intervals above it would be thinner, not thicker. It is most likely that the additional sands present only within the inferred downdropped blocks are erosional remnants of what was originally a more widespread sandstone. The thin, "spiky" sands at the top of the BP#1 and #32-1 wells are interpreted to be lags of the originally widely deposited sand, formed by the reworking of the uppermost Almond sands on uplifted blocks during transgression.

The thickness of the total upper Almond sand and the inferred locations of the faults that most strongly influenced the reservoir are also shown in Figure 3-8. Although no faults are indicated on the Geologic Map of Wyoming (Love and Christiansen, 1985) in this area, there is a distinct blocky geometry to both surface outcrop and drainage patterns that at least suggests fault control (Jaworowski and Simon, 1995). The presence of faults possibly associated with fractures may also help account for the different amounts of water produced by several wells in this area.

## CONCLUSIONS

The Almond-Lewis contact in the Washakie and Great Divide basins area stratigraphically rises from east to west, as does the Almond-Ericson contact. Where the Almond and Lewis intertongue, the tongues of Almond are denoted upper Almond, and comprise mainly open marine



28 Gross sand thickness "upper" Almond

— Structure contours top of Almond Fm. CI = 100'

○ dry hole

⊗ gas well, Almond

⊠ dry hole w/show of gas, Almond

○ other formation producer

◆ dry hole w/show of oil, Almond

△ cored in Almond

**Figure 3-8.** Base map of the Dripping Rock-Mulligan Draw Fields area, showing structure at the top of the upper Almond and the trend of syndepositional faults as interpreted from upper Almond sandstone distribution. The thickness of the upper Almond is given adjacent to each well. The locations of cross sections C-C' and D-D' in Plate 1 are indicated.

shoreface sandstones. The section of Almond below the Lewis Shale tongues is denoted main Almond. To the west, the marine sandstones in the upper Almond tongues grade into back-barrier tidal flat and lagoonal sediments, the tongues of Lewis Shale pinch out, and the upper Almond becomes indistinguishable from and merges with the main Almond.

In the subsurface, the Almond Formation can be grossly divided into three units. Unit 1 includes the upper Almond tongues and an underlying section of interbedded coal, carbonaceous shale, and fine to very-fine grained sandstones deposited in mostly back-barrier environments. Unit 1 is chronostratigraphically equivalent, at least in part, to the lower Almond member on the Rock Springs Uplift, and is transgressive. Unit 2 comprises multiple coarsening-upward shale-to-sandstone successions (parasequences), which have a high degree of continuity and were deposited mainly in shoreface to back-barrier environments. Unit 3 comprises interbedded coals, carbonaceous shales, siltstones, and very-fine grained sandstones deposited in a coastal plain environment. Unit 3 may be chronostratigraphically equivalent to the Pine Ridge Sandstone of the Rawlins Uplift. To the west, it is unclear whether Unit 3 is erosionally truncated, changes facies and is included in the Ericson, or is equivalent to the lowermost lower Almond of the Rock Springs Uplift.

The contact between Units 1 and 2 is a lowstand unconformity that progressively cuts down-section to the west, and the contact between Units 2 and 3 is a transgressive disconformity or a transgressively modified lowstand unconformity. Unit 2 pinches out to the west by a combination of erosional truncation below the lowstand unconformity and onlap onto Unit 3. West of where Unit 2 pinches out, both the lowstand unconformity and the transgressive disconformity become difficult to correlate.

Facies present in the Almond of the Washakie and Great Divide basins range from continental through brackish to open marine, and are similar overall to the Almond facies identified in outcrop on the Rock Springs Uplift. However, the number of tidal channel or tidal inlet facies observed in the "upper" Almond facies of the Echo Springs area are far fewer than the number present in "upper" Almond facies in the area of Patrick Draw. This observation is consistent with Van Horn's (1979) conclusion that tidal influence was greater in younger Almond deposits due to the focusing influence of tides in the Hallville embayment, which increased through time.

The presence of numerous, mature coals in the main Almond suggests that the main Almond may produce a significant amount of gas. The marine sandstones identified in Unit 2 are depositively similar to the productive upper Almond sands, and may be viable reservoirs.

As has been observed in outcrop, syndepositional movement along dominantly northeast-trending faults during Almond deposition is indicated by gross patterns in lithofacies and thickness distributions. Deposition and preservation of the upper Almond Sandstone reservoirs in the Dripping Rock Field were strongly influenced by syndepositional fault movements.

## ACKNOWLEDGEMENTS

The authors wish to thank the Gas Research Institute for support for this study under GRI contract number 5091-221-2146; Kathy Kirkaldie and David Copeland for editorial help and Allory Deiss for graphic creativity, all at the Institute for Energy Research; and Phyllis Ranz, Wyoming State Geological Survey, for monumental drafting.

## Chapter 4

# Joint Sets in the Wamsutter Area: Relation to Fracture History of the Rawlins and Rock Springs Uplifts, Washakie Basin, Southern Wyoming

*Earl R. Verbeek and Marilyn A. Grout  
U.S. Geological Survey*

*Cheryl Jaworowski  
Institute for Energy Research*

### ABSTRACT

A reconnaissance study of joint characteristics in resistant sandstone lenses of the lower Tertiary Wasatch Formation east of Wamsutter, in the Washakie Basin of southeastern Wyoming, indicates the existence of three joint sets: (1) a minor set (J1) of subvertical joints that strike N69-74°W, (2) a prominent set (J2) of subvertical joints that strike N61-84°E, and (3) a minor set (J3) of subvertical joints that strike N13°W. The dominant set is correlative with subsurface joints in oriented core from the Upper Cretaceous Almond Formation in the same area, and most likely corresponds to a major regional set of ENE-striking joints previously documented in Upper Cretaceous sandstones on both the Rawlins and Rock Springs uplifts. The two minor sets in the Wamsutter area also correlate to known sets on both uplifts. Three older sets on the uplifts are missing in the Wamsutter area, and likely predate the Wasatch rocks exposed there.

The three joint sets in the Wamsutter area are intermediate to late members of a complex regional fracture network of eight sets: the J1, J2, and J3 sets correspond to the fourth, fifth, and seventh sets, respectively, in the regional fracture sequence. The fifth set (J2) is the most prominent of all and is everywhere a major element of the fracture network; it also corresponds to a major set of face cleats in coal in lower Tertiary and

Upper Cretaceous beds on the Rock Springs Uplift. Although these cleats were once thought to be related to Cordilleran thrusting events, nothing in the areal distribution, relative prominence from place to place, or probable young age of this set suggests such a relation. The present study indicates that these fractures are an expression of post-Laramide extensional strain, as documented for several other basins on the Colorado Plateau farther south.

Among the eight known regional sets of joints in Upper Cretaceous rocks, six of them can be matched between the Rawlins and Rock Springs uplifts; thus, they are probable elements of the subsurface fracture network in correlative rocks beneath the intervening basin. The geometric properties of all six sets in outcrop are so closely related to rock type, bed thickness, stratal sequence, and previous joint history that the prospects for successful prediction of fracture-network properties at depth appear more promising for the Washakie Basin than for most other areas.

### INTRODUCTION

This report (1) summarizes the description of joint sets in the main body of the lower Tertiary Wasatch Formation (Love and Christiansen, 1985) in the area east of Wamsutter in the Washakie Basin and (2) interprets the sequence of formation of joint

sets within the context of the fracture history documented previously on the Rawlins and Rock Springs uplifts along the eastern and western margins of the basin, respectively (Grout and Verbeek, 1992a). The field methods used are summarized in Grout and Verbeek (1983; 1992a). Six localities in the Wasatch Formation were studied in the Creston 7.5' quadrangle in southern Sweetwater and northern Carbon counties (Figure 4-1). Outcrops at all six localities consist of thin, resistant ledges of gray, very-fine to fine-grained, calcareous sandstone interbedded with much thicker, nonresistant mudstone. Fracture data gathered at these six localities supplement data from 57 other localities in older, dominantly Upper Cretaceous rocks (Grout and Verbeek, 1992A; Grout et al., unpublished data, 1994) and provide a preliminary view of the regional fracture network.

## DESCRIPTION OF OUTCROPS AND JOINT SETS

Joints in the Wamsutter area (Figure 4-1) are confined to moderately to well-indurated sandstone lenses within friable mudstone of the main body of the lower Tertiary Wasatch Formation. The lenses are exposed for 0.25-0.6 m (10-24 in) vertically and several tens of meters (30-50 ft) horizontally; many cap eroded knobs. The bases and tops of most of the lenses are obscured by rubble and soil; the joints within them are thus best exposed in vertical section. The sandstone within the lenses is ripple- to cross-laminated with thin, shaly partings. Local rip-up clasts are common at the base. Bedding in some lenses is highly contorted, apparently from penecontemporaneous slump.

Three joint sets were documented at the six localities studied east of Wamsutter (Table 4-1). The joints of all three sets are vertical to subvertical and are thus roughly perpendicular to bedding, but they differ markedly in strike. Joints of the oldest set (J1) are present at only two localities,

Stations 54 and 58, and have median strikes of N69-74°W. The next set to form, J2, is the dominant one of the area and is present at all localities studied (Table 4-1). Median strikes of J2 joints at five localities are in the range N61-84°E, but at one locality, Station 55, their orientation was influenced by the geometry of the narrow sandstone lens within which they formed, as will be discussed in a later section. Joints of the youngest set, J3, are the sparsest of all, and were documented at only one locality, Station 58; their median strike is N13°W.

### Joint Set 1: N69-74°W

The J1 set, the first joints to form in the sandstone lenses of the main body of the Wasatch Formation in the Wamsutter area (Figure 4-1), are present at only two of the six localities studied (Table 4-1). Median strikes of these joints are N69°W (Station 54) and N74°W (Station 58); their dips are nearly vertical. Most of the J1 joints span the full thickness of the sandstone lenses within which they formed and, thus, have heights of 0.2-0.5 m (8-20 in). Few of the joints can be followed any great distance because of the narrowness of the outcrop; their exposed lengths of 0.2-1.6 m (0.6-5 ft) doubtless are only a fraction of their true lengths. The J1 joints are variably spaced at the outcrop scale, locally as close as 0.04 m (1.5 in) or as wide as 2-3 m (610 ft), but most commonly at 0.2-0.6 m (8-24 in).

Common plumose structure and twist-hackle fringes on the surfaces of J1 joints show that they are extension fractures. The J1 joints are planar or nearly so and have smooth surface except in the areas of twist hackle. Where terminations of these joints were observed, they end as hairline cracks within the rock body, in contrast to joints of later sets which commonly terminate against older joints. The faces of J1 joints are lightly to prominently coated with limonite and locally with pale tan to white, opaque calcite.

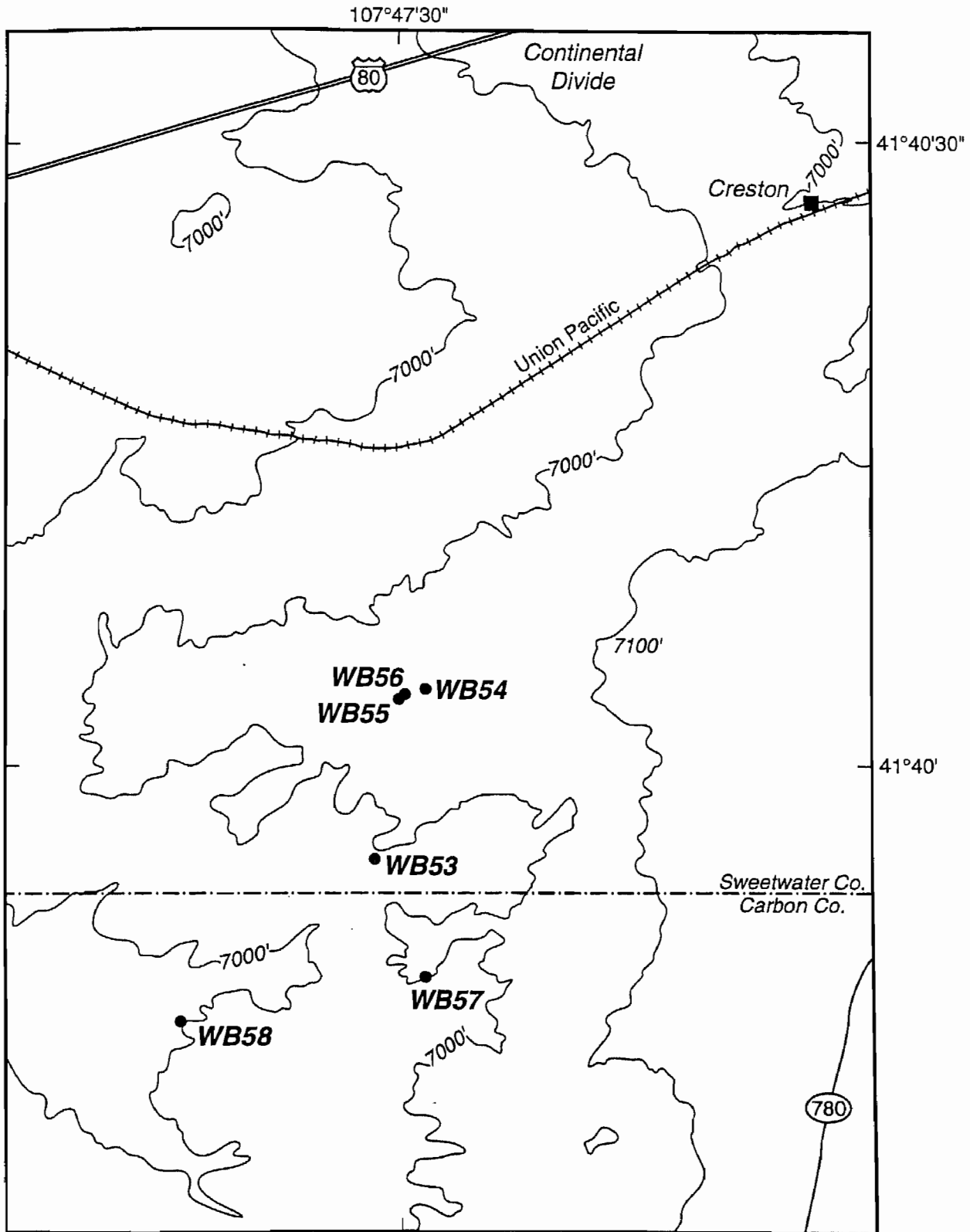


**Figure 4-1.** Map of joint stations east of Wamsutter in the Washakie Basin, southern Wyoming. Width of map is 6.33 km.

**Table 4-1.** Station number and set designation for joints in horizontally-bedded lower Tertiary Wasatch Formation sandstone lenses in the Wamsutter area of the Washakie Basin, Creston 7.5' quadrangle (Figure 4-1). N64E/83SE = median joint strike of N64°E and median dip of 83°SE.

Station No.	Joint-Set Designation, Relative Age, And Orientation		
	(oldest) J1	J2	(youngest) J3
53		N64E/83SE	
54	N69W/90	N84E/90	
55		N52E/89SE*	
56		N61E/88NW	
57		N62E/90	
58	N74W/90	N70E/84SE	N13W/85SW

\*more northerly strike influenced by the geometry of the sandstone lens

### Joint Set 2: N61-84°E

All six outcrops studied contained joints of the N61-84°E-striking J2 set, the second set to form in the Wamsutter area (Table 4-1). The J2 joints are prominent, abundant, and visually obvious in outcrop; they are the major set in this area. Heights of the J2 joints generally equal the exposed bed thickness of 0.2-0.95 m (8-37 in), but locally some are shorter and cut only about half the thickness of the beds. Exposed lengths of the J2 joints range from 0.2-4.0 m (0.7-13 ft), and many are exposed for 1 m (3 ft) or more. Their true lengths are not known, but are probably at least 2-3 m (6-10 ft) long for most of the joints. The seemingly longest J2 joints are actually thin zones of closely spaced, shorter, overlapping fractures whose ends curve toward and join one another to form a continuous break. The J2 joints commonly are spaced 0.1-1.5 m (4-20 in) apart, but the observed range of spacing is considerably greater, 0.01-1.85 m (0.4-72 in). They are more closely spaced in the thinner beds than in the thicker beds.

Most joints of the J2 set are nearly planar, but some are slightly curved or sinuous along strike. This planarity is interrupted where the joints hook into one another as described above, and also near the edges of sandstone lenses where individual J2 joints curve to terminate against the contact with

the enclosing mudstone at right angles. A related effect, seen only in the very narrowest sandstone lenses, is the tendency of J2 joints to form perpendicular to the long axis of the lens. At one locality, Station 55, the J2 joints strike more northerly (N52°E) than usual because of this effect, but other J2 joints in wider lenses nearby show strikes within the normal range. A similar effect is commonly seen in petrified logs, which tend to break perpendicular to the log regardless of the azimuth of the log axis; Petrified Forest National Park in east-central Arizona contains thousands of examples.

Common fracture-surface structures, such as arrest lines, twist-hackle fringes, and plumose structure confirm that the J2 joints are extension fractures. Where joints of the J1 set are present, the J2 joints either terminate against or cut across them; the latter is most common where the J1 joints were previously filled with calcite cement. All the joints of the J2 set are lightly coated with brown limonite that impregnates the wall rock generally 0.01-0.03 m (0.4-1.2 in) perpendicular to the joint face. At one locality, Station 57, diffusion bands adjacent to the joint wall for 0.8-0.12 m (3-5 in) are superimposed on earlier bands along or across bedding planes, indicating at least two periods of redistribution of iron in solution in these rocks. Locally, thin coatings of white calcite were noted on some J2 joints.

### **Joint Set 3: N13°W**

The NNW-striking joints of the young J3 set are present at only one of the six localities studied (Station 58). These joints are smaller than those of the older sets; exposed heights of 0.12-0.5 (4.5-20 in) are typical, and most are only 0.13-0.5 m (5-20 in) long. The stunted lengths reflect the previous fracture history of the rock: most J3 joints could propagate only short distances laterally before encountering a preexisting J1 or J2 joint, which arrested their growth. The resultant terminations of J3 joints against J1 and J2 joints amply demonstrate the relatively young age of the J3 set in the Wamsutter area. Other J3 joints began their growth at a point on a preexisting joint surface; the origin points for some of them are visible in outcrop, and again demonstrate their relatively young age. The J3 joints are variably spaced, from 0.1 m to about 0.6 m (4-23 in). They are subplanar in shape, commonly sinuous along strike and broadly curved in dip. Only light patchy stains of limonite are present on their surfaces. The J3 joints constitute a minor set of sparse, weakly expressed joints. Their small size, subplanar shape, and lack of mineral coatings other than light limonite stains are typical of late-formed joint sets in many areas.

### **SUMMARY OF FRACTURE NETWORK ON RAWLINS AND ROCK SPRINGS UPLIFTS**

Upper Cretaceous sandstones on both the Rawlins and Rock Springs uplifts record a complex history of pre- and post-uplift fracture events (Grout and Verbeek, 1992a). The fracture history of these rocks is of interest in predicting properties of the fracture network in reservoir rocks of similar age at depth between the two uplifts. Specifically, if individual fracture sets can be correlated from one uplift to the other, and if some of the same sets are

found in exposed Tertiary rocks of the Washakie Basin, then chances of successful prediction are much enhanced. Here, we briefly review the fracture history of the Rawlins and Rock Springs uplifts and in the following section, discuss possible correlation of some of the sets to those in buried Cretaceous and exposed Tertiary rocks in the Wamsutter area.

Eight sets of extension joints are present in Upper Cretaceous sandstones on the Rawlins Uplift, and six sets have been recognized in the Rock Springs area (Table 4-2). The fracture histories of the two uplifts are similar for the most part; six of the sets formed in identical sequence and have comparable orientations in the two areas. Most of the sets thus appear to correlate well across at least 100 km (62 mi) of the basin proper, but there are notable exceptions. The oldest set known on the Rawlins Uplift is one; it has no known counterpart on the Rock Springs Uplift, suggesting that fracturing began earlier along the eastern border of the Washakie Basin than in some areas farther west. One additional, much younger set likewise appears unique to the Rawlins Uplift. Joints of all but the youngest sets on each uplift are nearly perpendicular to bedding, regardless of present bed dip, showing that most of the joint sets predate the final phases of tilting along the basin margins. Though of regional extent, the six correlative joint sets differ markedly in prominence from one uplift to the other (Table 4-2), which is hardly surprising in view of the 100-km (62-mi) distance involved. Only the ENE-striking set is a major component of the joint network of both uplifts. In addition to the geographic differences, the character of the fracture network shows wide variation from bed to bed in the same outcrop, but much of the variation is systematic and predictable. For any given joint set, the three factors that most affect joint size, spacing, and shape are (1) lithology (esp. degree of cementation), (2) bed thickness, and (3) previous joint history.

**Table 4-2.** Possible correlations between median strikes of joints in Upper Cretaceous clastic rocks on the Rawlins and Rock Springs uplifts (Grout and Verbeek, 1992a) and in lower Tertiary rocks of the Wamsutter area (Table 4-1).

Rawlins Uplift	Rock Springs Uplift	Wamsutter Area	
(oldest)			
F1 N10-30°E*			
F2 N05-30°W	Fa N30-40°W*		
F3 N45-65°W*	Fb N55-65°W		
(Ft. Union unconformity)			
F4 N75-80°W		J1	N69-74°W
F5 N50-75°E*	Fd N60-80°E*	J2	N61-84°E*
— N27-44°E <sup>1</sup>	Fc N20-45°E		
F6 N25-45°W	Fe N20-45°W	J3	N13°W
F7 N55-65°W	Ff N55-85°W		
(youngest)			

\* = Major joint set present in >1/3 of the outcrops studied and thus is considered a major set of sets. <sup>1</sup>Unnumbered set found after publication of 1992a report of Grout and Verbeek. Set is present on south end of Rawlins Uplift and is correlative with Fc set on Rock Springs Uplift.

Many examples of the effect of rock type and rock-body geometry on the characteristics of the joint network in Cretaceous rocks bordering the Washakie Basin were mentioned in an earlier paper (Grout and Verbeek, 1992b). Other than these expected effects, we note no major changes in the overall fracture network from the base of the Mesaverde Group to the top of the Fox Hills Sandstone on either uplift (Grout and Verbeek, 1992a). The presence of the same joint sets within an appreciable thickness of strata, and the broad similarity of the fracture history from one uplift to another, increase our confidence that elements of fracture-network geometry in Cretaceous reservoir rocks buried beneath the Wamsutter area can indeed be predicted successfully.

## DISCUSSION

### Correlation of ENE-Striking Joints Across the Basin

On a basinwide scale, the prominent set of N61-84E-striking joints in outcropping sandstone lenses of the lower Tertiary Wasatch Formation near Wamsutter almost

certainly corresponds to (1) the set of N70-80°E-striking joints in oriented core of the Upper Cretaceous Almond Formation in the same area (Jaworowski and Simon, 1995; Hill, 1995); (2) the major set of N50-75° E-striking joints in Upper Cretaceous sandstones on the Rawlins Uplift; and (3) the major set of N60-80°E-striking joints in correlative rocks on the Rock Springs Uplift (Table 4-2; Grout and Verbeek, 1992a). Likewise, the two additional, minor sets in lower Tertiary rocks in the Wamsutter area (Table 4-1) most likely correspond to minor sets of similar relative age and orientation in the Upper Cretaceous rocks on both margins of the basin (Table 4-2). If the three joints sets in the Wamsutter area sets are indeed correlative with the sets in Upper Cretaceous rocks on the uplifts, then they represent intermediate to young members of a documented joint network of eight regional sets (Grout and Verbeek, 1992a).

### Age of Joint Sets

Two joint stations were established near an unconformity in the Paleocene lower

Fort Union Formation to gain further information on which of the eight recognized regional sets are of probable pre-Tertiary age. Station 59 is in steeply dipping beds (N16°W/59°W) below the unconformity; Station 60 is located above it in moderately dipping beds (N°3E/20°NW). Table 4-3 shows the orientations and relative ages of the tilted joint sets, and the bedding correction for tilt, both above and below the unconformity.

The oldest set below the unconformity, set F2 of Grout and Verbeek (1992a), is not present above it, suggesting that set F2 is of Paleocene (Fort Union) age and thus explaining its apparent absence from the younger Tertiary beds of the Wamsutter area. However, documentation of additional outcrops as the unconformity is traced north and south is required to see if this relation holds. The next set, whose joints strike WNW after tilt correction, is present both above and below the unconformity and correlates with the oldest set (J1 of this report; Table 4-1) documented in the lower Tertiary Wasatch Formation in the Wamsutter area. The youngest set is present only above the unconformity; whether or not this set postdates tilting of the beds is unknown, for its joints are nearly vertical both before and after the tilt correction is applied. This set correlates well with (1) the major set of prominent ENE-striking joints in the Upper Cretaceous rocks on the Rawlins Uplift to the south, (2) a similar major set in stratigraphically correlative rocks on the Rock Springs Uplift to the west, (3) the most prominent joint set in outcrops of Tertiary rocks in the Wamsutter area, and (4) a major set in the Upper Cretaceous subsurface rocks in the same area. This set of joints is the only one of eight sets known that is prominent throughout the region; fracture data from oriented core (Jaworowski and Simon, 1995; Hill, 1995) suggest that it is the dominant set in subsurface reservoir rocks as well.

Joints in the Miocene beds of the Browns Park Formation were documented at two localities on the southern part of the Rawlins Uplift to further bracket the absolute age of some of the younger joint sets of the region. A well-developed set of NNE-striking joints at both localities correlates to the Fc set (Table 4-2) of the Rock Springs Uplift; this set was found only recently on the Rawlins Uplift and is intermediate in age between the F5 and F6 sets of Grout and Verbeek (1992a). Also present within Browns Park Formation is a younger and equally well developed set of joints that corresponds to the F7 set on the Rawlins Uplift and the Ff set on the Rock Springs Uplift. These results suggest that the three youngest regional joint sets on both uplifts (Table 4-2) are of Miocene age or younger.

The J1, J2, and J3 sets in surface exposures of the Wamsutter area correspond to the F4, F5, and F6 sets, respectively, on the Rawlins Uplift (Table 4-2). The last of these is Miocene or younger in age; in the Wamsutter area it constitutes only a minor element of the fracture network in the Lower Tertiary beds. Ages of the prominent J2 and weakly developed J1 sets in the Wamsutter area remain somewhat loosely bracketed as probably a post-Wasatch and pre-Browns Park.

### **Relation of Joint Sets to Cordilleran Thrust Belt**

Face cleats (major joints) in coal-bearing units in the lower Tertiary Fort Union Formation and the Upper Cretaceous Mesaverde Group on the Rock Springs Uplift were measured by Laubach et al., 1992 and Tyler et al., 1993. These fractures strike N60-85°E. Face cleats of another, younger set strike N30-60°E. A still younger set of butt cleats, which terminate against the face cleats and strike northwest, complete the fracture network in the coals. Laubach et al.

**Table 4-3.** Orientations and relative ages of joints within the context of the Rawlins Uplift fracture history (Table 4-2; Grout and Verbeek, 1992a), in both tilted beds and beds corrected for rotation to horizontal, above and below the unconformity in the lower Paleocene Fort Union Formation. Location at Honey and Roberts' (1994) measured Sec. 10, 22 km northwest of Rawlins in small hogbacks of the Rawlins Uplift, 0.5 km east of Separation Creek, T22N, R89W, E1/2 Sec. 5, Shamrock Hills 7.5' quadrangle.

Station No.	Rawlins Uplift Joint-Set Designation		
	(oldest) F2	F4	(youngest) F5
Above Unconformity:			
60 (tilted N3°E/20°NW) Corrected		N77W/77NE N69W/84NE	N68E/86SE N68E/87NW
Below Unconformity:			
59 (tilted N16°W/59°SW) Corrected	N21W/32NE N20W/90	N82E/69NW N84W/86NE	

N21W/32SE = median joint strike of N21°W and median dip of 32° SE.

(1991; 1992) and Tyler et al. (1992; 1993) suggest that the face-cleats strike parallel to tectonic shortening directions and are at right angles to the Cordilleran thrust front. Any variation in face-cleat strike was suggested by them to reflect variation in fold-axis orientation in the foreland within the vicinity of the coalbeds. The orientations and relative ages of the two sets of face cleats on the Rock Springs Uplift correlate well with the Fd and Fc joint sets documented by Grout and Verbeek (1992a) in clastic rocks of the same area; strikes of the two sets are N6080°E and N25-45°E, respectively. Both of these sets are present on the Rawlins Uplift as well (Table 4-2), and one of them, the Fd set, corresponds to the major set documented both in outcrop and in core from the Wamsutter area. The sets thus are of regional extent and are present in both coal and clastic rocks alike. To date, we see nothing in the geographic distribution of these joints or in their relative prominence from one area to another to suggest any relation to thrusting. The presence of one of these sets in Miocene beds of the Browns Park Formation sug-

gests instead that the sets are due to post-Laramide regional extension, as shown by Grout and Verbeek (1992b) and Verbeek and Grout (1993) for several other basins farther south, on the Colorado Plateau. However, the possibility of local thrust-related joints in and near the Washakie Basin is not denied. Similar joints elsewhere, along the Colorado Plateau/Rocky Mountain foreland boundary in northwestern Colorado, are confined to the upper plates of low-angle thrust sheets. The influence of thrusting is felt for only a few kilometers into the basin (Grout et al., 1991; Grout and Verbeek, 1992b).

In the present report, we stress a complication in the integration of the regional tectonic and fracture histories of the Washakie Basin and its bordering uplifts. As noted repeatedly above, several of the youngest joint sets known from the region appear to be geologically young; this conclusion is based primarily on their presence in the Browns Park Formation. However, joints of the same sets—the F5 through F7 sets of the Rawlins Uplift—were noted by Grout and Verbeek (1992a) to be tilted

along the western flank of the uplift, where bed dips at three of the localities studied (Stations 16,17, and 41) range from 40° to 60°. These observations suggest either that the joint sets observed in the Browns Park Formation are not equivalents of those in older beds, or that some thrusting in the area is of much younger age than generally thought. Resolution of this problem will require more data than currently exist from the Browns Park Formation and from tilted beds along the flanks of the uplifts bordering the Washakie Basin.

## CONCLUSIONS

Paleocene sandstone lenses of the Wasatch Formation in the Wamsutter area contain (1) a minor set of subvertical joints that strike N69-N74°W, (2) a major set of subvertical joints that strike N61-84°E, and (3) a minor set of sparse, subvertical joints that strike N13°W (Table 4-1). Oriented core from subsurface Cretaceous rocks of the Almond Formation in the same area contains natural joints corresponding to the second of these sets (Jaworowski and Simon, 1995; Hill, 1995), which is the only prominent set of the three present in surface rocks. These ENE-striking joints most likely correspond to a major set of similar orientation in Upper Cretaceous rocks on the Rawlins and Rock Springs uplifts (Table 4-2). An excellent correlation thus appears to exist between joints in Tertiary and Cretaceous sandstones across the Washakie Basin. This suggests the presence of a unified, regional joint system across the basin rather than a disjointed series of local ones compartmentalized by faults. We recognize, however, that additional joints may be present near faults. Such joints, if present, most likely will prove to be restricted to zones a few meters wide adjacent to the fault surface. Despite their local nature, the faults and related joints could prove important to fluid flow if the faults are not sealed by relatively impermeable gouge and the joints by miner-

als precipitated within them. The detailed geometry of faults in the Washakie Basin so far remains unstudied.

Among the eight known joint sets in Upper Cretaceous rocks, the first three appear to predate an unconformity surface within the lower Paleocene Fort Union Formation and thus are of Late Cretaceous or early Paleocene age. These sets accordingly are expected to be absent from the bulk of the Tertiary section within the Washakie Basin. The other five sets are of post-Wasatch age or younger; the three youngest of these have apparent correlatives in Miocene beds of the Browns Park Formation. Bracketing the absolute ages of the various sets more closely will require additional work in the Tertiary part of the section.

The regional nature of the fracture network and the close correlation between fracture style and lithology suggest that properties of the fracture network in subsurface reservoir strata are potentially predictable from detailed outcrop studies.

## ACKNOWLEDGMENTS

Funding for M.A. Grout and E.R. Verbeek was provided by the U.S. Geological Survey Energy Resources Surveys and National Geological Mapping programs. Funding for C. Jaworowski was provided by the Institute for Energy Research, University of Wyoming and the Gas Research Institute under Contract No. 5091221-2146. We thank Niels Hansen for access to private land in the Wamsutter area.

# Chapter 5

## Oil And Gas Production Data

*William P. Iverson*

### ABSTRACT

Our study area includes 181 defined oil and gas fields in Wyoming. Production from these fields is extremely variable in terms of both volume and composition. Most of the fields are classified as gas fields (GOR>100Mscf/bbl), although the largest fields are oil producers or gas-condensate reservoirs. Boundaries of some of the larger fields correlate with the lineaments and linear features defined by remote sensing techniques. Although a lineament itself cannot confine hydrocarbons, it does influence the sediments and structures that have led to the development of structural and stratigraphic traps. Thus, the use of lineaments in hydrocarbon exploration should be considered as another tool aiding an exploration strategy, but not as an absolute, independent delineation strategy.

### INTRODUCTION

Data on linear features, joints, and lineaments can be of value in planning field development. It is well known that in Wyoming Laramide basins, highly productive gas wells occur along producing trends. Although an individual well provides data at only one point, this data point can be extrapolated in the context of a producing trend with lineaments defined through independent remote sensing techniques. For example, in the Washakie Basin study areas presented in this report, the highly productive trends are bounded by lineaments. A lineament can be used to differentiate between productive and nonproductive areas. It may also represent the boundary between areas with slightly

different geologic histories (e.g., differences in deposition, uplift, or diagenesis; the exact mechanism often cannot be defined).

Wells are often drilled on both sides of defined lineaments, but typically only one side is productive. Field development should proceed on the productive side, as development is difficult when a lineament is crossed. On the productive side, wells are put into production and little analysis generally is undertaken. On the non-productive side, a sand that is apparently equivalent to the producing sand can be identified, but generally the sand is too tight or too difficult to produce gas from successfully. These sands receive considerable attention, as their lack of production is frustrating when geologically similar sands nearby are quite productive.

Such concentrated attention to nonproductive wells has been applied to two detailed study areas in the Washakie Basin where Amoco drilled horizontal wells. The sands in these study areas definitely contain gas, but have experienced something in their geologic history to make them tight and unproductive.

This chapter presents only gas production data in the regions discussed in previous chapters of this report. It presents details of the production data used for comparison with linear features and lineaments. Previous chapters should be consulted for discussion of the linear features and lineaments.

### DATA SOURCES

Oil and gas production data within the State of Wyoming are tracked by the Wyoming Oil and Gas Conservation Commission

(WO&GCC), in Casper. Annual summaries list all named fields in the State, their location, number of wells, current production, and cumulative production. Data in this chapter are extracted from the most recent book available, published in 1994, and are cumulative to January 1, 1994. As this study deals with production trends and not with detailed production specifics, these data are considered sufficiently accurate. Field production statistics are presented in the first half of this chapter.

Individual well production is also tabulated by the WO&GCC, but not published directly. Data from individual wells are summed by WO&GCC into field production figures, and released as field totals as discussed above. Individual well production figures cited in the second half of this chapter use data compiled from Petroleum Information (PI), published in 1995; thus, individual well production data for the detail study areas is current as of January 1, 1995.

### FIELD PRODUCTION: FIELDS IN STUDY AREA

A simple oil and gas map of the State of Wyoming (DeBruin and Boyd, 1991) gives the impression that the Washakie Basin is covered with many productive fields. Upon more detailed examination, most of the defined fields are found to be nearly insignificant. Economically significant fields correlate well with lineaments.

For purposes of compiling production data, the study area of this chapter is defined as T12N through T28N and R88W through R105W, in Wyoming. There are 181 named oil and gas fields in this area; they are listed in Appendix A. These fields have produced a cumulative total of 4.2 Tcf of gas and 531 MMbbl of oil and condensate. Production records do not distinguish true crude from gas condensate, but list both as oil.

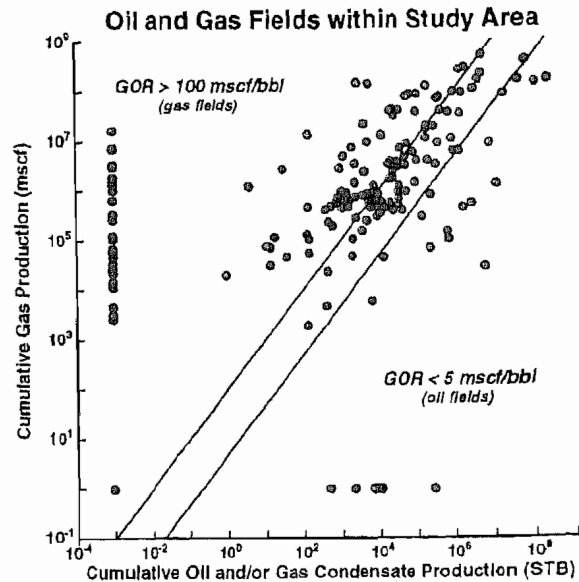


**Figure 5-1.** Cumulative gas production versus cumulative oil production for the 181 fields in the study area. Vertical line of points represents dry gas producers, with no oil or condensate reported by the WO&GCC.

Figure 5-1 presents cumulative gas production versus cumulative oil production for the 181 fields within the study area. The vertical line of points on the left side represents dry gas producers, with no oil or condensate reported by the WO&GCC. Most of these fields do produce condensate, but in such small quantities that it is used up or disposed of on site. To avoid a zero error on logarithms and ratios, the dry gas fields are assigned an arbitrary production of 0.000999 bbl of oil. The horizontal line of points on the lower right side represents the few oil fields of the study area with zero gas production reported. An arbitrary 0.999 Mcf of gas is assigned to these fields to avoid zero errors. A single point near the origin represents the named fields that have yet to produce any reported gas or oil.

Most fields in the study area display gas-oil ratios above 5000 scf of gas per barrel of condensate (Figure 5-1); thus, this area is considered to be a gas-producing region. The two sloped lines in Figure 5-1 represent gas-oil ratios of 5000 scf per

barrel and 100,000 scf per barrel, the cut-off values commonly used to distinguish oil wells from gas-condensate wells and gas wells. The importance of liquids production in this region should not be ignored. In fact, the most economically productive fields are oil fields with very low gas-to-oil ratios. The next most significant fields are gas-rich condensate reservoirs, in which, again, liquids production must be considered.

Estimates of the gross hydrocarbon production in billion standard cubic feet equivalent (Bscfe) of both oil and gas are used as measures of total production. Exact equivalence between oil and gas is a function of composition for each component, the heating value in Btu, the expansion of gas from the reservoir, shrinkage of oil, and the separation of free gas from solution gas from gas-condensate. A universal factor cannot be derived for the entire basin, so a more economic approach (in terms of time and real dollars to operators) is taken. Because cumulative production across many decades of price and market fluctuations complicates production estimates, historical values are not used in estimates of Bscfe. At present, gas is selling in this region for slightly over \$1 per Mcf (up to \$1.50), but when long-term cumulative production is considered, the low prices of a few years ago must be considered. Conversely, oil is well below \$20/bbl at present (about \$17/bbl), but much of this oil is condensate, which has garnered higher prices in recent years. A simple estimate of net present worth (NPW) is made by approximating one Mscf of gas as \$1, and one bbl of oil or condensate as \$20; one barrel of oil would therefore be equivalent to 20 Mscf of gas. Thus, a rough value of estimated cumulative production can be obtained from cumulative (gas + (20 × oil)) in terms of dollars, dividing by 10<sup>6</sup> to obtain Bscfe in millions of dollars. Each million units from this calculation is roughly one billion cubic feet of gas (Bscfe).

Some explorationists use a 1:5 or 1:10 ratio, rather than the 1:20 ratio used in the preceding estimates. These lower numbers

tend to place less emphasis on oil production. Because this area produces rich condensates, which are of great value to operators, if a 1:5 ratio were used here, fields like Patrick Draw or Arch would appear to be no better than Echo Springs. All of these fields are significant, but Patrick Draw and Arch are considered to be more productive due to the condensates present. Thus, a 1:20 ratio has been used for economic reasons.

Figure 5-2 shows this defined worth for each of the 181 fields in the study area plotted against year of discovery. This plot is used to separate these 181 fields into four categories as listed in Appendix A. The *largest* fields are those that have produced over 500 Bscfe (\$500 million), as calculated above. *Significant* fields have produced 50-500 Bscfe (\$50-\$500 million), *small* fields have produced 5-50 Bscfe (\$5-\$50 million), and *smallest* fields have produced less than 5 Bscfe (\$5 million). When production is less than 5 Bscfe (\$5 million), a field is considered to be unprofitable to marginal.

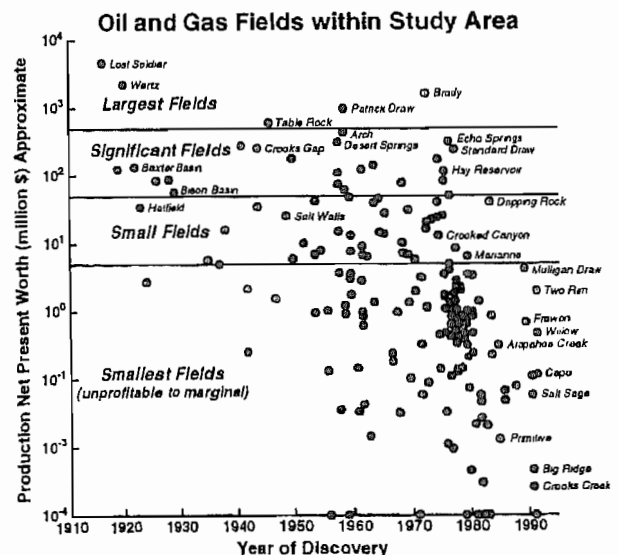


Figure 5-2. Defined worth for each of the 181 fields in the study area plotted against year of discovery. This plot defines the four categories of fields as described in the report and as listed in Appendix A.

This classification scheme provides a rough estimate of where the significant hydrocarbon accumulations exist within the study area. In summary,

Category	Gross Production (NPW)
Largest Fields	= >500 Bscfe (> \$500 million)
Significant Fields	= 50-500 Bscfe (\$50 to \$500 million)
Small Fields	= 5-50 Bscfe (\$5 to \$50 million)
Smallest Fields	= < 5 Bscfe (<\$5 million)

Gas is cumulative gas production in Mcf and oil is cumulative oil and condensate in bbl.

The *largest* fields in this area include Lost Soldier and Wertz, which are both located on top of a classic shallow anticline above a thrust fault. These fields were discovered on the basis of surface geology 75 years ago, and continue oil production to date. Brady, the third largest field in the area, is a deep dome structure that required seismic data for discovery. A dozen pay intervals are productive at Brady. Patrick Draw and Arch are two productive units within a single producing trend of the Cretaceous Almond Formation, which is the only stratigraphic field of the largest fields; all other fields are structural traps. Table Rock is another structure that is productive from a dozen intervals; it has been a prolific producer over the years. These four areas account for 75% of the total production from the study area.

*Significant* fields in the study area are mostly stratigraphic plays, such as the Echo Springs - Standard Draw producing trend from a barrier bar sand within the Almond Formation. The Hay Reservoir is a significant sand body encapsulated within the Lewis Shale. In general, the significant gas and gas-condensate fields tend to be stratigraphic traps, while the few significant oil fields (e.g., Mahoney Dome) are structures. The 23 significant fields in the study area have produced 26% of the dollar value of hydrocarbons.

*Small* fields, mainly stratigraphic plays, contribute a little less than 1% of the total dollar value of hydrocarbon production within the study area. A few of these fields were only recently discovered (e.g., Dripping Rock, Mulligan Draw), and will probably become significant fields in the future.

Another 114 *smallest* fields, most them abandoned or not yet developed, exist within the study area, but have contributed only 0.06% of the total production in this area. Again, some of the recent discoveries (Two Rim, Frewen, Willow) have promise of becoming significant fields in the future, but have yet to prove their potential.

## INDIVIDUAL WELL PRODUCTION: DETAILED STUDY AREAS

In a sense, the exploration for gas in the Washakie Basin is trivial; no matter where one drills, eventually one will encounter significant quantities of gas within the Cretaceous sands. The real exploration problem is to find sands capable of producing gas economically. Amoco Production (Denver, Colorado) selected two sites where developing such sands was particularly frustrating, the Wamsutter and Red Desert areas. Both display good gas shows and each is within a few miles of highly productive areas; geologically equivalent sands can easily be correlated between the productive and the nonproductive wells.

Horizontal wells were thought to be a possible solution to the production problem primarily for two reasons. First, the oriented natural fractures could possibly be transversed perpendicularly to intersect more fractures and, thus, enhance production from the fractures. Second, a horizontal well would expose more sand surface to the wellbore and possibly add additional pay into the wellbore. Drilling such a well would also allow lateral changes in geology to be recorded, which is not possible in a routine vertical well. In this context, both horizontal wells were technical successes. However, the

wells were not economically viable; the additional gas produced could not cover the higher costs of horizontal drilling.

### Detailed Study Area 1: Wamsutter Area

As discussed in Chapter 2, the first horizontal well, Champlin 254 Amoco B 2H in the Wamsutter area of the Washakie Basin, has been the focus of attention for studying the relationship between fractures, lineaments, linear features, and production.

The Champlin 254 Amoco B 2-H vertical parent well, Amoco B-1, is located on the northern fringe of the Echo Springs field and represents the far northern extension of this significant gas field (Figure 5-3). Figure 5-3 clearly shows the northern end of the Echo Springs - Standard Draw producing trend,

which is centered to the south in T18N-R93W, where NPW production exceeds \$30 million for some prolific wells. An infill drilling program was initiated in 1992 to drill Echo Springs on 320-acre spacing. These infill wells were omitted from the contour map (Figure 5-3), as their cumulative production has not yet reached economically significant levels. Many of the infill wells currently produce at rates higher than the original wells within the same sections; production from the original wells has declined exponentially at approximately 10% per year.

There is a marked change in sand productivity in this area, with no comparable change in well-log response. Numerous explanations have been given for this discrepancy, including natural fractures, diagenesis, and tidal channel inlets. In any case, a major lineament at the north edge of

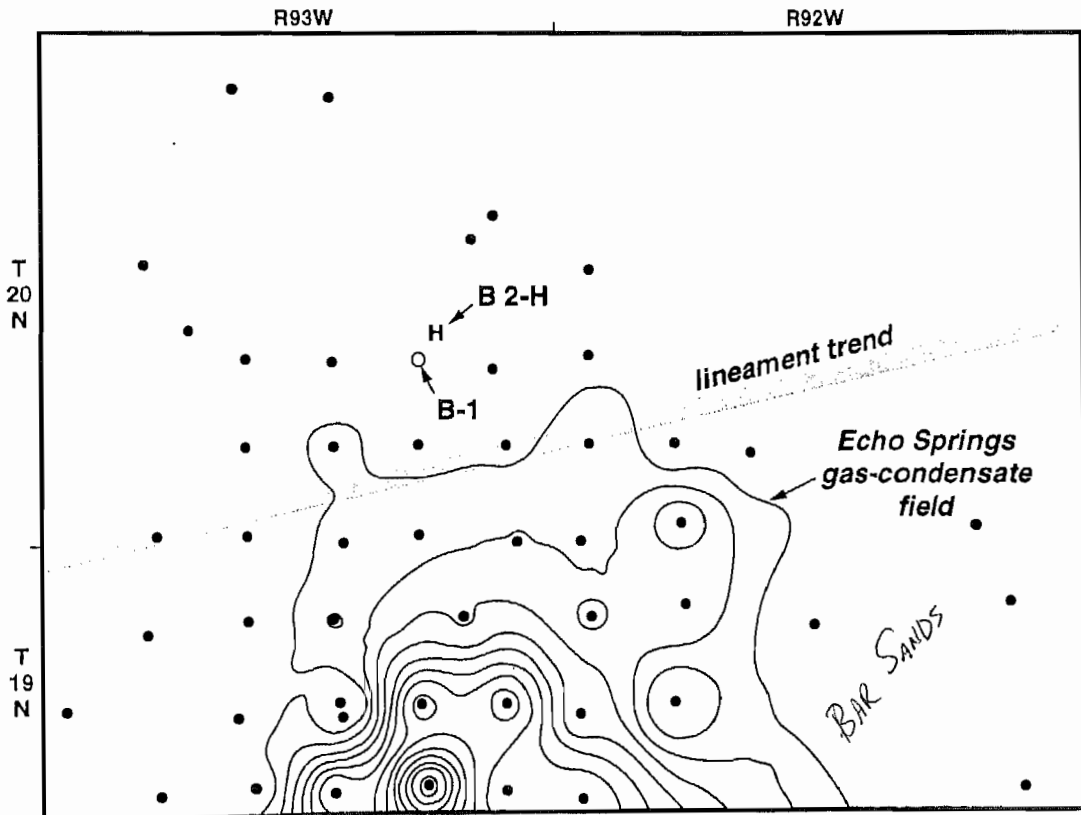


**Figure 5-3.** Contour map of the net present worth (NPW) of individual wells in this area, defined as (gas + (20 × oil)) for an estimate of the dollar value of cumulative production. The minimum contour level is 3 Bscfe (\$3 million).

Echo Springs appears to coincide with this abrupt change in sand productivity. Well logs from the Amoco B-1 well are shown in Figure 5-4. Comparison of these logs with logs from PTS #14-4 (Figure 5-5), a prolific Echo Springs producer, indicates a general similarity in log character. Both wells contain roughly 20 feet of sand at about 12% porosity and 80 ohm-m resistivity, but the Amoco B-1 has produced only 2 Bcf, while the PTS #14-4 has produced 20 Bcf. Cumulative production

from the Amoco B-1 well is 2.2 Bcf gas and 16 bbl condensate, for an approximate net worth of \$2.5 million. The Amoco B-1 well is probably economically profitable, but is marginal compared with the 20-Bcf wells to the south. Thus, Amoco chose to drill the first horizontal well in this area to determine if production could be improved.

The Champlin 254 Amoco B 2-H well was one of the first attempts to enhance gas production from tight gas sands by drilling

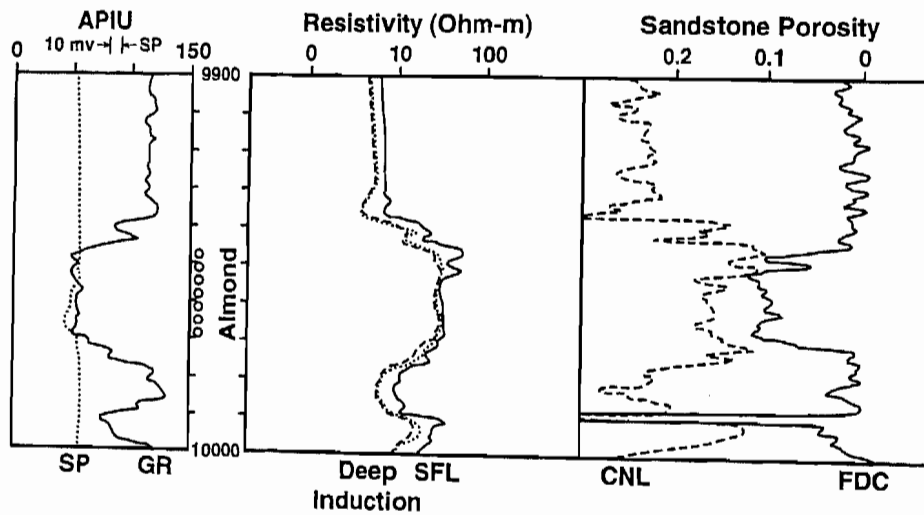


Figure 5-4. Well logs from the Champlin 254 Amoco B 2-H well in the Wamsutter area.

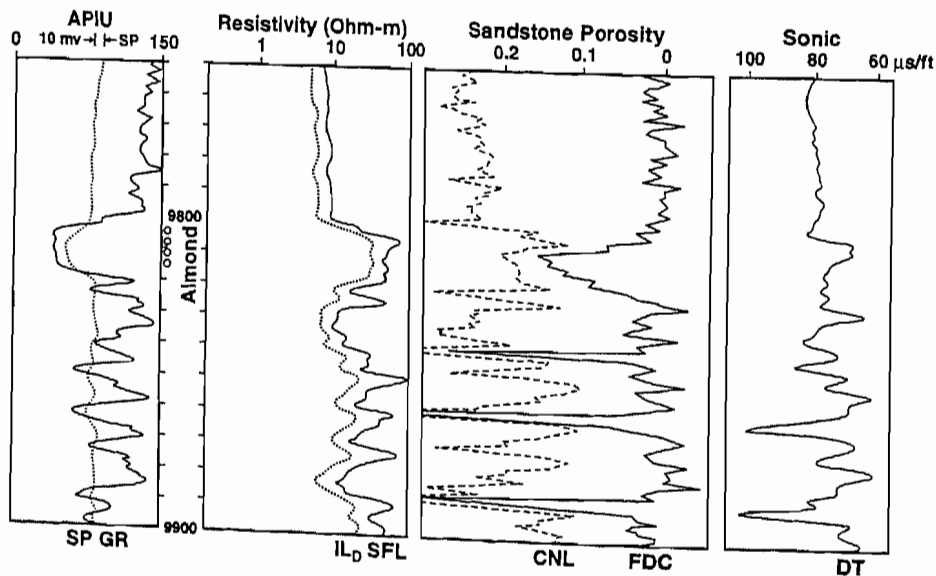


Figure 5-5. Well logs from PTS #14-4 well, a prolific Echo Springs producer with log character similar to the Champlin 254 Amoco B 2-H well.

horizontally in a direction thought to be perpendicular to the natural fracture planes. As stated above, it was hoped that the lateral extent of a horizontal well would replace the need for massive hydraulic fracturing and, overall, would offset the additional cost of drilling a horizontal well. It was also hoped that increased gas production from these wells would help compensate for the higher drilling costs.

Oil and gas production data from the area around the Champlin 254 Amoco B 2-H horizontal well have been tabulated from Petroleum Information and contoured to show the producing trend. Figure 5-3 shows a contour map of the gross hydrocarbon production in billion cubic standard feet equivalent (Bscfe) of individual wells in this area, as defined above, used to estimate the dollar value of cumulative production. The minimum contour level is 3 Bscfe (\$3 million); as a gas well in this area costs nearly \$2 million to drill, complete, fracture, and operate for the ten years needed to obtain economic production, the 3 Bscfe (\$3 million) cutoff ensures that all wells represented will be profitable.

Unfortunately, the horizontal well did not significantly improve production. The plane of fracture orientation was very accurately predicted by joints and linear surface trends (Chapters 2 and 4, this volume), but the enhancements to production via horizontal drilling were disappointing. There appear to be various geologic differences between productive and nonproductive regions in the Wamsutter area; their relation to the present study has yet to be explored. In any case, that the boundary between these regions correlates nicely with a distinct lineament indicates that the use of lineaments as exploration tools is viable.

### Detailed Study Area 2: Red Desert

As discussed in Chapter 2, the second horizontal well drilled by Amoco in 1994, Champlin 320 C-1A-H, was located in the

Red Desert area, Sec. 1-T22N-R96W (Figure 5-6). Figure 5-6 shows high production northwest of this area in the Great Divide gas field, which is a small field. The isolated producing wells in the center and southeast of the Red Desert area are part of the Lost Creek gas field, a smallest field. Lost Creek has not yet produced enough gas to even pay-out the first well in the field. For this field to ever turn a profit will require either many years or significant changes in the gas industry. The Great Divide field produces both gas and condensate, and is probably profitable even at today's low gas prices.

The Great Divide gas field is bounded on the southeast by a photo-linear feature (Figure 5-6). This linear feature does not correlate directly with productive regions of the area, but does coincide with a production boundary. North of this linear feature, some sands have proven productive, but the sands to the south are very tight, have few natural fractures, and are not easily stimulated by hydraulic fracturing.

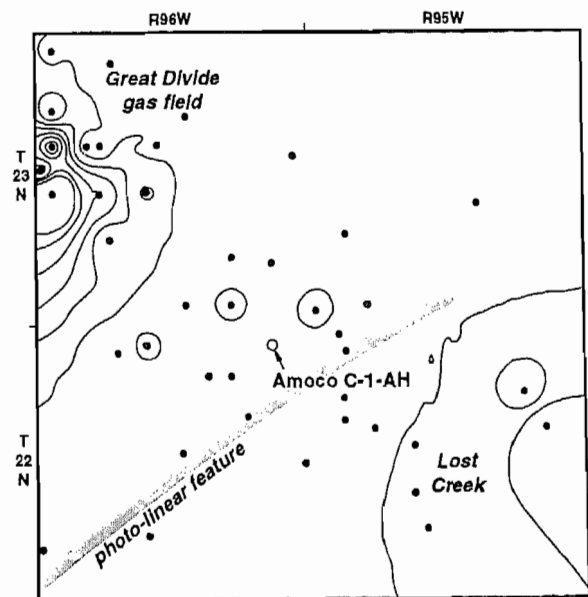


Figure 5-6. The Red Desert study area, including Great Divide and Lost Creek gas fields, in which the second horizontal well, Champlin 320 C-1A-H, was drilled.

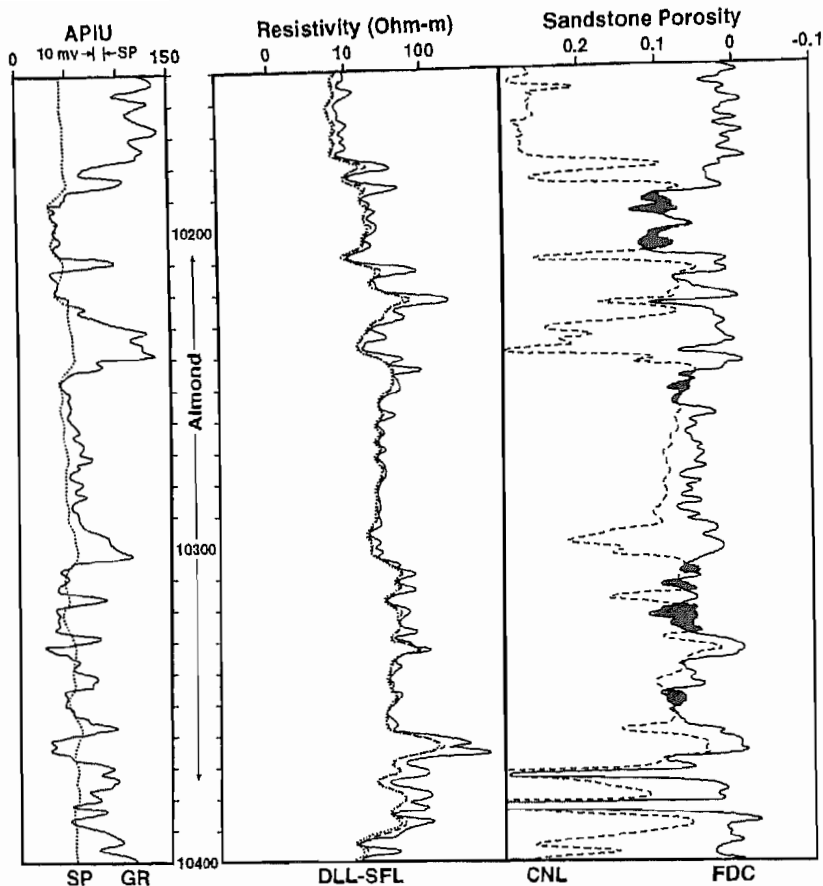


Figure 5-7. Well logs from the vertical parent of the horizontal well Champlin 320 C-1A-H (grain density of 2.68 gm/cc).

Well logs from the vertical parent of the Red Desert well are shown in Figure 57. Although numerous sands in the upper Almond Formation have fair porosity and gas crossover in neutron-density, no commercial production has been obtained from the wells penetrating them, even after extensive hydraulic fracturing and stimulation. This is what prompted Amoco to attempt a horizontal completion along the obvious gas-bearing sandstones. The Champlin 320 C-1A-H well was not successful at reaching commercial levels of gas production and, thus, was abandoned.

## CONCLUSIONS

Lineaments and linear features have been shown to correlate with structure, stratigraphy, and fractures in this report.

Although the dominant structural trends correlate very well with major lineaments, the precise localization of fields will require other, independent means to define the structural highs where oil and gas fields are discovered. Stratigraphic trap boundaries are often reflected by the presence of lineaments; the margin of a producing trend from a stratigraphic trap is often coincident with a lineament. The orientation of subsurface natural fractures can be accurately predicted from surface linear features and joints.

Structural plays appear to correlate most directly with lineaments. Fields such as Lost Soldier and Table Rock are structurally controlled by the presence of thrust faults; these fields lie along lineaments, but in positions that are relatively high. Because thrust faults are easily

correlated to lineaments, the next exploration question becomes how to find the tops of these structures, as vertical relief along anticlines is probably not reflected by lineaments.

Stratigraphic traps are localized by a complex interaction of processes that leaves productive sands in isolated locations. The processes can be associated either with primary deposition (e.g., in a valley) or with subsequent diagenesis (e.g., along the downthrow of a fault). Either way, these processes often enhance gas production in some areas but not in others, in effect creating a boundary between productive and nonproductive sands. While the processes involved are often too complicated to completely describe, the boundary that results from them can often be well recognized after enough wells have been drilled. Alternatively, a lineament may imply the location of a producing trend boundary, or at least the orientation of the boundary, which may result in lower exploration risk.

A productive well in the vicinity of a distinctive lineament implies that the next drilling location should be offset from the productive well in a direction parallel to the defined lineament. Such boundaries do not provide direct definition of precise locations to drill, but can be used as factors in sorting out exploration prospects. Every development company has countless drilling prospects to select from, seldom with an obvious definitive reason to select one site over another. The selection is usually based upon maximum likelihood of success as measured by many techniques. Definition of lineaments provides another tool in that selection process.

That lineaments correspond very well with the orientation of natural fracturing may be quite valuable in field development when natural fracturing is the primary mechanism of oil and gas production. In such a field, horizontal drilling is best oriented perpendicular to the plane of natural fractures. The determination of

wellbore trajectory in new horizontal drilling projects should be guided by consideration of surface trends.

Unfortunately, gas production in the Washakie Basin does not appear to be primarily controlled by natural fractures. They exist, but they cannot solely account for the producing trends of the significant fields. However, it is interesting to note that the Champlin 320 C-1A-H well encountered very few natural fractures, while the Champlin 254 Amoco B 2-H encountered many natural fractures. Even though production did not improve as much as expected in the Wamsutter well, it still was more successful than the Red Desert well; evidently, the subsurface fractures may have had some impact on productivity.

The correlation of linear features with natural fracture trends and of lineaments with production boundaries in the Washakie Basin are successful results of the present study. Although such correlations have yet to yield economically significant results, the potential to use lineaments, linear features, and regional features as exploration tools that can help to define production boundaries and lower exploration risk in economically viable wells is very good.

## **ACKNOWLEDGEMENTS**

The author wishes to thank the Gas Research Institute for supporting this study under contract no. 5091-221-2146. Kathy Kirkaldie and David Copeland provided editorial assistance.

## Chapter 6

# Automated Recognition Of Lineaments From Linear Features

*Robert Simon and Cheryl Jaworowski*

### ABSTRACT

This study and others indicate that recurrent movement along basement-related faults is an important mechanism influencing the overlying sedimentary section in Rocky Mountain basins. A program is being developed to map these basement-related faults (lineaments). This program is intended to be used with other datasets to generate a more reliable (i.e., reproducible) map of lineaments than currently exists. Ideally, this computer-generated map of lineaments would be compared visually and digitally with a human-interpreted map of lineaments to illustrate biases in both maps. The ultimate result of this effort will be the most accurate map of basement-related faults (i.e., lineaments) available.

Our initial attempt to use a Hough transform to map lineaments from a simple image identifies many northwest-trending lineaments and shows limited success in identifying the prominent east-northeast and north-east-trending lineaments recognized by numerous researchers in the Greater Green River Basin (GGRB). Continued testing of an algorithm to map lineaments from a simple image of linear features or a complex satellite image is needed to map geologically relevant lineaments.

### INTRODUCTION

As previously discussed in Chapters 2 and 4, surface lineaments may correspond to basement faults and influence hydrocarbon production by affecting sedimentary thickness, facies, and structure. Since the

advent of satellite imaging, many researchers have identified lineaments—zones of structural discordance—on satellite images for hydrocarbon exploration, mineral resources, hydrogeology, neotectonic study, geothermal resources, and geologic mapping (Berger, 1994; Brown, 1994; Goetz and Rowan, 1983; Lang et al., 1987; Mason et al., 1994; Sabins, 1987). Methods that standardize and automate lineament identification, as well as integrate lineaments with other sources of geologic data, have been a goal of numerous research efforts (Marrs and Raines, 1984; Oldfield, 1988; Saether et al., 1991; Raghavan, 1994, 1995; Foley, 1991; Zlatopolsky, 1992).

The terms lineament and linear feature are defined differently by various authors (Hoppin, 1974; Saether et al., 1991; Raghavan et al., 1994). We follow the definitions proposed by Hoppin (1974). According to Hoppin (1974), lineaments are “generally rectilinear lines or zones of structural discordance of regional (100 km or longer) extent,” and linear features are “...single rectilinear elements commonly, but not necessarily, of structural origin.”

In an attempt to test our identification of surface lineaments derived from SPOT satellite images, we developed and tested a program that generated lineaments from small linear features. Using a human interpreter, structural linear features on digital satellite images were recognized by changes in grey-levels on SPOT panchromatic images. The program uses a Hough Transformation to derive the large, regional lineaments from small, local linear features.

The algorithm is an extension of a program developed by R. Simon in a University of Wyoming digital image processing class. We hope to replace a "human" edge filter by an algorithm that reliably maps structural linear features.

## PREVIOUS STUDIES

Raghavan et al. (1994) attribute the limited use of automated techniques of lineament extraction in part to the lack of ready-to-use computer programs. Automated extraction of lineaments from digital satellite images typically is broken into two logical parts: (1) enhancement of edges and lines and (2) detection of edges. Application of a directional gradient filter to the satellite image and thresholding of the filtered image is a common pre-processing approach to edge enhancement for lineament extraction (Sabins, 1987; Saether et al., 1991; Zlatopolsky, 1992). Nonfiltering approaches to detect grey levels and extract lineaments from a digital image have also been developed (Desai et al., 1994; Raghavan et al., 1995). Raghavan et al. (1995) developed a segment tracing and rotation transformation algorithm that can be adjusted to delineate linear topographic and geologic features such as valleys and dike swarms. Desai et al. (1994) used artificial neural networks for edge enhancement and detection of geological lineaments. We follow Duda and Hart's (1972) use of the Hough transform to detect linear trends.

## THE HOUGH TRANSFORMATION ALGORITHM

We will not attempt to describe the Hough Transformation Algorithm completely. For a complete description of the algorithm see Duda and Hart (1972). We will discuss only those concepts that are relevant to the input parameters of our program.

In order to use the Hough Transformation, a two-dimensional parameter space is selected such that lines in the plane of the original image are mapped to points in the

parameter space. We choose to use the parameterization suggested by Duda and Hart (1992),

$$x \cos \theta + y \sin \theta = \rho.$$

See Figure 6-1 for a geometric representation of the parameterization.

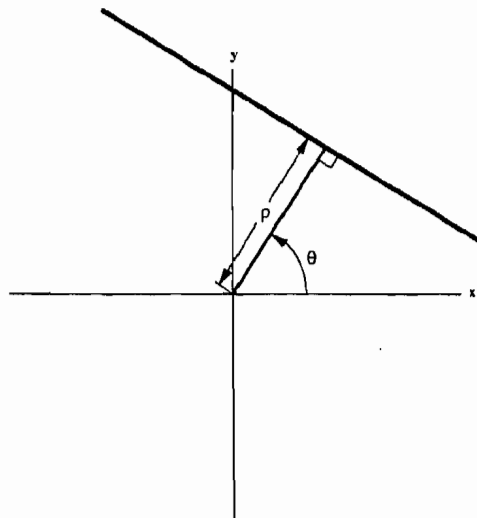
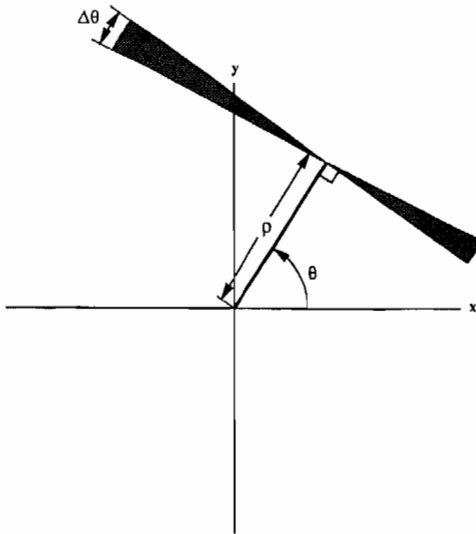


Figure 6-1. Parameterization of a line

The parameter space is discretized by approximating the  $r$ - $q$  plane by an  $N$  by  $M$  array,  $H(r, q)$ . This array,  $H$ , is sometimes called the *Hough accumulator*. The difference in  $r$  between consecutive elements of  $H$  is denoted as  $\Delta\rho$  and the difference in  $q$  as  $\Delta\theta$ . That is,

$$\begin{aligned} \Delta\rho &= H(i, j) - H(i-1, j), \\ \Delta\theta &= H(i, j) - H(i, j-1). \end{aligned}$$

With the discretization of the parameter space, points in the parameter space are mapped to areas in the image space. Figure 6-2 shows the general shape in the image space of a point in the parameter space when  $\Delta\theta$  is large compared to  $\Delta\rho$ ; Figure 6-3 shows the area when  $\Delta\rho$  is large compared to  $\Delta\theta$ . We will say that a



**Figure 6-2.** Shape in the image space of a point when  $\Delta\theta$  is large.

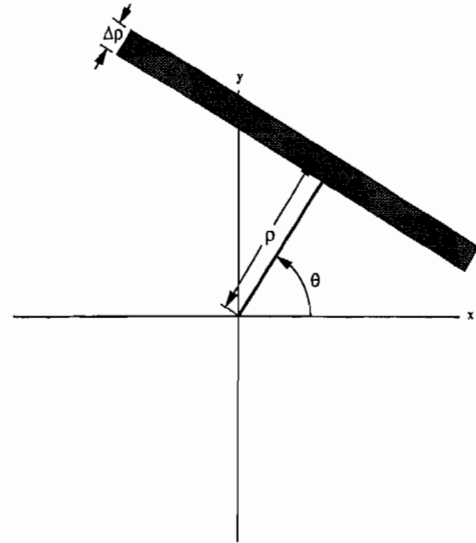


**Figure 6-3.** Shape in the image space of a point when  $\Delta\rho$  is large.

pixel in the image plane belongs to the line  $l(\rho_0, \theta_0)$  if the pixel is inside the area mapped from the point  $(\rho_0, \theta_0)$  in the discretized parameter space. Note that a pixel belongs to many lines, in fact  $M$  of them. The Hough transform chooses the lines with the highest counts of belonging pixels.

We have found that the algorithm chooses more reasonable lines if a relatively small  $\Delta\theta$  is chosen such that the area belonging to a line is more like that in Figure 6-3. Choosing a relatively large  $\Delta\theta$  (as in Figure 6-2) is more likely to result in the algorithm choosing a line between two clusters of pixels that are separated by a large distance, with one cluster on each end of the line.

## MODIFICATIONS TO THE ALGORITHM

The Hough Transform in its simplest form finds the most prominent lines that continue through the entire image. There may be strong lineaments that do not cross the entire image, and these may not be treated as particularly strong lines by the algorithm. The program allows lineaments to be found on different scales by partitioning the image into sections. Then the Hough

transform is performed on each of these subimages. This allows the user to choose the approximate scale of the lineaments being searched, but does introduce a bias against lineaments spanning the arbitrary sections of the image. This problem is alleviated somewhat by making the sections overlap. The overlap was set at 20% for images in this report.

The program also attempts to eliminate portions of a line that are not associated with pixels in the image. This is accomplished by extending the lines only to the last pixels of the image, not the entire image or section of the image. A future improvement may be to consider the density of pixels along a line and accept only segments of that line above a specified density.

## TESTING THE PROGRAM WITH SYNTHETIC INPUT

There are four input parameters for the program. The first three parameters, discussed in previous sections, are  $\Delta\theta$ ,  $\Delta\rho$  and the number of sections into which to split the image. The input for the number of section specifies the number of sections in the  $x$

direction. The program chooses a number for  $y$  that maintains a roughly one-to-one aspect ratio for each section. The fourth parameter is the minimum number of pixels of the input image that must belong to a line in order for the line to be output. Changing the minimum number of pixels does not affect the location or size of any of the lineaments; it only changes the number of lineaments output by the program. If all other parameters are held constant, then the set of lineaments output with a higher minimum number of pixels is a subset of the lineaments output with a lower number. This fourth

parameter is used to adjust the total number of output lineaments.

We found that  $\Delta\theta$  should be kept small, on the order of one or two degrees. The number of sections chosen appears to have the most impact on the nature of the lineaments. Recall that altering the number of sections essentially changes the scale on which the lineaments are found, that is, the length of the lineaments. We usually had a number of sections in mind and then tweaked  $\Delta\rho$  and the minimum number of pixels in order to get reasonable results.

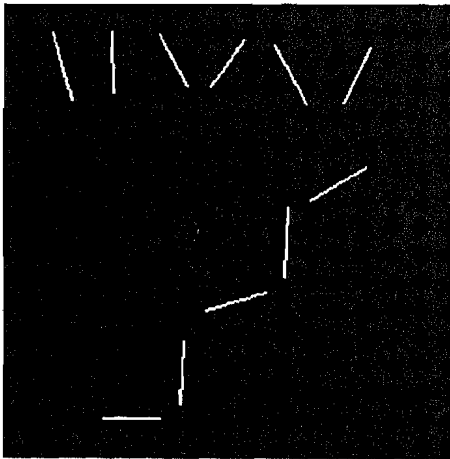


Figure 6-4. Input for test.

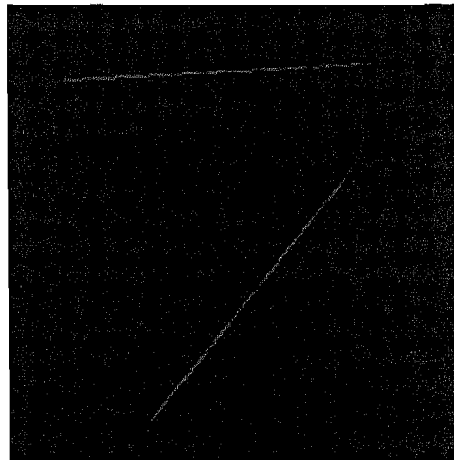


Figure 6-5A. Output for test using various parameters.  $sections = 1$ ,  $\Delta\rho = 10$ ,  $minipixels = 60$ ,  $\Delta\theta = 1$ .

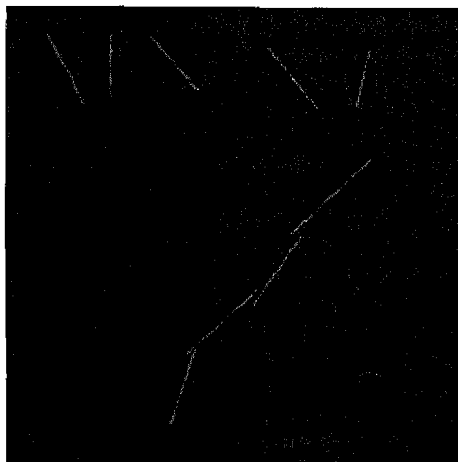


Figure 6-5B.  $sections = 4$ ,  $\Delta\rho = 10$ ,  $minipixels = 30$ ,  $\Delta\theta = 1$ .

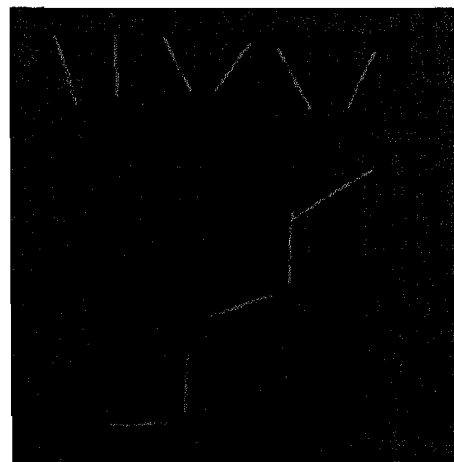


Figure 6-5C.  $sections = 8$ ,  $\Delta\rho = 1$ ,  $minipixels = 10$ ,  $\Delta\theta = 1$ .

A simple set of test linear features and the resulting lineaments generated by the program are shown in Figures 6-4 and 6-5A-C.

### TESTING THE ALGORITHM: DRAWING LINEAMENTS FROM LINEAR FEATURES

Application of the algorithm to the nearly 17, 300 linear features mapped over a 6430 mi<sup>2</sup> (16,655 km<sup>2</sup>) area of the east-central Greater Green River Basin shows limited success in identifying major east-northeast, northeast, and northwest-trending lineaments (Figures 6-6 through 6-9). The number of sections into which an image is partitioned (in the direction of the x-axis) is a significant variable. The longest lineaments are drawn when an image is partitioned into six sections (Figure 6-6). The "best" lineaments are drawn by increasing the number of sections (from 6 to 24), decreasing the value of mini-

mum pixels (from 300 to 90) and decreasing the value of  $\Delta\rho$  (from 30 to 10) (Figure 6-9). In order to draw "reasonable" lines,  $\Delta\theta$  is kept small and constant (2) in all tests (Figures 6-6 to 6-9).

Many significant east-northeast and northeast trends were not drawn by this algorithm. However, the algorithm did define more northwest-trending lineaments not drawn by the image analyst. Northwest-trending lineaments are expected in the Greater Green River Basin. The drawing of lineaments from linear features is a simple test of an algorithm's ability to define linear features or lineaments from a more complex satellite image. Continued work on automated recognition of lineaments from simple images of linear features and more complex satellite images is needed to generate a map of lineaments that reliably shows the most prominent east-northeast lineaments. The initial test of a Hough transformation in

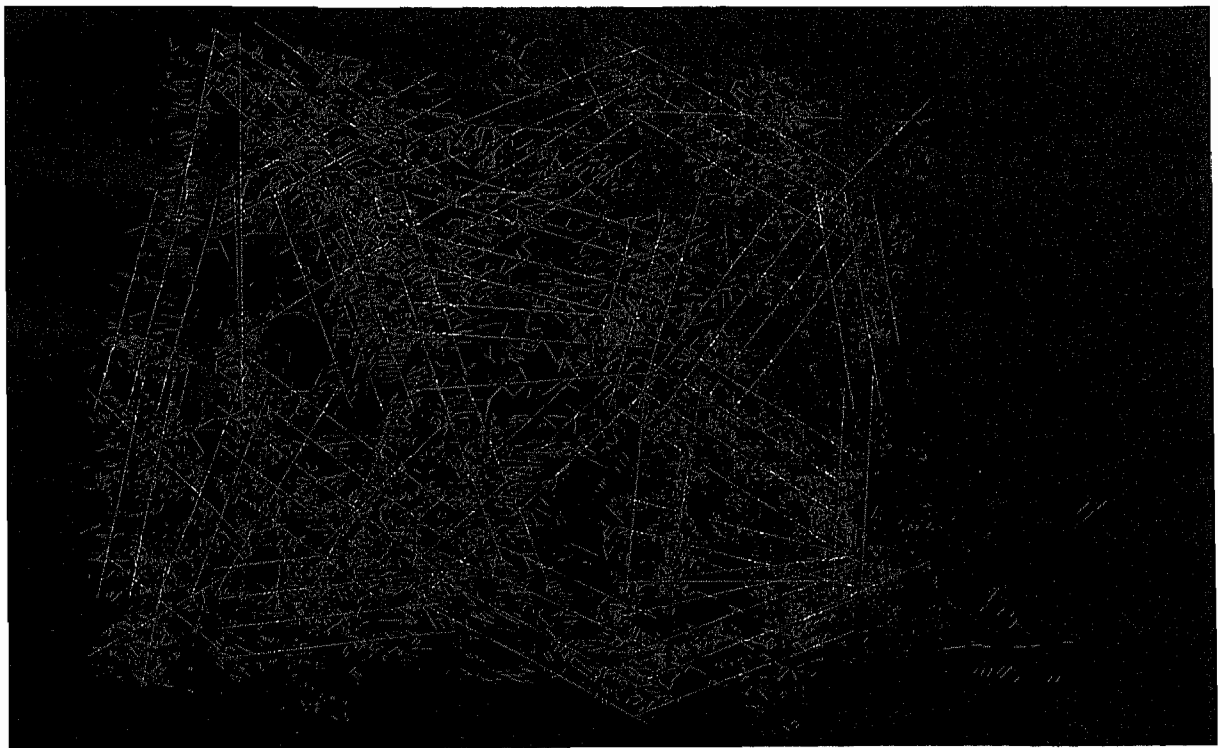


**Figure 6-6.** Parameters set to draw large lineaments: number of sections 6, minimum pixels 300,  $\Delta\rho$  30 and  $\Delta\theta$  2. Red lines represent linear features, and green lines represent lineaments.

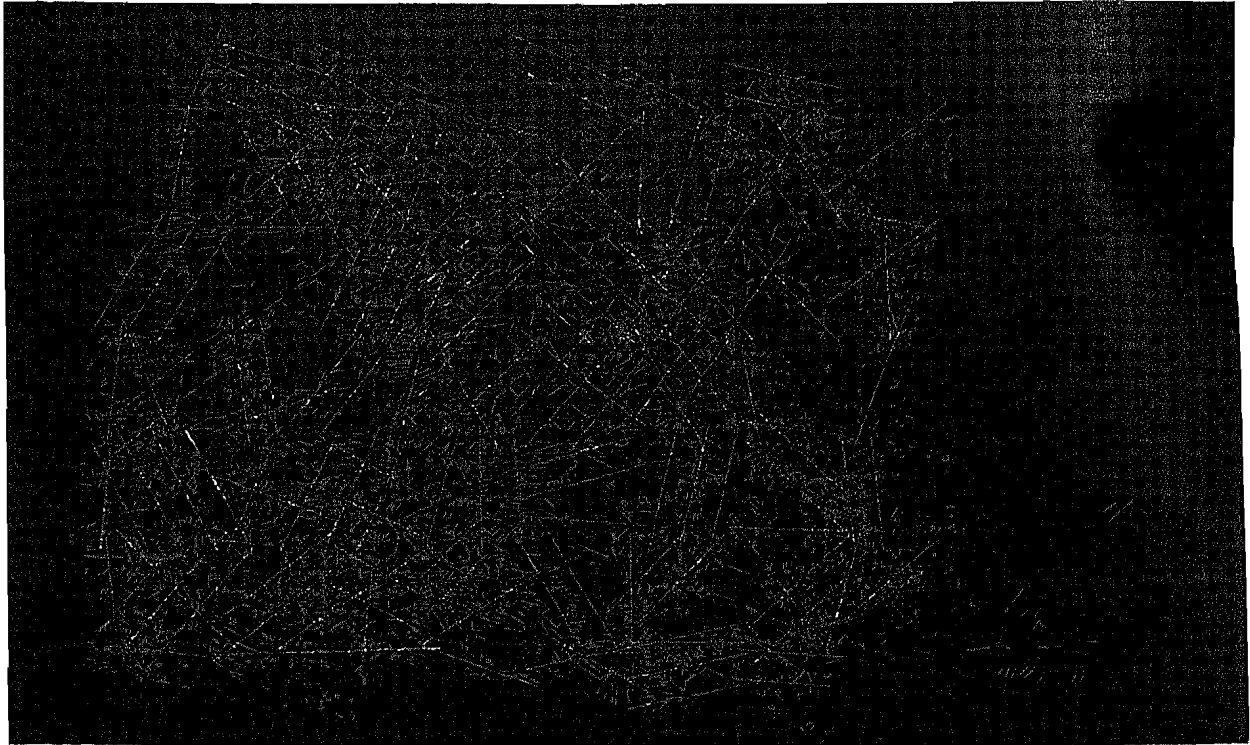


**Figure 6-7.** The values of  $\Delta\rho$  (30) and  $\Delta\theta$  (2), are the same as Figures 6-6, but the number of sections increases (from 6 to 12) and the minimum pixel value decreases (from 300 to 200), which decreases the size of the lineaments. A high minimum pixel value (200) generates numerous subparallel lines in a particular direction.

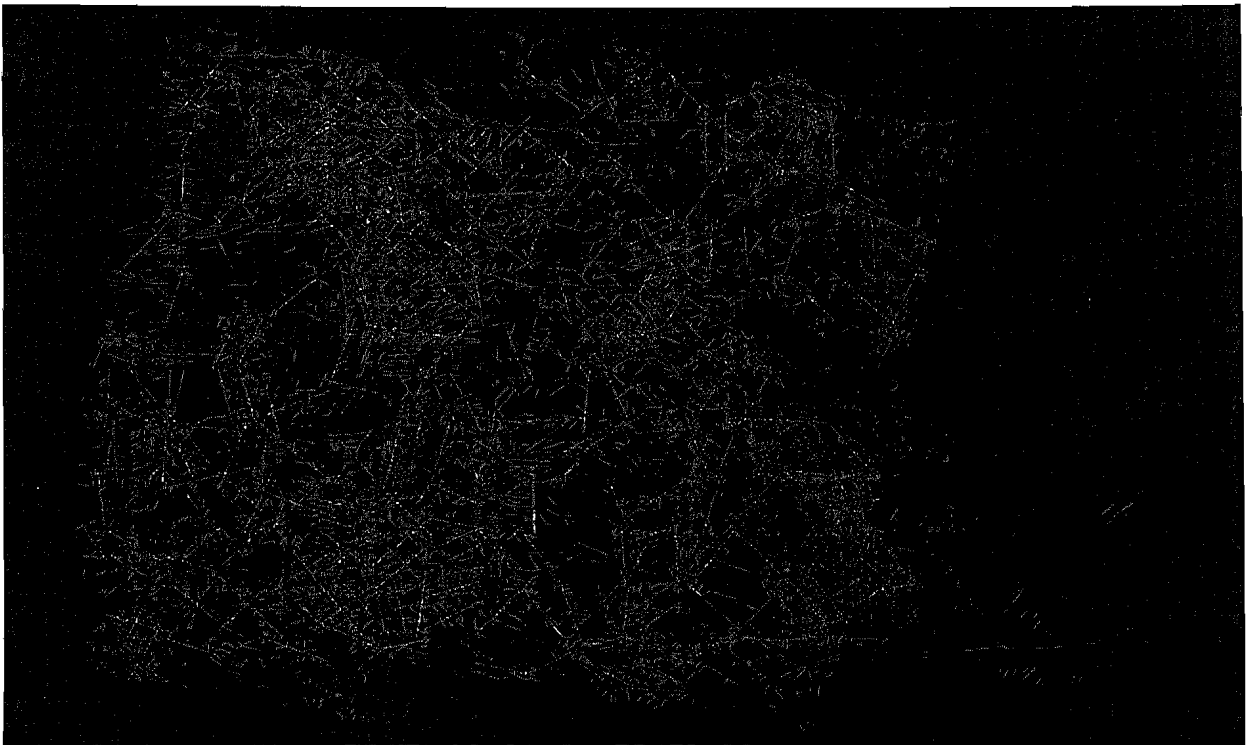


**Figure 6-8.** Smaller lineaments are drawn when the following parameters are used: number of sections 24, minimum pixels 100,  $\Delta\rho$  20, and  $\Delta\theta$  2.

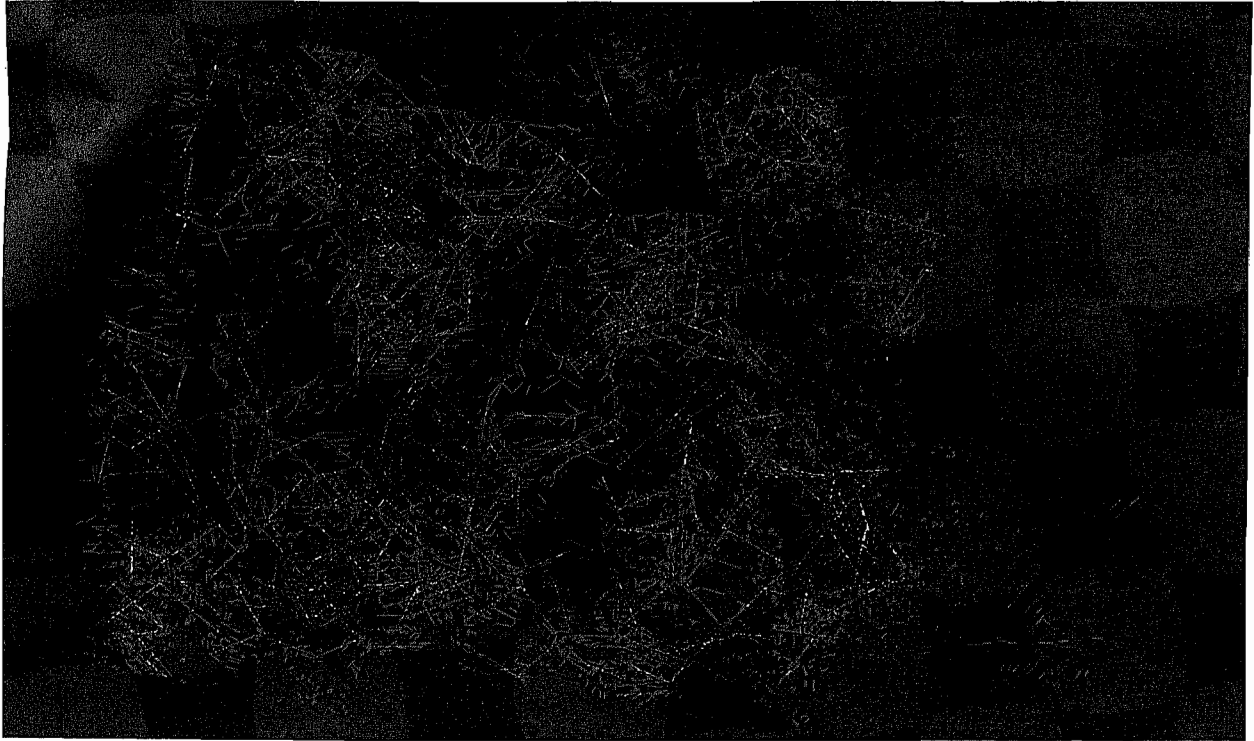


**Figure 6-9.** The "best" lineaments are drawn when the following parameters were used; number of sections 24, minimum pixels 90,  $\Delta\rho$  10, and  $\Delta\theta$  2.

detecting lineaments shows limited success in drawing lineaments from linear features. The fact that the Hough transformation detected northwest-trending lineaments not recognized by the image analyst demonstrates that the program can be useful in highlighting an interpreter's bias. Better success in detecting the dominant east-northeast-trending lineaments may be achieved by further modifications to the algorithm. Continued work on this algorithm and the application of other programs to mapping lineaments from linear features, satellite images, and digital elevation data will provide the image analyst with an independent assessment of significant linear features and lineaments.

## **FUTURE WORK**

As discussed in Duda and Hart (1972) and the present paper, the classical algo-

rithm for the detection of lines applies the Hough transformation to an edge-filtered image and finds a single point of maximum support in the transform space. After this point of a maximum support is identified, the appropriate pixels are removed from the edge-filtered image. The Hough transformation is applied again, and a new point of maximum support in the transform space is found. This process continues until there are no more significant points in the transform space.

We have had preliminary success in mapping lineaments directly from the SPOT satellite image with a slightly different algorithm, which performs a Hough transformation only once. Using this algorithm, we examine the transformed image for local maxima, which correspond to prominent lines in the original image. The new algorithm appears to result in better detection of dominant northeast-trending lineaments than the classical algorithm. We think that

continued modifications to this algorithm will result in not only a more easy-to-use program, but ultimately a map of reproducible lineaments.

## **ACKNOWLEDGEMENTS**

The authors appreciate the support of the Gas Research Institute (Contract No. 5091-221-2146) and the NSF-EPSCoR-ADP Fossil Energy program (Contract No. EHR-910-8774). Also, we wish to thank the editors and reviewers of this manuscript for their suggestions.

## Chapter 7

# Comparison Of Lineaments And Potentiometric Surfaces

*Henry Heasler and Cheryl Jaworowski*

### ABSTRACT

Potentiometric maps of the Cretaceous Mesaverde and Frontier formations in the Greater Green River Basin show discontinuities in the fluid-flow regime. Graphical display of these potentiometric maps with SPOT-derived lineaments and previously mapped faults demonstrates a spatial correlation between faults, SPOT lineaments, geophysical gradients, areas of high hydraulic head, and production of hydrocarbons. This unique combination of digital geologic data illustrates the new insights and questions that develop by integrating available geologic data in a digital database.

### INTRODUCTION

Comparison of surface lineaments with geophysical data (Bouguer gravity and magnetics) is a common procedure for establishing the subsurface significance of satellite-derived lineaments. This chapter introduces an innovative approach to establish the subsurface significance of lineaments by using potentiometric surfaces to define areas of high hydraulic head and high permeability ("sweet spots"). The "sweet spots" are compared with the spatial location of lineaments as reported in Chapter 2 of this volume.

### METHODOLOGY

Potentiometric maps were constructed for the Frontier and Mesaverde formations using the techniques described in Heasler and Surdam (1992) and Heasler et al. (1995).

Basically, drill stem test (DST) pressures from oil and gas wells contained in Petroleum Information's historical well database were converted to values of hydraulic head. Hydraulic head  $h$  was calculated using

$$h = \frac{p}{\rho g} + z$$

where  $p/\rho g$  is the pressure potential ( $p$  is pressure,  $\rho$  is fluid density, and  $g$  is gravitational acceleration), and  $z$  is the elevation potential (the elevation of the pressure measurement above sea level). In the present study, the pressure potential is standardized to the density of pure water.

Thus, hydraulic head represents the total potential energy of fluids contained within a reservoir. Using hydraulic head values, zones of unusually high potential energy may be defined. By contouring hydraulic head values, a potentiometric surface is created. Such a surface allows a spatial comparison of areas of low potential energy with those of high potential energy.

For example, Figure 7-1 shows a potentiometric surface for the Mesaverde Formation in the Greater Green River Basin. As discussed by Heasler and Surdam (1992), this map indicates discontinuities in the fluid-flow regime in the Mesaverde Formation and has been used as evidence for the existence and the delineation of pressure compartments in the Greater Green River Basin. Figure 7-1 shows areas of high hydraulic head (greater than 8000 ft elevation) adjacent to and surrounded by areas of low hydraulic head (less

*How does this relate to overpressure reservoirs?*

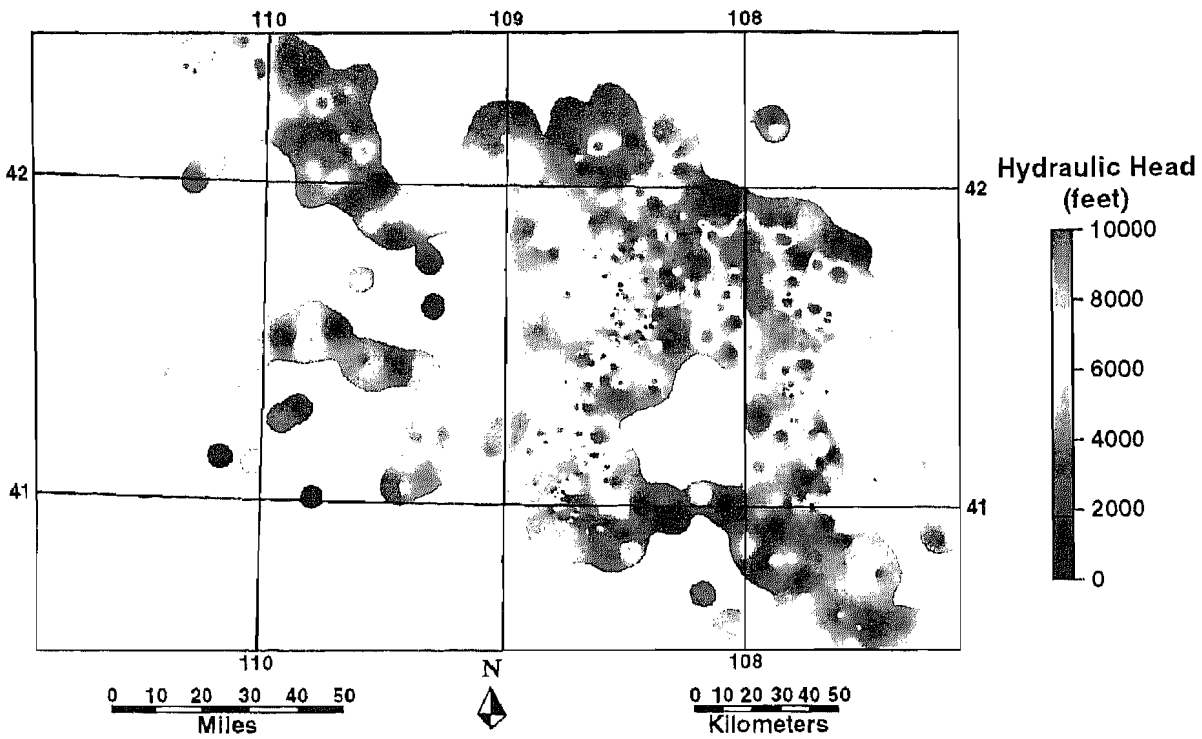


Figure 7-1. Contoured potentiometric surface of 2345 drill stem tests (1176 wells) within the Mesaverde Formation in the GGRB.

than 2000 ft elevation). The preferred interpretation by Heasler and Surdam (1992) of this potentiometric surface is that the areas of high hydraulic head (the red areas on Figure 7-1) indicate both high pressure and relatively high permeability, whereas the areas of low hydraulic head (the blue areas on Figure 7-1) indicate low permeability.

### RESULTS

Figure 7-2 graphically demonstrates that many surface lineaments coincide with previously mapped faults (Love and Christiansen, 1985). Only surface lineaments with the highest degree of certainty are shown. As discussed below, these major surface faults and lineaments show good correlation with areas of high permeability and porosity in the Cretaceous Mesaverde and Frontier formations. Areas of high porosity and permeability are known as "sweet spots."

Figure 7-3 shows the relationship of these "sweet spots" (as defined by the red anomalies on the Mesaverde Formation potentiometric surface) to surface faults (as compiled by Love and Christiansen, 1985). In general, the mapped faults are in areas of moderate hydraulic head (about 6000 to 7000 ft elevation). Some faults clearly bound the red anomalies in the general areas of latitude 41.7°N and longitude 108°W, and latitude 41.2°N and longitude 108.6°W. Additional work is proceeding to further classify the fault systems in an effort to understand the nature of the anomaly bounding faults.

Figure 7-4 shows the relationship of Frontier Formation "sweet spots" (also red anomalies on the potentiometric surface) to surface faults as compiled by Love and Christiansen (1985). Similar to Figure 7-3, the mapped faults are in areas of moderate hydraulic head (about 6000 to 7000 ft elevation). However, very little surface fault data exist over these "sweet spots."

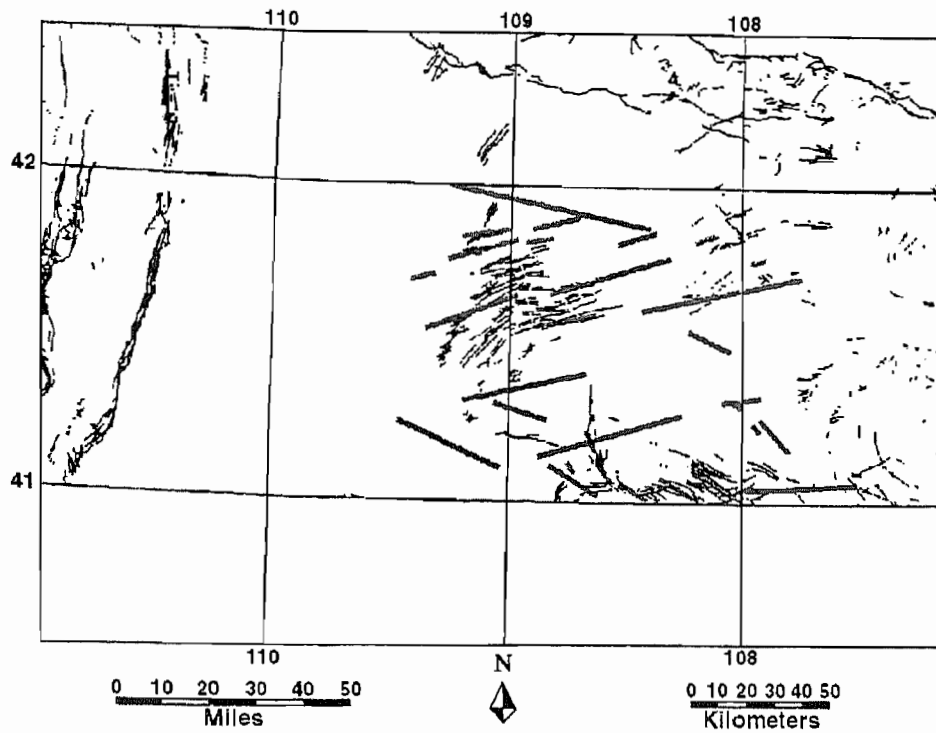


Figure 7-2. Many faults shown by black lines (Love and Christiansen, 1985) are associated with SPOT lineaments (grey lines: Chapter 2, this volume).

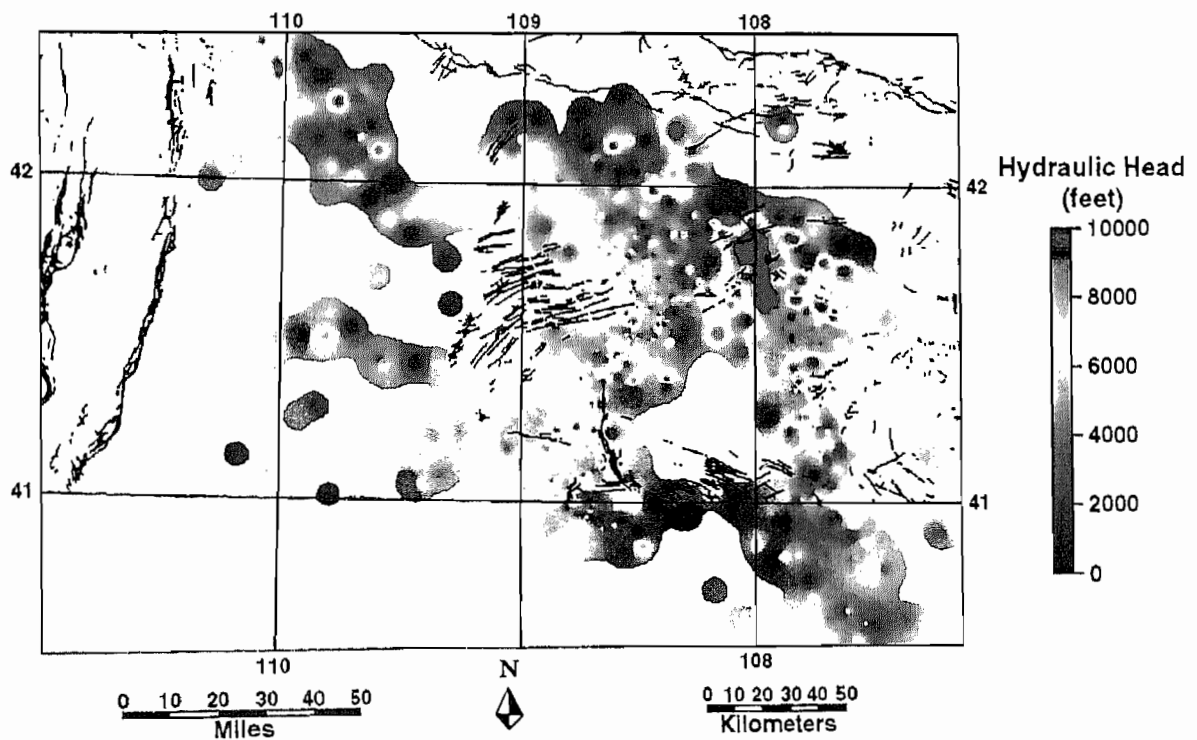
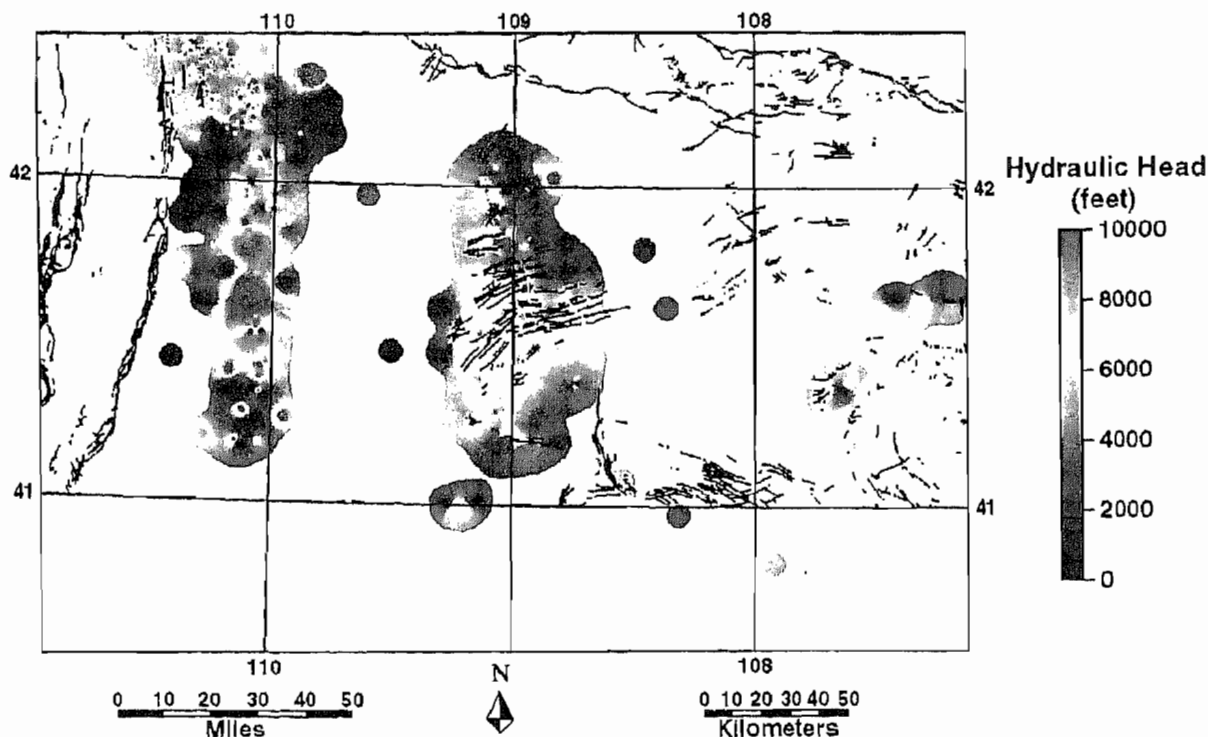


Figure 7-3. Contoured potentiometric surface of 2345 drill stem tests (1176 wells) within the Mesaverde Formation in the GGRB. Faults are shown by heavy black lines (Love and Christiansen, 1985).



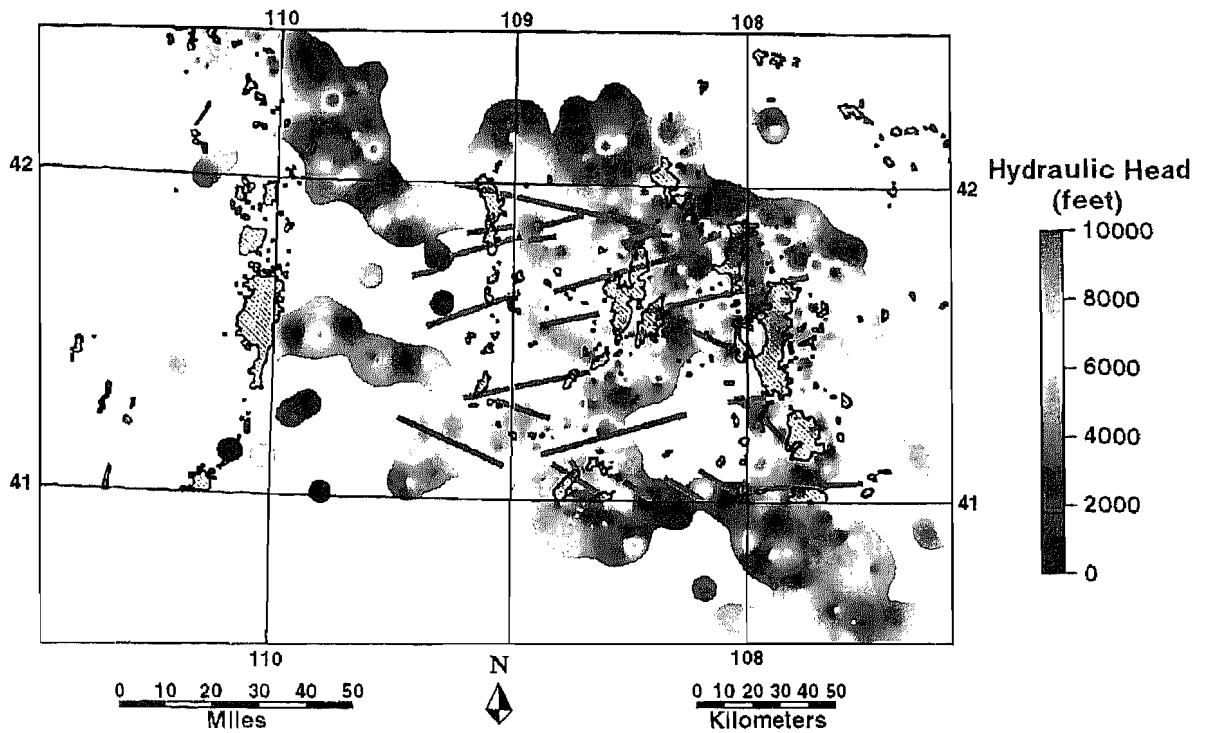
**Figure 7-4.** Contoured potentiometric surface of 1321 drill stem tests (731 well) within the Frontier Formation in the GGRB. Faults are shown by heavy black lines (Love and Christiansen, 1985).

Figure 7-5 shows the relationship of the Mesaverde Formation potentiometric surface to SPOT lineaments (Chapter 2, this volume) and oil and gas fields (DeBruin and Boyd, 1991). Lineaments frequently separate areas of high hydraulic head from areas of low hydraulic head. Along a lineament, hydraulic head values are generally in the moderate to high range. This suggests that lineaments may be useful in defining zones of high permeability as defined from the potentiometric surface. The defined oil and gas fields also overlie areas of moderate to high hydraulic head. However, some areas of high hydraulic head are not overlain by defined oil and gas fields.

A similar relationship is observed in Figure 7-6 between the Mesaverde Formation potentiometric surface and gravity gradients (Jaworowski and Simon, 1995; Chapter 2, this volume). Gravity gradients are also generally in the range of moderate to high hydraulic heads.

This suggests a correlation between the gravity gradients and the areas of increased permeability as defined from the Mesaverde potentiometric surface. These gradients typically bound both oil and gas fields and potentiometric highs; in one area (latitude  $41.7^{\circ}\text{N}$  and longitude  $108^{\circ}\text{W}$ ), a gravity gradient crosscuts a potentiometric high.

Figure 7-7 shows the relationship of the Frontier Formation potentiometric surface to oil and gas fields (DeBruin and Boyd, 1991) and gravity gradients (Jaworowski and Simon, 1995; Chapter 2, this volume). In general, the gravity gradients do not correlate well with either the boundaries of potentiometric highs or with areas of moderate to high hydraulic head. However, in the vicinity of the Brady Field (latitude  $41.4^{\circ}\text{N}$  and longitude  $108.75^{\circ}\text{W}$ ) a northeast-trending gravity gradient parallels a zone of moderate hydraulic head.



**Figure 7-5.** Contoured potentiometric surface of 1321 drill stem tests (731 wells) within the Frontier Formation in the GGRB. Faults are shown by heavy grey lines (Love and Christiansen, 1985)

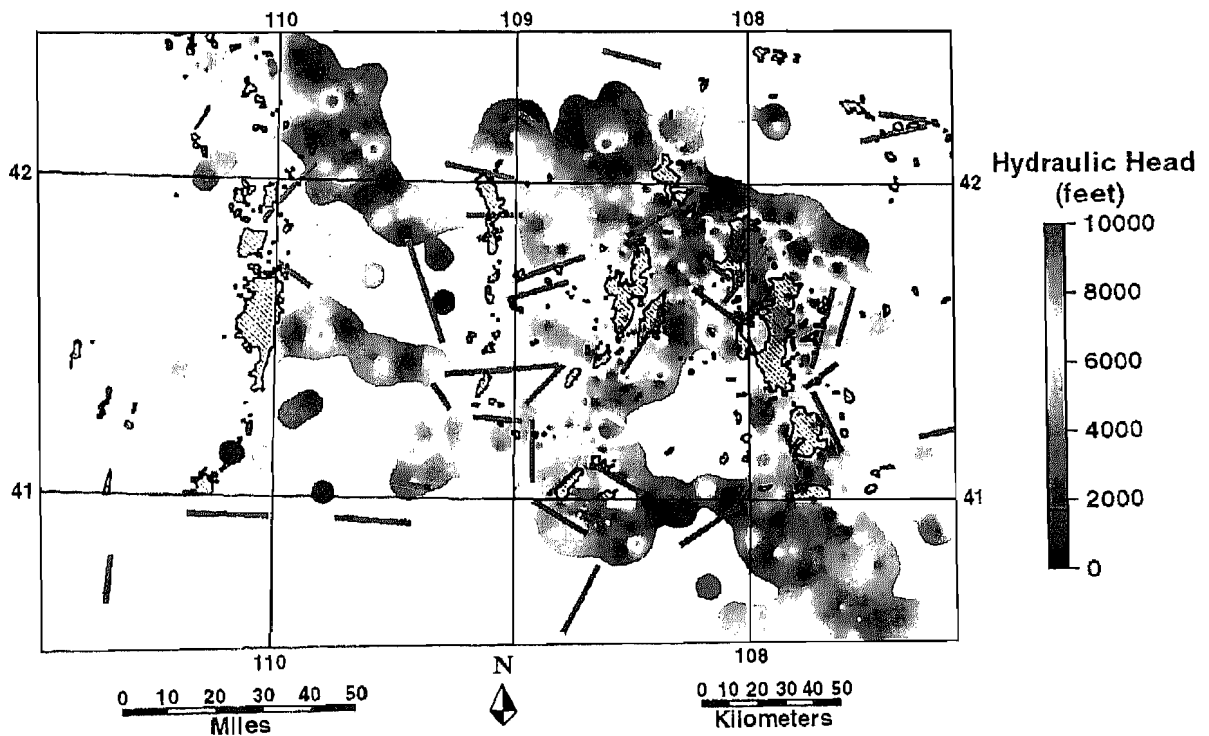


**Figure 7-6.** Contoured potentiometric surface of 2435 drill stem tests (1176 wells) within the Mesaverde Formation in the GGRB. Oil and gas fields, as defined by DeBruin and Boyd (1991), are shown by diagonal line pattern areas. Gravity gradients or lineaments (Chapter 2, this volume) are shown by heavy grey lines.

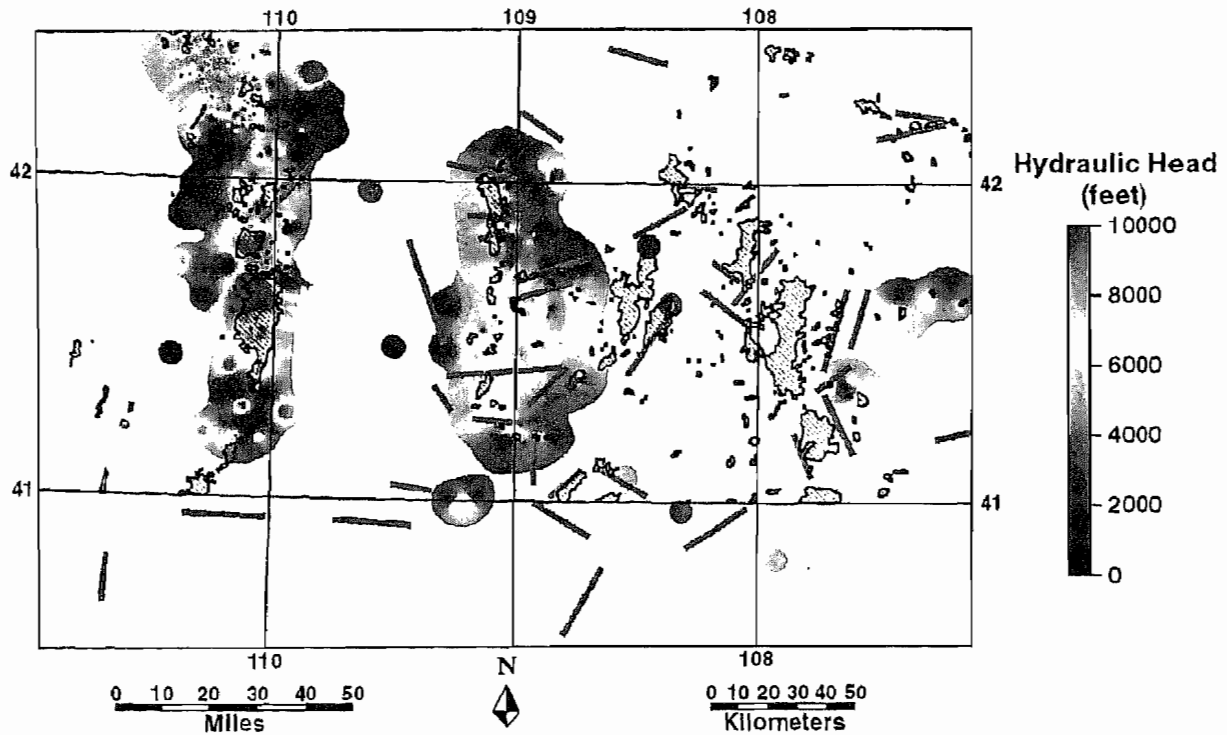


Figure 7-7. Contoured potentiometric surface of 1321 drill stem tests (731 wells) within the Frontier Formation in the GGRB. Oil and gas fields are shown by hatched areas (DeBruin and Boyd, 1991). Gravity lineaments are shown by heavy grey lines (Chapter 2, this volume).

## CONCLUSIONS

The acquisition, generation, and compilation of digital geologic data (lineaments, faults, gravity, and potentiometric surfaces) for the Greater Green River Basin have made possible this preliminary comparison of Mesaverde and Frontier fluid flow with faults, SPOT lineaments, and geophysical gradients. In the Mesaverde, SPOT lineaments frequently separate areas of high hydraulic head from areas of low hydraulic head. Along a SPOT lineament, hydraulic head values are generally in the moderate to high range. This suggests that SPOT lineaments may be useful in defining zones of high permeability as identified from the potentiometric surface. A similar relationship was observed between the Mesaverde potentiometric surface and gravity gradients.

The explanation for the correlation between the Mesaverde potentiometric surface, gravity gradients, SPOT linea-

ments, and surface faults is unclear. Additional mapping, laboratory analyses, and modeling must be undertaken to investigate probable causes of the correlations. Understanding the causes of the correlations will help in using the lineaments to predict the spatial occurrence of "sweet spots."

## ACKNOWLEDGEMENTS

The authors wish to thank the Gas Research Institute for supporting this study under contract No. 5091-221-2146.

# References

- Bankey, Viki, and D.M. Kulik, 1989, Gravity survey data and a complete Bouguer gravity anomaly map of southwestern Wyoming, northeastern Utah and northwestern Colorado: U.S. Geological Survey Open File Report 89-175-A, 31 p.
- Berger, Z., 1994, Satellite Hydrocarbon Exploration: Springer-Verlag, 319 p.
- Blackstone, D.L., Jr., 1972, Tectonic analysis of southwestern Wyoming from ERTS-1 imagery: University of Wyoming Remote Sensing Laboratory Special Report, 4 p.
- Blackstone, D.L., Jr., 1973, Geology of photo-linear elements, Great Divide Basin, Wyoming: University of Wyoming Remote Sensing Laboratory Special Report, 11 p.
- Bradley, W.H., 1961, Geologic map of a part of southwestern Wyoming and adjacent states: U.S. Geological Survey Miscellaneous Geological Investigations Map I-332.
- Brown, N.N., 1994, Integrating structural geology with remote sensing in hydrogeological resource evaluation and exploration: Tenth thematic conference on geologic remote sensing, San Antonio, p. I144-I154.
- Christiansen, G.E., 1995, Factors Influencing Differential Natural Gas Production from the Upper Cretaceous Upper Almond Formation, Wamsutter Arch Area, Sweetwater and Carbon Counties, Wyoming: M.S. thesis, University of Wyoming, 106 p.
- Davis, D.G., 1977, Geophysical logging of coal, in D. Murray, ed., Geology of Rocky Mountain Coal: Rocky Mountain Association of Geologists, 1976 Symposium, p. 115-119.
- DeBruin, R.H., and C.S. Boyd, 1991, Oil and gas map of Wyoming: Wyoming State Geological Survey, Map Series 35, scale 1:500,000.
- Desai, P.V., K. Chidananda Gowda, and P. Nagabhushan, 1994, Edge enhancement using neural network: Proceedings of the Tenth Thematic Conference on Geologic Remote Sensing, San Antonio, pp. II425-II426.
- Dickinson, R.G., 1992, Table Rock Field - Frontier Formation, an overpressured reservoir: Wyoming Geological Association 43rd Annual Field Conference Guidebook, p. 139-144.
- Doeringsfeld, W.W., Jr., and J.B. Ivey, 1992, Use of photogeology and geomorphic criteria to locate subsurface structure, in N. Foster and E. Baumont, eds., Photogeology and Photogeomorphology: AAPG Treatise of Petroleum Geology, Reprint Series No. 18, p. 147-159.
- Duda P.O., and P.E. Hart, 1972, Use of the Hough Transformation to detect lines and curves in pictures: Comm. Assoc. Comp. Machinery, v. 15, pp. 11-15.
- Earle, J., 1975, A re-evaluation of tectonics of Wyoming and adjacent areas using photo linear elements mapped from Landsat-1 and Skylab imagery: Progress Report for NASA/Goddard Space Flight Center, 78 p.
- Flores, R.M., 1978, Barrier and back-barrier environments of the deposition of the Upper Cretaceous Almond Formation, Rock Springs Uplift, Wyoming: The Mountain Geologist, v. 15, p. 57-65.
- Foley, M.G., 1991, Three-dimensional visualization for evaluating automated geomorphic pattern recognition analyses of crustal structures in The Eight Thematic Conference on Geologic Remote Sensing, Denver, p.287-292.

- García-González, M., 1992, Joint azimuth on the Mesaverde Group in the Rock Springs Uplift: unpublished data, Institute for Energy Research, Laramie, Wyoming, 13 p.
- García-González, M., and R.C. Surdam, 1992, Coal as a source rock of petroleum: A comparison between the petrology of the Mesaverde Group coals, in burial and hydrous pyrolysis, in C. Mullen, ed., *Rediscover the Rockies: Wyoming Geological Association 43rd Field Conference Guidebook*, p. 237-244.
- Gill, J.R., E.A. Merewether, and W.A. Cobban, 1970, Stratigraphy and nomenclature of some Upper Cretaceous and lower Tertiary rocks in south-central Wyoming: U.S. Geological Survey Professional Paper 667, p. 19-20.
- Goetz, A.F.G., and B.N. Rock, 1983, Remote sensing for exploration-an overview: *Economic Geology*, v.78, pp. 573-590.
- Grout, M.A., and E.R. Verbeek, 1983, Field studies of joints—Insufficiencies and solutions, with examples from the Piceance basin, Colorado, in J.H. Gary, ed., 16th Oil Shale Symposium, Proceedings: Golden, Colorado School of Mines Press, p. 68-80.
- Grout, M.A., and E.R. Verbeek, 1992a, Joint-history summary and orientation data for Upper Cretaceous sandstones, Rawlins and Rock Springs Uplifts, Washakie Basin, southern Wyoming: U.S. Geological Survey Open-File Report 92-388, 30 p.
- Grout, M.A., and E.R. Verbeek, 1992b, Fracture history of the Divide Creek and Wolf Creek anticlines and its relation to Laramide basin-margin tectonism of the southern Piceance basin: U.S. Geological Survey Bulletin B-1787-Z, 32 p.
- Grout, M.A., and Verbeek, E.R., in press, Regional joint sets and faulted evaporite-cored anticlines in the Paradox Basin, southeastern Utah, in Friedman, J.D., and Huffman, A.C., Jr., eds., *Laccolith complexes of southeastern Utah—Tectonic control and time of emplacement*: U.S. Geological Survey Bulletin, 49 ms. p.
- Grout, M.A., G.A. Abrams, R.L. Tang, T.J. Hainsworth, and E.R. Verbeek, 1991, Late Laramide thrust-related and evaporite-domed anticlines in the southern Piceance basin, northeastern Colorado Plateau: *American Association of Petroleum Geologists Bulletin*, v. 75, no. 2, p. 205-218.
- Hale, L.A., 1950, Stratigraphy of the Upper Cretaceous Montana Group in the Rock Springs Uplift, Sweetwater County, Wyoming, in *Geology of Southwest Wyoming: Wyoming Geological Association 5th Annual Field Conference Guidebook*, p. 49-58.
- Hansen, W.R., 1969, Development of the Green River drainage system across the Uinta Mountains, in *Geologic Guidebook of the Uinta Mountains: Intermountain Association Geologists and Utah Geological Society 16th Annual Field Conference*, p. 93-100.
- Hansen, W.R., 1984, Post-Laramide tectonic history of the eastern Uinta Mountains, Utah, Colorado, and Wyoming: *The Mountain Geologist*, v. 21, no. 1, p. 5-29.
- Hansen, W.R., 1985, Drainage development of the Green River Basin in southwestern Wyoming and its bearing on fish biogeography, neotectonics, and paleoclimates: *The Mountain Geologist*, v. 22, no. 4, p. 192-204.
- Heasler, H.P., and R.C. Surdam, 1992, Pressure compartments in the Mesaverde Formation of the Green River and Washakie Basins, as determined from drill stem test data: *Wyoming Geological Association 43rd Annual Field Conference Guidebook*, p. 207-220.
- Heasler, H.P., J.H. George, and R.C. Surdam, 1995, Pressure compartments in the Powder River Basin, Wyoming and Montana, as determined from drill stem test data, in P. Orteleva, ed., *Basin Compartments and Seals: American Association of Petroleum Geologists Bulletin Memoir 61*, p. 235-262.

- Hendricks, M.L., 1983, *Stratigraphy and Tectonic History of the Mesaverde Group (Upper Cretaceous), East Flank of the Rock Springs Uplift, Sweetwater County, Wyoming*: Ph.D. dissertation, Colorado School of Mines, 213 p.
- Hill, R.E., in press, *Natural fractures and stress orientations in the Almond Formation, Wamsutter area, Green River Basin, Wyoming*, in *An Engineering and Geologic Evaluation of a Horizontal Gas Well Completion in the Almond Sandstone, Echo Springs Field, Greater Green River Basin, Wyoming*: Gas Research Institute Topical Report.
- Honey, J.G., and Roberts, S.B., 1994, *Sedimentologic framework of the lower Fort Union Formation (Paleocene), eastern Great Divide Basin, Wyoming, and implications for tectonic influence on coal-forming environments [abs.]*: American Association of Petroleum Geologists Annual Meeting, June 12-15, 1994, Denver, Colorado, 1 p.
- Hoppin, R.A., 1974, *Lineaments: Their role in tectonics of central Rocky Mountains*: American Association of Petroleum Geologists Bulletin, v. 58, p. 2260-2273.
- Iverson, W., and R.C. Surdam, 1995, *Tight gas sand production from the Almond Formation, Washakie Basin, Wyoming*: SPE 29559, Society of Petroleum Engineers Regional / Low Permeability Reservoirs Symposium, Denver, p. 163-176.
- Jacka, A.D., 1965, *Depositional dynamics of the Almond Formation, Rock Springs Uplift, Wyoming*: Wyoming Geological Association 29th Annual Field Conference Guidebook, p. 81-100.
- Jackson, S.R., and V. Rawn-Schatzinger, 1993, *Data from Selected Almond Formation Outcrops—Sweetwater County, Wyoming*: U.S. Department of Energy, Topical Report NIPER-724, 72 p.
- Jaworowski, C., 1993, *Joints and linear features of the east-central Greater Green River Basin, Wyoming*, in *Natural Gas Resource Characterization Study of the Mesaverde Group in the Greater Green River Basin, Wyoming: A Strategic Plan for the Exploration of Tight Gas Sands*.
- Jaworowski, C., and R. Simon, 1995, in press, *Joints and linear features of the east-central southwestern Wyoming*: Wyoming Geological Association Guidebook.
- Jaworowski, C., and R. Simon, in press, *Relating fractures in the eastern Greater Green River Basin to oil and gas fields: integrating field measurements, linear features, and digital geologic data*: Wyoming Geological Association 46th Annual Field Conference Guidebook.
- Kolm, K.E., 1982, *Predicting the surface wind characteristics of southern Wyoming from remote sensing and eolian geomorphology*, in R. Marrs and K. Kolm, eds., *Interpretation of Windflow Characteristics From Eolian Landforms*: Geological Society of America Special Paper 192, p. 25-53.
- Lang, H.R., S.L., Adams, J.E. Conel, B.A. McGuffie, E.D. Paylor, and R.E. Walker, 1987, *Multispectral Remote Sensing as a stratigraphic and structural tool, Wind River Basin and Bighorn Basin areas, Wyoming*: American Association of Petroleum Geologists Bulletin, v.71, no.4, pp.389-402.
- Laubach, S.E., R.Tyler, C.M. Tremain, M.A. Grout, and W.A. Ambrose, 1991, *Fracture patterns in coal in the western United States—observation and implications for development of coalbed methane resources [abs.]*: Geological Society of America Abstracts with Programs, v. 23, no. 5, p. A38-A39.
- Laubach, S.E., Tyler, Roger, Ambrose, W.A., Tremain, C.M., and Grout, M.A., 1992, *Preliminary map of fracture patterns in coal in the western United States*, in C.E. Mullen, ed., *Rediscover the Rockies*: Wyoming Geological Association 43rd Field Conference Guidebook, p. 253-267.
- Law, B.E., and C.R. Smith, 1983, *Subsurface temperature map showing depth to 180 degrees Fahrenheit in the Greater Green River Basin, Wyoming, Colorado, and Utah*: U.S. Geological Survey, Miscellaneous Field Studies

Map MF-1504, scale 1:500,000.

- Leite, M.B., 1992, Joint azimuths in sandstones of the Mesaverde Group, Upper Cretaceous of the Rock Springs Uplift, Wyoming: unpublished internal report, Institute for Energy Research, Laramie, Wyoming, 6 p.
- Lewis, J.L. 1961, The stratigraphy and depositional history of the Almond Formation in the Great Divide Basin, Sweetwater County, Wyoming: Wyoming Geological Association 16th Annual Field Conference Guidebook, p. 87-95.
- Love, J.D., and A.C. Christiansen, 1985, Geologic Map of Wyoming: U.S. Geological Survey Map, scale 1:500,000.
- Marrs, R.W., and D.R. Gaylord, 1982, Techniques for interpretation of windflow characteristics from eolian landforms, in R. Marrs and K. Kolm, eds., Interpretation of Windflow Characteristics from Eolian Landforms: Geological Society of America Special Paper 192, p. 3-17.
- Marrs, R.W., and G.L. Raines, 1984, Tectonic framework of Powder River Basin, Wyoming and Montana, interpreted from Landsat imagery: American Association of Petroleum Geologists Bulletin, v. 68, p. 1718-1731.
- Martinsen, O.J., 1994, Fluvial sheet sandstone development above a tectonically-controlled sequence boundary: Canyon Creek Member, Ericson Sandstone (Campion), Rock Springs Uplift, Wyoming: American Association of Petroleum Geologists 1994 Annual Convention Program with Abstracts, p. 206.
- Martinsen, R.S., and R.W. Marrs, 1985, Comparison of major lineament trends to sedimentary rock thickness and facies distribution, Powder River Basin, Wyoming: Proceedings, Fourth Thematic Conference on Remote Sensing for Exploration Geology, p. 9-19.
- Mason, P.J., L.J. Guo, and M. Moore, 1994, Integration of Landsat TM with SPOT panchromatic data and ERS-1 SAR imagery for neotectonic studies: Tenth thematic conference on geologic remote sensing, San Antonio, p. I253-I262.
- Masursky, H., 1962, Uranium-Bearing Coal in the Eastern Part of the Red Desert Area, Great Divide Basin, Sweetwater County, Wyoming: U.S. Geological Survey Bulletin 1099-B, 152 p.
- McCubbin, D.C., and M.C. Brady, 1969, Depositional environment of the Almond reservoirs, Patrick Draw Field, Wyoming: Mountain Geologist, v. 6, p. 3-26.
- McGrew, P.O., and J.E. Berman, 1955, Geology of the Tabernacle Butte area: Wyoming Geological Association 10th Annual Field Conference Guidebook, p. 108-111.
- Meyers, W.W., 1977, Environmental Analysis of the Almond Formation (Upper Cretaceous) from the Rock Springs Uplift: Ph.D. dissertation, University of Tulsa, 366 p.
- Oldfield, B., 1988, Graphical integration and correlation of multispectral scanner and subsurface geologic data for hydrocarbon exploration in Appalachian Basin industrial associates Fall program, October 1988, West Virginia University, v.14, p.140-156.
- Paylor, E.D., II, 1983, Investigation of Surface Features Interpreted From Remote Sensing Data of the Table Rock Gas Field: M.S. thesis, University of Wyoming, 81 p.
- Peiterson, M.N., 1992, Lineament analysis of the Washakie Basin: unpublished data, Institute for Energy Research, Laramie, Wyoming, 8 p.
- Penney, F.A., 1992, The local surface expression of some deep discoveries in the central Rocky Mountains, in N. Foster and E. Baumont, eds., Photogeology and Photogeomorphology: American Association of Petroleum Geologists Treatise of Petroleum Geology, Reprint Series No. 18, p. 499-505.

- Pipiringos, G.N., 1961, Uranium-Bearing Coal in the Central Part of the Great Divide Basin, Sweetwater County, Wyoming: U.S. Geological Survey Bulletin 1099-A, 104 p.
- Raghavan, V., K. Wadatsumi, and S. Masumoto, 1994, SMILES, A Fortran-77 program for sequential machine interpreted lineament extraction using digital images: *Computers and Geosciences* v.20, no.2, pp.121-159.
- Raghavan, V., S. Masumoto, K. Kioke, and S. Nagano, 1995, Automatic lineament extraction from digital images using a segment tracing and rotation transformation approach: *Computers and Geosciences*, v.21, no.4, pp.555-591.
- Richers, D.M., J.R. Reed, K.C. Horstman, G.D. Michels, R.N. Baker, L.Lundell, and W. Marrs, 1982, Landsat and geochemical study of Patrick Draw Oil Field, Sweetwater County, Wyoming: *American Association of Petroleum Geologists Bulletin*, v. 66, p. 903-922.
- Roehler, H.W., 1988, The Pintail Coal Bed and Barrier Bar G—A model for Coal of Barrier Bar Lagoon Origin, Upper Cretaceous Almond Formation, Rock Springs Coal Field, Wyoming: U.S. Geological Survey Professional Paper 1398, 60 p.
- Roehler, H.W., 1990, Stratigraphy of the Mesaverde Group in the Central and Eastern Greater Green River Basin, Wyoming, Colorado, and Utah: U.S. Geological Survey Professional Paper 1508, 52 p.
- Roehler, H.W., and D.E. Hansen, 1989, Surface and subsurface correlations showing depositional environments of the Upper Cretaceous Mesaverde Group and associated formations, Lost Soldier Field to Cow Creek, Southwest Wyoming: U.S. Geological Survey, Miscellaneous Field Studies Map MF-2076.
- Russell, C.B., and D.S. Stone, 1995, Table Rock 3-D Survey—Structural Interpretation in 3-D Seismic Symposium: Rocky Mountain Association of Geologists and Denver Geophysical Society, Denver, CO (expanded abstract).
- Sabins, F.F., 1987, Resource Exploration *in* Remote Sensing Principles and Interpretation: Remote Sensing Enterprises, pp.279-316.
- Saether, B.M., H.G. Rueslatten, and T.H. Henningsen, 1991, Advanced techniques for lineament analysis *in* The Eight Thematic Conference on Geologic Remote Sensing: Denver, pp. 983-988.
- Sherman, T.F., 1983, Sedimentology of the Upper Cretaceous Ericson Formation, Rock Springs Uplift, Wyoming: Colorado State University, M.S. thesis, Fort Collins, Colorado, 192 p.
- Shurr, G.W., L.M. Monson, and D.F. Lund, 1991, Importance of Landsat linear features in hydrocarbon exploration on Fort Peck Reservation, northeastern Montana: Proceedings, Eighth Thematic Conference on Geologic Remote Sensing, p. 45-58.
- Slack, P.B., 1981, Paleotectonics and hydrocarbon accumulation, Powder River Basin, Wyoming: *American Association of Petroleum Geologists Bulletin*, v. 65, p. 730-743.
- Stone, D.S., 1995, Structure and Kinematic Genesis of the Quealy Wrench Duplex: Transpressional Reactivation of the Precambrian Cheyenne Belt in the Laramie Basin, Wyoming: *American Association of Petroleum Geologists Bulletin*, v. 79, no. 9, pp. 1349-1376.
- Szpakiewicz, M., R. Schatzinger, S. Jackson, B. Sharma, A. Cheng, and M. Honarpour, 1991, Selection and Initial Characterization of a Second Barrier Island Reservoir System and Refining of Methodology for Characterization of Shoreline Barrier Reservoirs: U.S. Department of Energy, Topical Report No. NIPER-484, 170 p.
- Thomas, G.E., 1971, Continental plate tectonics: southwest Wyoming: Wyoming Geological Association 23rd

- Annual Field Conference Guidebook, p. 103-123.
- Thomas, G.E., 1973, Evanston lineament, Green River Basin, Wyoming: Wyoming Geological Association 25th Annual Field Conference Guidebook, p. 93-95.
- Tyler, Roger, S.E. Laubach, W.A. Ambrose, M.A. Grout, and C.M. Tremain, 1992, Face-creat patterns in Rocky Mountain foreland basins, Western United States—permeability indicators for coalbed methane [abs.]: American Association of Petroleum Geologists Bulletin, v. 76, no. 9, p. 1269-1270.
- Tyler, Roger, S.E. Laubach, W.A. Ambrose, C.M. Tremain, and M.A. Grout, 1993, Coal fracture patterns in the foreland of the Cordilleran thrust belt, western United States: Proceedings 9379 of the 1993 International Coalbed Methane Symposium, May 17-21, 1993, Birmingham, Alabama, p. 695-704.
- Union Pacific Resources, 1992, Almond / Mesaverde Formation, Echo Springs Field: Wyoming Oil and Gas Commission, Cause No. 1, Order No. 9, Docket no. 90-92.
- Van Horn, M.D., 1979, Stratigraphic relationships and depositional environments of the Almond and associated formations, east-central flank of the Rock Springs Uplift: Rocky Mountain Section, Society of Economic Paleontologists and Mineralogists, Field Trip Guide, 1979, p. 50-63.
- Van Wagonner, J.C., R.M. Mitchum, K.M. Campion, and V.D. Rahmenian, 1990, Siliclastic Sequence Stratigraphy in Well Logs, Cores, and Outcrops: Concepts for High-Resolution Correlation of Time and Facies: American Association of Petroleum Geologists, Methods in Exploration Series, No. 7, 55 p.
- Verbeek, E.R., and M.A. Grout, 1993, Geometry and structural evolution of gilsonite dikes in the eastern Uinta Basin, Utah: U.S. Geological Survey Bulletin B-1787-HH, 42 p.
- Verbeek, E.R., M.A. Grout, and C. Jaworowski, 1994: unpublished field data.
- Weimer, R.J., 1965, Stratigraphy and petroleum occurrences, Almond and Lewis Formations (Upper Cretaceous), Wamsutter Arch, Wyoming: Wyoming Geological Association 19th Annual Field Conference Guidebook, p. 65-81.
- Weimer, R.J., 1966, Time-stratigraphic analysis and petroleum accumulation, Patrick Draw Field, Sweetwater County, Wyoming: American Association of Petroleum Geologists Bulletin, v. 50, pp. 2150-2175.
- Weimer, R.J., 1980, Recurrent movement on basement faults, a tectonic style for Colorado and adjacent areas, *in* H. Kent and K. Porter, eds., Colorado Geology: Rocky Mountain Association of Geologists, Denver, p. 23-46.
- Weimer, R.J., K.W. Porter, and C.B. Land, 1985, Depositional Modeling of Detrital Rocks: Society of Economic Paleontologists and Mineralogists, Core Workshop No. 8, 252 p.
- Wyoming Geological Association, 1979, Wyoming Oil and Gas Fields Symposium, Greater Green River Basin, 1979: Casper, Vol. II, 428 p.
- Wyoming Geological Association, 1992, Wyoming Oil and Gas Fields Symposium, Greater Green River Basin, 1992, Casper, Vol. I, 373 p.
- Wyoming State Geological Survey, 1987, Preliminary SSC Site Map - Red Desert Basin, Wyoming, scale 1:100,000.
- Zlatopolsky, A.A., 1992, Program LESSA (Lineament extraction and stripe statistical analysis) automated linear image features analysis-experimental results: Computers and Geosciences, v. 18, no. 9, pp.1121-1126.

# Appendix A

## List of Fields by Production

# List of Fields by Production

Field Name	Twp	Rng	Discovery	Active Wells, '93	Cum oil (bbls)	Cum gas (Mscf)	(7+(20x6)/10 <sup>6</sup> )	GOR
<b>Largest Fields</b>								
Arch	19	98	1959	15	18,538,910	86,759,910	457.5381	4.679882
Brady	16	101	1973	25	62,571,620	401,319,600	1652.752	6.413764
Lost Soldier	26	90	1916	99	226,807,600	160,684,500	4696.836	0.7084617
Patrick Draw	18	99	1959	41	42,714,060	160,845,300	1015.127	3.765629
X Table Rock	19	98	1946	101	5,426,136	508,643,300	617.166	93.7395
Wertz	26	90	1920	67	109,249,200	143,327,700	2328.312	1.311934
<b>Total</b>					<b>465,307,500</b>	<b>1,461,580,000</b>		
<b>Significant Fields</b>								
Baxter Basin Middle	18	103	1938	4	0.000999	16,206,370	16.20637	16,222,590,000
Baxter Basin North	20	103	1926	15	71,681	84,263,780	85.6974	1175.538
Baxter Basin South	16	104	1922	16	5934	137,182,800	137.3015	23,118.1
Bison Basin	27	95	1929	14	2,916,277	555,845	58.88139	0.1906009
Canyon Creek	12	101	1941	37	1,303,843	257,385,600	283.4625	197.4054
Coal Gulch	17	93	1977	9	762,546	38,050,930	53.30185	49.89985
Crooks Gap	28	93	1944	8	13,250,060	1,342,034	266.3432	0.1012851
Desert Springs	21	98	1958	33	2,056,498	283,181,000	324.3109	137.7006
Desert Springs West	20	99	1959	18	1,466,237	34,542,350	63.86709	23.55851
X Echo Springs	19	93	1977	74	5,322,650	218,771,000	325.224	41.10189
Fabian Ditch	20	102	1976	55	414,760	77,931,960	86.22716	187.8965
Happy Springs	28	93	1950	10	8,739,204	8,969,381	183.7535	1.026338
Hay Reservoir	24	97	1976	42	1,589,948	87,616,140	119.4151	55.1063
Hiawatha	12	99	1928	17	115,311	85,660,800	87.96702	742.8676
Higgins	17	99	1969	9	55,336	78,850,860	79.95758	1424.947
Mahoney Dome	26	88	1919	19	6,401,392	30,000	128.0578	0.004686481
Nitchie Gulch	23	103	1962	50	198,547	123,554,300	127.5252	622.2925
Playa	20	98	1960	0	435,891	40,862,540	49.58036	93.74486
Standard Draw	18	93	1978	37	4,182,454	162,104,600	245.7537	38.75825
Trail Unit	13	100	1958	7	377,179	71,245,440	78.78902	188.8903
Wamsutter	20	95	1958	43	927,790	96,521,420	155.0772	104.0337
West Side Canal	12	91	1964	30	2912	145,475,300	145.5335	49,957.18
Wild Rose	18	94	1975	49	3,318,872	108,734,800	175.1122	32.76258
<b>Total</b>					<b>53,915,320</b>	<b>2,159,039,000</b>		
<b>Small Fields</b>								
Antelope	17	99	1970	5	26,368	31,506,040	32.0334	1194.859
Baggs South	12	92	1954	21	38,356	42,772,460	43.53958	1115.144
Bailey Dome	26	89	1944	3	1,755,474	457,344	35.56683	0.2605245
Barrel Springs	16	93	1965	55	451,189	38,278,660	47.30244	84.83952
Blue Gap	15	92	1974	40	197,929	19,678,900	23.63748	99.42403
Browning	14	91	1969	8	355,133	3,447,372	10.55003	9.707271
Bunker Hill	27	89	1937	0	1182	4,956,904	4.980544	4193.658
Cow Creek	16	92	1960	1	148	13,400,880	13.40384	90,546.48
Creston	19	92	1960	2	93,640	5,964,626	7.837,426	63.69741
Crooked Canyon	21	103	1975	13	12,200	13,027,960	13.27196	1067.866
Deadman Wash	20	101	1973	3	4319	21,431,420	21.5178	4962.125
Deep Creek	16	90	1950	2	46,901	5,189,815	6.127835	110.6547
Delaney Rim	18	97	1976	9	989,112	6,299,701	26.08194	6.369047
Drrping Rock	14	94	1984	12	19,674	41,791,160	42.18464	2124.182
Espy	19	89	1965	4	749,689	109,624	15.10336	0.1462264

## APPENDIX A (CONT.)

Field Name	Twp	Rng	Discovery	Active	Cum oil (bbls)	Cum gas (Mscf)	(7+(20x6)/10 <sup>6</sup> )	GOR
				Wells, '93				
Golden Goose	28	92	1966	1	702,363	155,459	14.20272	0.2213371
Great Divide	23	96	1978	8	226,589	4,151,774	8.683554	18.32293
Hatfield	20	88	1923	4	14,371,169	6,202,512	34.94589	4.315785
Joyce Creek	15	103	1958	9	190,807	11,698,290	15.51443	61.30954
Kinney	13	99	1975	8	25,040	41,194,500	41.6953	1645.148
Leucite Hills	22	103	1969	8	2110	7,304,921	7.347121	3462.048
Marianne	20	103	1980	7	0.000999	6,632,807	6.632807	6,639,446,000
Middle Mountain	12	103	1952	1	57,724	9,114,546	10.26903	157.8987
Mulligan Draw	15	95	1990	5	20,668	3,947,175	4.360535	190.98
Pine Canyon	23	103	1964	31	106,571	38,482,370	40.61379	361.0961
Point of Rocks	20	101	1963	3	117,392	4,139,226	6.487066	35.25986
Powder Springs	12	97	1970	1	66,2118	5,704,247	7.028607	86.14345
Robbers Gulch	14	91	1962	17	47,650	5,947,451	6.900451	124.8153
Robin	19	97	1971	1	251,435	821,558	5.850258	3.267477
Salt Wells	14	103	1949	4	316,578	20,296,250	26.62781	64.11137
Savery	13	89	1954	2	0.000999	7,136,297	7.136297	7,143,440,000
Sheep Creek	28	92	1935	4	291,930	0.000999	5.8386	3.42205E-09
Shell Creek	19	96	1977	0	253,635	72,661	5.145361	0.2864786
x Siberia Ridge	21	94	1975	32	203,140	20,550,420	24.61322	101.1638
Stage Stop	18	99	1966	10	865,958	11,091,720	28.41088	12.80861
Table Rock Southwest	18	98	1955	2	36,776	7,238,409	7.973929	196.8243
Ten Mile Draw	21	99	1962	5	5290	9,376,785	9.482585	1772.549
Tierney	19	94	1973	11	386,776	9,063,918	16.79944	23.43454
<b>Total</b>					<b>10,353,131</b>	<b>478,636,160</b>		
<b>Smallest Fields</b>								
Adobe Town	15	97	1981	1	0.000999	22,200	0.02220002	22,222,220
Airport	19	103	1972	2	0.000999	3,230,632	3.230632	3,233,866,000
Alkaline Creek	16	98	1977	1	5271	557,277	0.662697	105.7251
Antelope Springs	27	93	1947	0	0.000999	1,578,848	1.578848	1,580,428,000
Anthill Unit	12	93	1991	0	0.000999	0.000999	2.0979E-08	1
Arapahoe Creek	28	93	1985	0	13,689	48,417	0.322197	3.536927
Baldy Butte	17	92	1982	4	7921	1,283,525	1.441945	162.0408
Barteltt	19	102	1973	0	0.000999	1,177,140	1.17714	1,178,318,000
Bastard Butte	25	97	1978	0	6887	6078	0.143818	0.8825323
Battle Springs	23	94	1979	4	19,616	1,700,191	2.092511	86.677368
Baxter Siding	19	103	1980	0	13	74,550	0.07481	5734.615
Bell Springs	23	88	1924	3	31	2,750,623	2.751,243	88729.77
Big Ridge	14	93	1991	0	139	1971	0.004751	14.17986
Bitter Creek	16	99	1962	3	3801	779,884	0.855904	205.1786
Black Butte Creek	19	102	1959	2	4	1,244,751	1.244831	311,187.8
Blue Goose	13	92	1991	0	0.000999	0.000999	2.0979E-08	1
Boulder Dome	28	92	1984	0	11,781	0.000999	0.23562	8.47976E-08
Browns Hill	16	90	1982	0	0.000999	58,403	0.05840302	58,461,460
Buccaneer	26	102	1982	1	0.000999	47,519	0.04751902	47,566,560
Bush Lake	24	96	1978	1	4310	2,408,681	2.494881	558.8587
Camel Rock	18	102	1979	0	26,643	1,720,635	2.253495	64.58113
Cedar Breaks	13	94	1977	4	2439	1,501,639	1.550419	615.6782
Cepo	14	95	1992	1	18	116,948	0.117308	6497.111
Cherokee Creek	15	91	1960	3	40,574	2,925,286	3.736766	72.09755
Cherokee Ridge	12	96	1962	0	2165	0.000999	0.0433	4.61432E-07
Chimney Rock	18	102	1956	0	0.000999	0.000999	2.0979E-08	1
Cole Springs Draw	23	88	1960	0	0.000999	1,802,518	1.802,518	1,804,322,000
Continental Divide	22	93	1964	3	48,157	421,108	1.375248	8.557593

## APPENDIX A (CONT.)

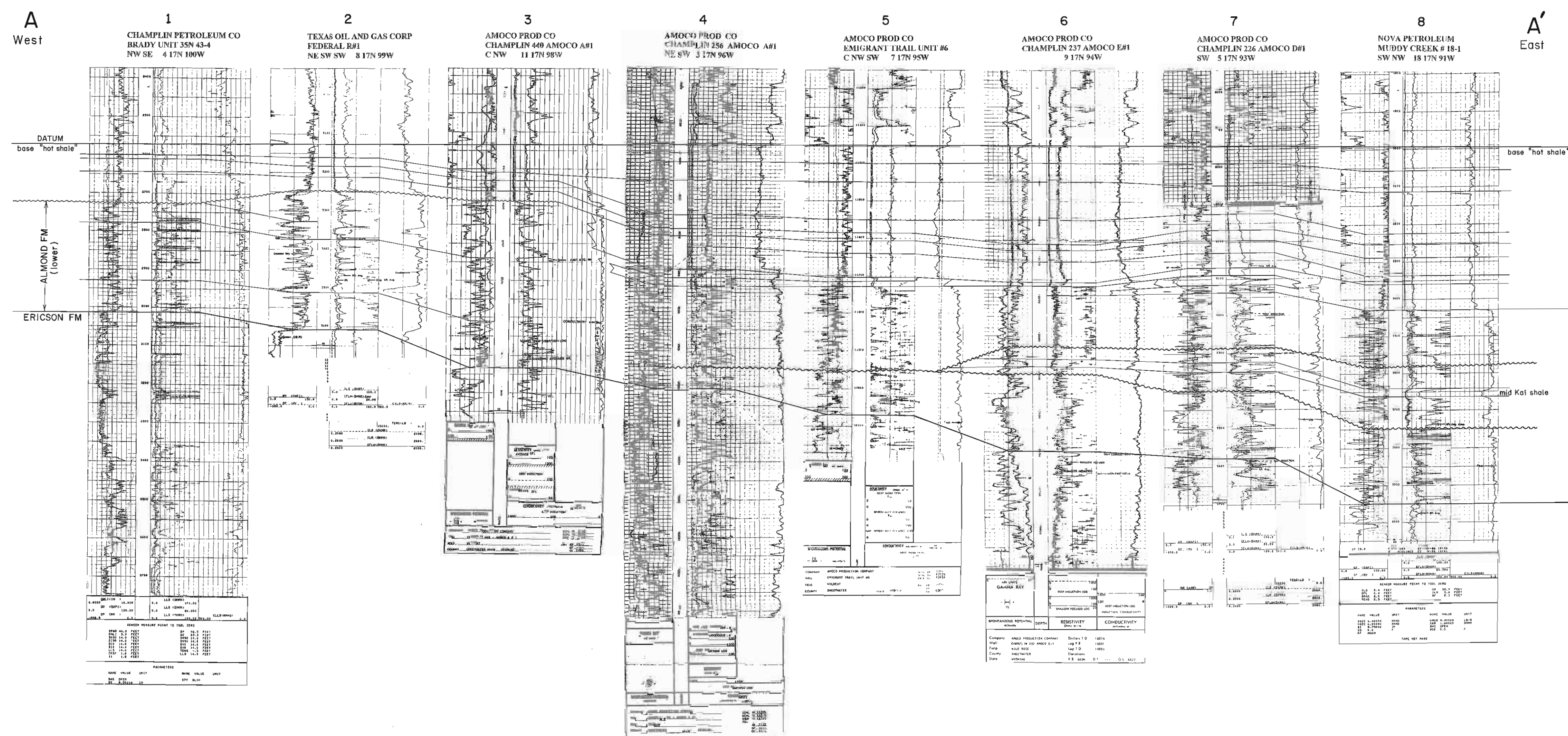
Field Name	Twp	Rng	Discovery	Active Wells, '93	Cum oil (bbls)	Cum gas (Mscf)	(7+(20x6)/10 <sup>6</sup> )	GOR
Crooks Creek	27	92	1991	0	0.000999	2659	0.00265902	2,661,662
Deep Gulch	16	91	1976	0	0.000999	1,805,065	1.805065	1,806,872,000
Desert Flats	19	95	1973	0	2056	49,720	0.09084	24.18288
Desert Rose	14	96	1986	0	0.000999	68,004	0.06800402	68,072,070
Dines	20	105	1986	0	40	48,333	0.049133	1208.325
Dixon	12	90	1991	11	0.000999	112,130	0.11213	112,242,200
Emigrant Trail	17	95	1981	2	23,347	546,709	1.013649	23.41667
Essex Mountain	24	104	1981	0	0.000999	0.000999	2.0979E-08	1
Fillmore	20	92	1976	6	103,650	1,465,401	3.538401	14.13797
Fireplace Rock	12	95	1978	1	873	763,118	0.780578	874.1329
Five Mile Gulch	21	93	1977	5	58,875	3,198,539	4.376039	54.32763
Freighter Gap	24	102	1981	0	4002	163,502	0.243542	40.85507
Frewen	19	95	1990	3	11,207	470,286	0.694426	41.96359
Gale	23	96	1980	1	4087	243,114	0.324854	59.48471
Gap Road	15	99	1983	0	1	20,799	0.020819	20,799
Girard	27	95	1972	0	0.000999	328,113	0.328113	328,441,400
Hansen Draw	17	96	1977	1	151	108,781	0.111801	720.404
Haystack	14	96	1978	0	0.000999	123,422	0.123422	123,545,500
Horn Canyon	24	100	1976	2	1810	460,049	0.496249	254.1707
Iron Pipe	16	98	1978	1	2570	283,897	0.335297	110.4658
Jade Ridge	28	93	1976	0	31,847	1,001,535	1.638475	31.44833
James Creek	15	103	1984	1	1301	845,299	0.871319	649.7302
Kinney Rim	14	100	1983	0	0.000999	0.000999	2.0979E-08	1
Kirk	28	92	1954	0	0.000999	967,418	0.967418	968,386,400
Lamont	25	89	1961	0	2254	103,194	0.148274	45.78261
Laney Wash	17	97	1979	2	5312	253,039	0.359279	47.63535
Little Snake	12	96	1962	0	0.000999	632,053	0.632053	632,685,600
Little Worm Creek	15	104	1958	0	16,561	3,481,879	3.813099	210.2457
Lost Creek	27	93	1976	0	0.000999	32,958	0.03295802	32,990,990
Lost Creek	23	97	1972	0	0.000999	60,000	0.06000002	60,060,060
Lost Creek Basin	23	95	1981	3	24,407	365,092	0.853232	14.9585
Lost Valley	25	98	1980	0	0.000999	4668	0.00466802	4,672,673
Mahoney Draw	21	90	1978	1	21,709	456,944	0.891124	21.0486
Mahoney South	25	88	1978	0	38,733	694,176	1.468836	17.92208
Masterson	20	102	1970	1	0.000999	1,400,298	1.400298	1,401,700,000
McPherson Springs	13	94	1980	3	600	201,228	0.213228	335.38
Monument Lake	21	92	1977	2	400	412,473	0.420473	1031.182
Mud Lake	23	98	1959	0	0.000999	0.000999	2.0979E-08	1
N.T.	15	96	1982	0	0.000999	0.000999	2.0979E-08	1
Neff	18	98	1968	0	14	32,504	0.032784	2321.714
Nickey	24	96	1980	2	892	666,782	0.684622	747.5134
Osborne Draw	26	93	1971	0	0.000999	0.000999	2.0979E-08	1
Pickett Lake	26	97	1978	2	23,555	2,482,491	2.953591	105.3913
Potter Mountain	14	103	1956	5	1073	1,018,687	1.040147	949.3821
Pretty Water Creek	15	104	1962	0	1461	964,338	0.993558	660.0534
Primitive	16	94	1985	1	425	4941	0.013441	11.62588
Red	16	94	1979	0	2240	106,418	0.151218	47.50804
Red Desert	22	96	1971	3	45,079	1,070,269	1.971849	23.74207
Red Hill	19	100	1963	0	0.000999	14,913	0.014191302	14,927,930
Rim	19	88	1975	0	7174	0.000999	0.14348	1.39253E-07
Rim Rock	24	103	1980	2	950	656,859	0.675859	691.4305
Rim Unit	14	95	1988	1	12	78,863	0.079103	6571.917
Roser	21	100	1971	0	0.000999	0.000999	2.0979E-08	1
Round Table	12	96	1967	0	9224	0.000999	0.18448	1.08304E-07
Saddle Bag	24	100	1981	0	0.000999	0.000999	2.0979E-08	1
Salazar	16	95	1975	1	1113	435,988	0.458248	391.7233

## APPENDIX A (CONT.)

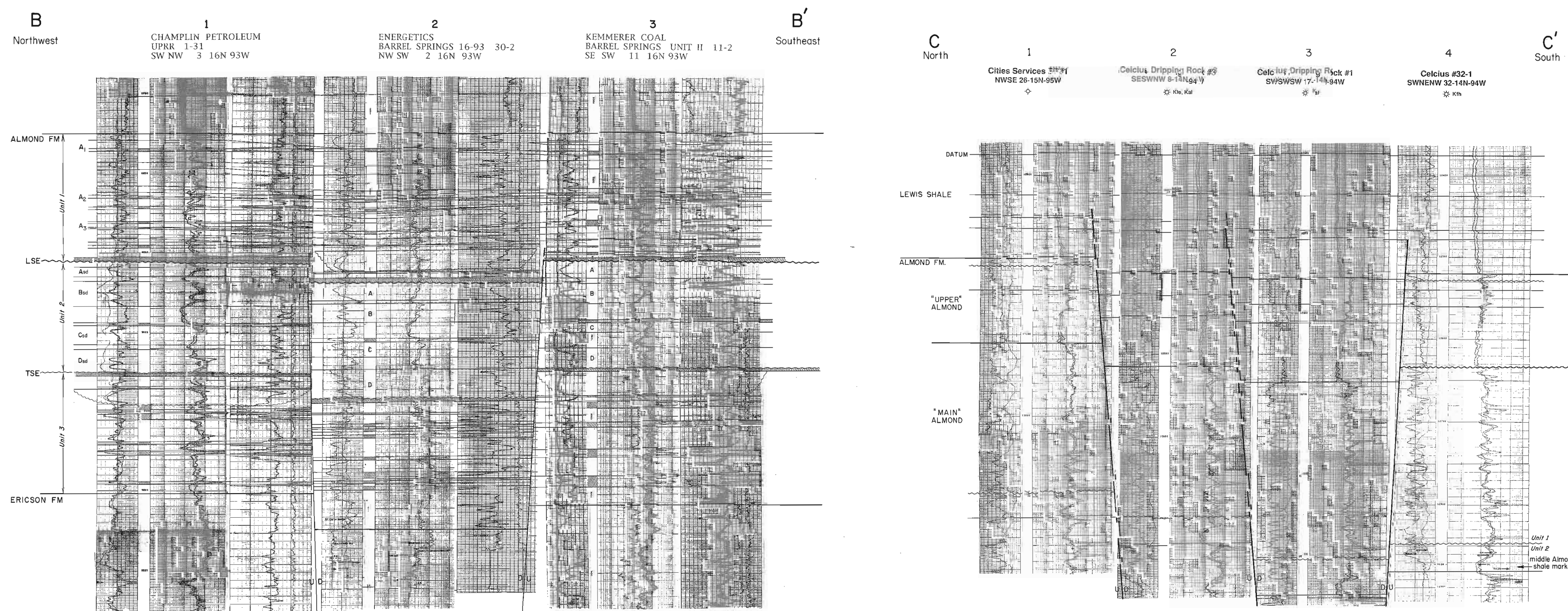
Field Name	Twp	Rng	Discovery	Active Wells, '93	Cum oil (bbls)	Cum gas (Mscf)	(7+(20x6)/10 <sup>6</sup> )	GOR
Salt Sage Draw	20	97	1991	1	148	57,159	0.060119	386.2095
Sand Butte	17	99	1960	3	0.000999	2,979,889	2.979889	2,982,872,000
Sentinel Ridge	23	94	1977	1	1225	801,109	0.825609	653.9666
Shallow Creek	16	94	1981	1	10,087	288,538	0.490278	28.60494
Sheep Camp	22	97	1976	2	11,296	855,323	1.081243	75.7191
Sherard	25	88	1942	2	59,984	965,164	2.164844	16.09036
Sherard North	25	89	1942	0	0.000999	256,781	0.256781	257,038,000
Sierra Madre	13	89	1981	17	155,672	297,869	3.411309	1.91344
Sixmile Spring	18	104	1962	5	959	2,863,927	2.883107	2986.386
Smith Ranch	12	93	1967	2	472	234,558	0.243998	496.9449
Smokey	15	99	1979	0	0.000999	0.000999	2.0979E-08	1
State Line	12	94	1959	1	19,016	562,460	0.94278	29.57825
Steamboat Mountain	23	102	1978	1	566	508,722	0.520042	898.8021
Stewart Creek	24	91	1977	0	482	0.000999	0.009640001	2.07261E-06
Stock Pond	22	95	1978	1	5165	743,853	0.847153	144.018
Stratton Draw	24	93	1982	0	0.000999	3114	0.00311402	3,117,117
Sugar Creek	19	90	1968	0	4858	887,989	0.985149	182.789
Tipton	19	97	1970	0	0.000999	103,993	0.103993	104,097,100
Trail Ridge	27	95	1958	0	0.000999	36,523	0.03652302	36,559,560
Treasure	24	101	1980	1	22,946	616,255	1.075175	26.86675
Triton	13	94	1980	4	2538	3,485,439	3.536199	1373.301
Twin Buttes	26	90	1976	0	0.000999	11,366	0.01136602	11,377,380
Twin Fork	14	97	1980	2	5955	461,925	0.581025	77.56927
Twin Rocks	21	103	1956	0	139	131,636	0.134416	947.0216
Two Rim	19	95	1992	4	37,825	1,253,599	2.010099	33.14207
Vermillion Creek	13	101	1961	0	453	24,204	0.033264	53.43046
Wells Bluff	18	96	1977	2	12,371	341,999	0.589419	27.64522
Willow Reservoir	16	95	1992	1	140	473,069	0.475869	3379.064
Windmill Draw	15	94	1979	2	1793	666,483	0.702343	371.7139
Windy Hill	21	91	1982	0	0.000999	27,465	0.02746502	27,492,490
<b>Total</b>					<b>11,349,690</b>	<b>74,097,180</b>		
<b>Totals</b>				<b>1446</b>	<b>530,572,500</b>	<b>4,173,353,000</b>	<b>14,784.8</b>	<b>7.865754</b>
<b>State of Wyoming</b>				<b>16,530</b>	<b>6,194,916,000</b>	<b>18,026,870,000</b>	<b>141,925.2</b>	<b>2.909946</b>

**PLATE 1**  
**ALMOND FORMATION**  
WELL LOG CROSS-SECTIONS  
A-A', B-B', C-C', & D-D'  
Washakie Basin, Wyo.

-  Coal
-  Channel
-  Inferred fault
-  Unconformity

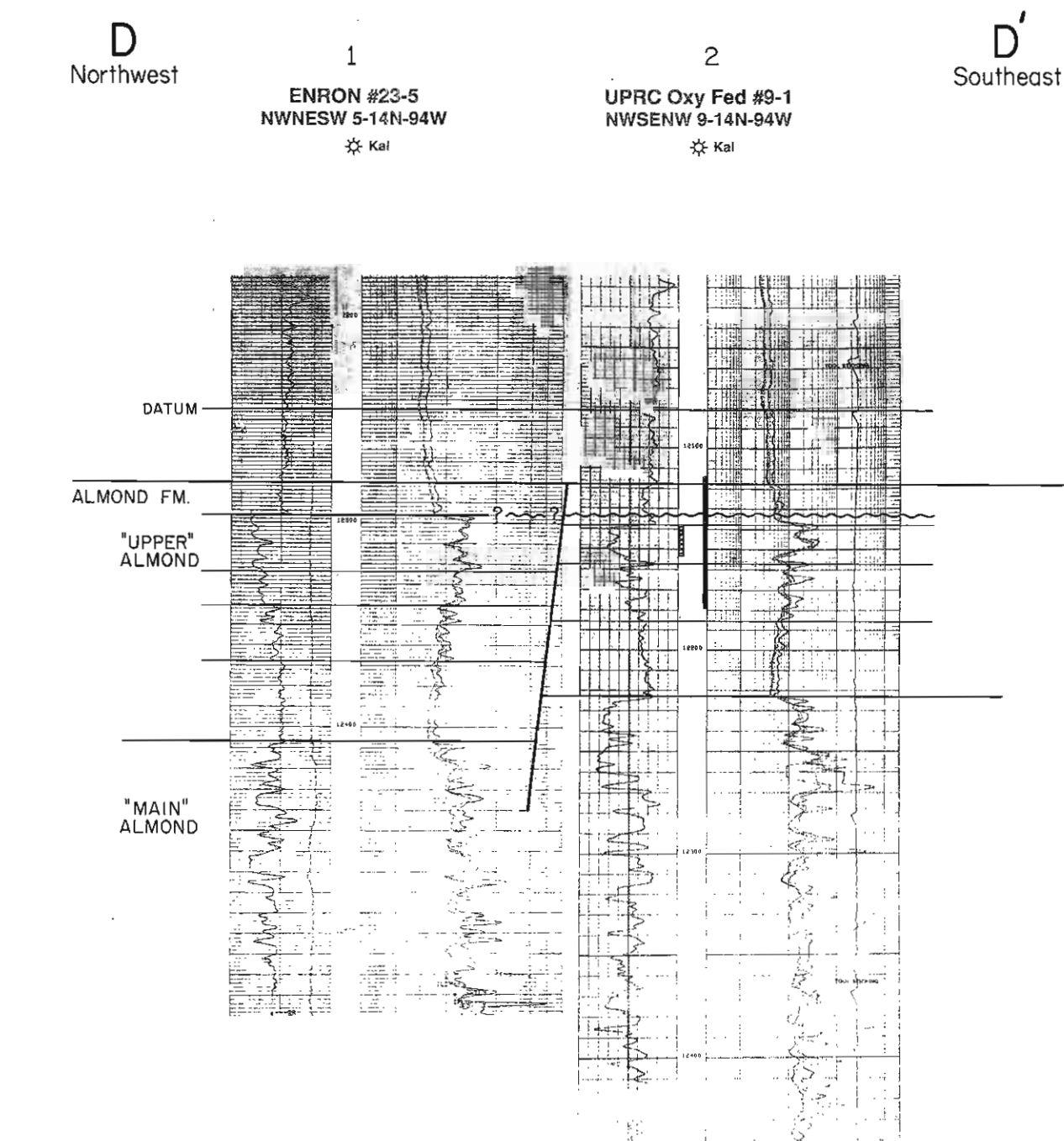


East-west well log cross section A-A' of the upper Ericson through lower Lewis interval. Cross section is hung on the base of the "hot shale." Line of section shown in **Figure 3-2**.



Northwest-southeast well log cross section B-B', Barrel Springs Field, showing stratigraphic relationships within the Almond and the location of inferred syndepositional faults. The interval designated "middle Almond shale marker" is correlatable across the central and eastern Washakie and Great Divide Basins. Datum is a marker in the lower Lewis. LSE= Lowstand surface of erosion; TSE=Transgressive surface of erosion. Line of section shown in **Figure 3-2**.

Gamma-ray - resistivity-log cross section C-C' of the Almond Formation in the Dripping Rock - Mulligan Draw fields area. Location of cross section shown in **Figure 3-8**. Cross section trends northwest-southeast and is hung on a bentonite datum in the Lewis Shale. Also shown are location and relative motion of inferred faults.



Gamma-ray - resistivity log cross section D-D' of the Almond Formation in the Dripping Rock Field. Cross section is of two adjacent wells, and is hung on a bentonite datum in the Lewis Shale. Also shown are location and relative motion of inferred fault. Location of cross section shown in **Figure 3-8**.

**PLATE 2**  
**ALMOND FORMATION**  
CROSS-SECTION GRID  
T 17 N R 93 W  
COAL GULCH  
Washakie Basin, Wyo.

 Coal

 Unconformity

